

# Catalytic Upgrading of Biomass-Derived Carboxylic Acids to Fuels and Chemicals

**Thèse N° 9247**

Présentée le 20 mars 2019

à la Faculté des sciences de base

Laboratoire des procédés durables et catalytiques

Programme doctoral en chimie et génie chimique

pour l'obtention du grade de Docteur ès Sciences

par

**Jher Hau YEAP**

Acceptée sur proposition du jury

Prof. A. Osterwalder, président du jury

Prof. J. Luterbacher, directeur de thèse

Prof. M. Studer, rapporteur

Prof. J. Bond, rapporteur

Prof. W. Queen, rapporteuse

2019



# Acknowledgements

When I first met Jeremy Luterbacher, he was still a postdoctoral researcher at the University of Wisconsin - Madison, and I was just a clueless undergraduate researcher. He took me under his wing, taught me how to properly operate a flow reactor, and invited me to join his new lab when he became a professor. In a sense, my life as a PhD student at EPFL would not have been possible without Jeremy. An extremely kind and approachable advisor, Jeremy put on no airs with regards to his position and still discusses both scientific problems and daily matters with me like a friend. I cannot thank him enough for his patience when I was just starting out as a researcher, and I feel extremely lucky to have a friendly and perhaps brotherly relationship with him over the last 6 years.

The 4 years that I have spent in LPDC can be said as both exciting and fulfilling, mainly due to the lab members I have met throughout the years. Ydna Questell-Santiago, whom I met briefly in Madison, turned out to be one of my closest friends. No silly or funny topic would be off-limits for discussions, and no difficulties or problems would be too hard to talk about during our weekly Starbucks or McDonald's sessions. I will also be always grateful to Florent Héroguel for always watching out for me when we first arrived in Lausanne, and for our morning coffee breaks. I'm also thankful to Jessica Rohrbach, who has been an excellent next table neighbor in the office and who has been incredibly patient with my antics. I would also like to extend my appreciation and gratitude to all the other members of LPDC (Stefania, Lorenz, Yuan-Peng, Benjamin, Masoud, Wu, Li, Raquel, Rémy, Luca, Kris, Jean, Chloé, Gaël, Nathalie), whose company I cherish.

Additionally, I would be amiss to not mention David Martin Alonso and Stephanie

Wettstein, who both set me out on the path of a researcher when they showed me how to use a glass reactor, and the late Steve Rader, whose pen I still keep until now.

I would also like to thank all my friends who have been with me through thick and thin. To my old ZxG buddies in Malaysia, may our friendship never end no matter how far away we are. To my good friends who I've had the pleasure of meeting in UW-Madison, once a Badger, always a Badger.

Most important of all, I would like to acknowledge my loving and supportive family, without which all of this would not be possible. My brother-in-law (Kai Kiat) and my baby nephew (Dylan Zi Hong), the newest addition to the family. My three sisters (Sze Ling, Szu Ling and Yi Jiun) and my cousin (Cheong Min), who have been role models to me. My late eldest aunt, who loved me like her own son. My late father, who sacrificed everything for us and was the pillar of the family. And my mum and my aunt, whose unconditional love, care and guidance for me shaped who I am now. I dedicate this thesis to both of you, Mummy and Koko. Thank you for everything.

# Abstract

Our reliance on fossil fuels, which is unsustainable due to dwindling reserves, has led to various environmental issues. Lignocellulosic biomass could serve as a renewable source of carbon and energy for the production of fuels and chemicals. While several valorization routes of biomass-derived sugars (via furans or sugar alcohols) exist, the upgrading of the biological carboxylate platform is relatively unexplored, mainly due to historical focus on ethanol production via fermentation. Research on biomass-derived carboxylic acids could increase our knowledge on carboxylic acid upgrading and open up new avenues towards sustainable production of fuels and chemicals from lignocellulosic biomass.

The production of olefins from carboxylic acids via tandem hydrogenation/dehydration was carried out, with olefin selectivities  $> 90\%$  at close to 99% conversion of carboxylic acids using a  $\text{Cu/SiO}_2\text{-Al}_2\text{O}_3$  catalyst. Interestingly, a sudden selectivity switch from olefins to predominantly alkanes was observed at full conversion. Using various intermediate products and catalyst surface studies, this selectivity switch phenomenon was ascertained to originate from the adsorption of small amounts of carboxylic acid on the catalyst surface, which prevented the binding and subsequent overhydrogenation of olefins. This finding suggests that carboxylic acids has potential to be used in influencing product distributions of other catalytic reactions, especially if selective double bond preservation is required. This phenomena could also be used to explain the difference in catalyst performance observed when using commercial model compounds versus real biomass-derived feed, given the prevalence of carboxylic acid impurities in biomass-derived streams. This route represents a single-step upgrading of carboxylic acids to olefins with no loss in carbon efficiency and without use of expensive stoichiometric reagents, which is important

for economical production of bulk chemicals from lignocellulosic biomass.

In parallel, a study on carboxylic acid upgrading via single-step ketonization/cascade aldol condensation to an aviation fuel additive was performed over Cu/ZrO<sub>2</sub>. Biomass-derived acetic acid and butanoic acid was converted to an organic oil composed of aromatics and cycloalkenes with a carbon number range of C<sub>8</sub> - C<sub>16</sub> at mass yields of around 20 wt %. By-products include gaseous hydrocarbons (mainly propylene) and water resulting from condensation. This organic oil represents up to 96% deoxygenation of the starting carboxylic acids, and has been tested to be compatible as a 10 vol % blend with Jet A-1 fuel in terms of specific energy and distillation properties. While previous research on ketonization and aldol condensation have performed the reactions separately, this route combines both in a single step to upgrade short carboxylic acids to long chain hydrocarbons, while valorizing the often neglected acetate fraction of biomass. This study shows a combination of C-C coupling and extensive deoxygenation, both crucial towards successful upgrading of lignocellulosic biomass to fuels.

**Keywords** *carboxylic acids, olefins, aviation fuel, heterogeneous catalysis, lignocellulosic biomass, carboxylate platform, fundamental catalyst-substrate interactions, copper*

# Résumé

Notre dépendance aux énergies fossiles est non-durable et conduit à de nombreux problèmes environnementaux. Dans ce contexte, la biomasse lignocellulosique se présente comme une source de carbone et d'énergie alternative pour la production de carburants et substances chimiques. Alors que plusieurs procédés de conversion de la biomasse en sucre (par le biais de furanes ou polyols) existent, sa valorisation en carboxylate reste encore peu explorée, notamment dû au fort accent mis historiquement sur la production d'éthanol par fermentation. La recherche sur les acides carboxyliques dérivés de la biomasse peut améliorer notre connaissance sur leur valorisation et ainsi ouvrir de nouvelles voies pour une production durable de produits chimiques à partir de la biomasse lignocellulosique.

La production d'oléfines à partir d'acides carboxyliques via un tandem d'hydrogénation /déshydratation a été conduite, avec une haute sélectivité ( $> 90\%$ ) envers les oléfines pour une conversion d'acides proche de 99%, sur un catalyseur  $\text{Cu/SiO}_2\text{-Al}_2\text{O}_3$ . A conversion totale, un changement soudain de sélectivité, favorisant la formation d'alcanes, a été observé; ce fait a pu être attribué à l'adsorption en faible quantité d'acide carboxylique sur la surface du catalyseur, empêchant ainsi la liaison des oléfines et par conséquent leur hydrogénation en alcanes. Ce résultat suggère le potentiel d'utilisation des acides carboxyliques pour influencer la distribution des produits obtenue par réactions catalytiques, en particulier lorsque la conservation sélective de la double liaison est cruciale. De même, ce phénomène peut expliquer la différence de performance des catalyseurs observée lorsqu'un flux réel dérivé de la biomasse, contenant des acides carboxyliques, est utilisé au lieu de composés modèles. Ce procédé représente une réaction en une seule étape, sans perte de carbone et non basé sur l'utilisation stoechiométrique de réactifs onéreux,

critères fondamentaux pour une production de masse de produits chimiques issus de la biomasse lignocellulosique.

En parallèle, la conversion d'acides carboxyliques en additif pour kérosène, par un tandem cétonisation/condensation d'aldols en cascade sur un catalyseur Cu/ZrO<sub>2</sub> en une seule étape, a été étudiée. La production d'une huile organique constituée d'aromatiques et de cycloalcènes (C<sub>8</sub> - C<sub>16</sub>) a été réalisée à partir d'acide acétique et butyrique dérivés de la biomasse, avec des rendements massiques à hauteur de 20%; sous-produits de cette réaction incluent des hydrocarbures gazeux (principalement propylène) et de l'eau émanant de la condensation. L'huile organique obtenue représente jusqu'à 96% de désoxygénation des produits de départ et s'est avérée compatible, en terme de densité d'énergie et propriétés de distillation, lorsque mélangée à un volume de 10% avec du kérosène Jet A-1. Alors que de précédentes recherches ont traité la cétonisation et la condensation en aldol de manière individuelle, ce procédé les combine en une seule étape afin d'obtenir de longues chaînes d'hydrocarbures à partir d'acides carboxyliques courts, tout en valorisant une fraction de la biomasse souvent inutilisée. Cette recherche présente un couplage carbone-carbone associée à une désoxygénation extensive, phénomènes cruciaux pour la réussite de la valorisation la biomasse en carburants.

**Mots-clés** *acide carboxylique, oléfine, carburant aviation, catalyse hétérogène, biomasse lignocellulosique, carboxylate plate-forme, catalyseur-substrat interactions, cuivre*



# Contents

<b>Acknowledgements</b>	<b>iii</b>
<b>Abstract</b>	<b>v</b>
<b>Résumé</b>	<b>vii</b>
<b>Table of contents</b>	<b>ix</b>
<b>List of figures</b>	<b>xiii</b>
<b>List of tables</b>	<b>xvii</b>
<b>1 Introduction</b>	<b>1</b>
1.1 Current situation with fossil fuels . . . . .	1
1.2 Alternatives to fossil fuels . . . . .	3
1.2.1 Alternative energy sources . . . . .	4
1.2.2 Alternative carbon sources . . . . .	7
1.3 Biomass as a renewable source of carbon and energy . . . . .	9
1.3.1 First-generation biomass . . . . .	9
1.3.2 Second-generation biomass . . . . .	12
1.3.3 Third-generation biomass . . . . .	13
1.4 Lignocellulosic biomass as a feedstock for the production of fuels and chemicals . . . . .	14
1.5 Valorization of lignocellulosic biomass . . . . .	16
1.5.1 Direct usage . . . . .	17

1.5.2	Fractionation and subsequent upgrading . . . . .	19
1.6	Carboxylic acids as platform molecules to fuels and chemicals . . . . .	29
1.7	Current upgrading routes with carboxylic acids . . . . .	31
1.7.1	Addition/substitution reactions . . . . .	33
1.7.2	Decarboxylative reactions . . . . .	35
1.8	Challenges in upgrading carboxylic acids . . . . .	41
1.9	Objectives . . . . .	43
1.9.1	Objective 1: To study the direct conversion of carboxylic acids to olefins via tandem hydrogenation/dehydration . . . . .	43
1.9.2	Objective 2: To investigate the conversion of carboxylic acids to liquid transportation fuels via ketonization/aldol condensation . .	43
1.9.3	Objective 3: To use real biomass-derived carboxylic acids . . . . .	44
1.9.4	Objective 4: To understand the fundamental surface reaction phe- nomena occurring during catalytic upgrading of carboxylic acids .	44
<b>2</b>	<b>Selectivity control during the single-step conversion of aliphatic car- boxylic acids to linear olefins</b>	<b>45</b>
2.1	Results and discussion . . . . .	46
2.2	Conclusion . . . . .	54
<b>3</b>	<b>Catalytic valorization of the acetate fraction of biomass to aromatics and its integration into the carboxylate platform</b>	<b>57</b>
3.1	Results and discussion . . . . .	58
3.1.1	Proposed reaction pathway . . . . .	58
3.1.2	Upgrading of pure acetic acid . . . . .	61

3.1.3	Upgrading of dilute & biomass-derived acetic acid . . . . .	65
3.1.4	Upgrading of dilute & biomass-derived acetic/butanoic acid mixtures	69
3.1.5	Aviation fuel testing of organic oil as an additive . . . . .	73
3.2	Conclusion . . . . .	75
<b>4</b>	<b>Conclusion</b>	<b>77</b>
4.1	Summary . . . . .	77
4.2	Outlook . . . . .	78
<b>A</b>	<b>Appendix for Chapter 2</b>	<b>81</b>
A.1	Chemicals and materials . . . . .	81
A.2	Catalyst preparation . . . . .	82
A.3	Catalyst characterization . . . . .	82
A.4	Catalytic testing . . . . .	83
A.5	Temperature-programmed desorption (TPD) experiments . . . . .	85
A.6	Fourier-Transform Infrared Spectroscopy (FTIR) . . . . .	86
A.7	Production of butanoic acid from beech wood . . . . .	87
A.7.1	Steam pretreatment of beech wood . . . . .	87
A.7.2	Fungal and bacterial strains and culturing methods . . . . .	88
A.7.3	Biofilm membrane reactor . . . . .	89
A.8	Extraction and purification of biomass-derived butanoic acid . . . . .	89
A.9	Supplementary figures . . . . .	90
<b>B</b>	<b>Appendix for Chapter 3</b>	<b>93</b>
B.1	Chemicals and materials . . . . .	93
B.2	Catalyst preparation . . . . .	94

B.3 Catalyst characterization . . . . .	95
B.4 Catalytic testing . . . . .	96
B.5 Estimation of higher heating values (HHV) for the organic oil . . . . .	99
B.6 Inductively coupled plasma-mass spectrometry (ICP-MS) analysis . . . . .	100
B.7 Aviation fuel testing . . . . .	100
B.8 Production of acetic and butanoic acid from beech wood . . . . .	101
B.9 Steam pretreatment of beech wood . . . . .	101
B.10 Fungal and bacterial strains and culturing methods . . . . .	101
B.11 Biofilm membrane reactor . . . . .	102
B.12 Purification of biomass-derived acetic and butanoic acid in water . . . . .	103
B.13 Purification of acetic acid . . . . .	103
B.14 Purification of butanoic acid . . . . .	103
B.15 Supplementary figures and tables . . . . .	104
<b>References</b>	<b>113</b>
<b>Curriculum Vitae</b>	<b>133</b>

# List of figures

1.1	Global mean CO <sub>2</sub> concentration from 1980 to 2017. . . . .	3
1.2	Atmospheric and terrestrial carbon cycle. . . . .	7
1.3	Three generations of biomass feedstock and their components. . . . .	10
1.4	Three main fractions of lignocellulosic biomass. . . . .	14
1.5	An overview of lignocellulosic biomass valorization routes. . . . .	17
1.6	The furanic and sugar alcohol platform with their subsequent upgrading routes. . . . .	26
1.7	Consolidated bioprocessing of steam-pretreated beech wood to lactic acid in a membrane biofilm reactor by a cross-kingdom consortia of <i>T. reesei</i> / <i>L. pentosus</i> . . . . .	30
1.8	Common upgrading routes for carboxylic acids towards building block molecules and subsequently their family of end products. . . . .	32
1.9	Transesterification of triglycerides to fatty acid methyl esters (FAME). . . . .	34
1.10	Thermal decarboxylation of carboxylic acids to alkanes. . . . .	35
1.11	Oxidative decarboxylation of carboxylic acids to olefins. . . . .	36
1.12	Decarbonylation of carboxylic acids to olefins. . . . .	37
1.13	Decarboxylative coupling reactions. . . . .	37
1.14	Ketonization of carboxylic acids to ketones. . . . .	38
2.1	Graphical abstract for chapter 2 . . . . .	45
2.2	Proposed reaction pathway for the tandem hydrogenation/dehydration of hexanoic acid. . . . .	46

2.3	A) Conversion and molar product distribution of hexanoic acid tandem hydrogenation/dehydration as a function of time on stream. B) Average steady state conversion and molar product distribution of hexanoic acid tandem hydrogenation/dehydration at different WHSV. C) Molar product distribution of an intermediate products study as function of time on stream.	48
2.4	A) Temperature-programmed desorption (TPD) of different reaction species on the catalyst while using the MS to track mass 84 (molecular ion peak of 1-hexene). B) Subtracted FTIR spectra of different molecules adsorbed on the surface of the catalyst at 25 °C. C) Illustration depicting the accessibility of hydrogenation sites in the presence/absence of adsorbed hexanoic acid. . . . .	51
2.5	A) Conversion and molar product distribution of butanoic acid tandem hydrogenation/dehydration as a function of time on stream. B) Illustration of the consolidated bioprocessing of steam-exploded beech wood to butanoic acid, followed by tandem hydrogenation/dehydration to form butenes. C) Conversion and molar product distribution of biomass-derived butanoic acid tandem hydrogenation/dehydration as a function of time on stream.	53
3.1	Graphical abstract for chapter 3 . . . . .	57
3.2	Proposed and simplified reaction pathway for the ketonization of carboxylic acids and subsequent cascade aldol condensation reactions to form aromatic hydrocarbons with high carbon numbers. . . . .	59
3.3	Upgrading of pure acetic acid over 2 g 2 wt % Cu/ZrO <sub>2</sub> . . . . .	62
3.4	Upgrading of 50 wt % aqueous acetic acid over 2 g 0.5 wt % Cu/ZrO <sub>2</sub> . .	67

3.5	Upgrading of 28/12 wt % aqueous acetic/butanoic acid over 3 g 0.5 wt % Cu/ZrO <sub>2</sub> . . . . .	70
3.6	Steam-explosion of beech wood, followed by consolidated bioprocessing and secondary fermentation of the resulting polysaccharides to obtain biomass-derived acetic and butanoic acid. . . . .	72
A.1	Conversion and molar product distribution of 10 wt % hexanoic acid tandem hydrogenation/dehydration as a function of time on stream . . . . .	90
A.2	Conversion and molar product distribution of hexanoic acid tandem hydrogenation/dehydration as a function of time on stream with initial Ar flow . . . . .	90
A.3	Subtracted FTIR spectra of different molecules adsorbed on the surface of the catalyst at 25 °C. . . . .	91
B.1	Conversion of acetone as a function of time on stream during the upgrading of pure acetic acid over 2 g commercial ZrO <sub>2</sub> . . . . .	104
B.2	Gas chromatogram of the organic oil during the upgrading of pure acetic acid. . . . .	104
B.3	Molar carbon distribution of the organic oil during the upgrading of different carboxylic mixtures categorized by product functionality. . . . .	109
B.4	Molar carbon distribution of the product stream during the upgrading of 50 wt % aqueous acetic acid over 2 g of 2 wt % Cu/ZrO <sub>2</sub> . . . . .	110
B.5	Molar carbon distribution of the product stream during the upgrading of pure acetic acid over 2 g of 2 wt % Cu/ZrO <sub>2</sub> at 1 bar H <sub>2</sub> partial pressure . . . . .	110
B.6	Molar carbon distribution of the product stream during the upgrading of pure acetic acid over 2 g of 0.5 wt % Cu/ZrO <sub>2</sub> . . . . .	111

B.7 Biofilm membrane reactor used to produce butanoic acid from pretreated	
beech wood. . . . .	111



# List of tables

3.1	Aviation fuel testing results for a 10 vol % blend of organic oil with Jet A-1.	74
B.1	List of identified compounds from the gas chromatogram (Figure B.1) of the organic oil during the upgrading of pure acetic acid. . . . .	105
B.2	Characterization data for the two catalysts utilized in this study . . . . .	108



# Chapter 1

## Introduction

In this thesis, I will first review the current situation regarding carbon and energy usage, which mainly features fossil fuels, and then talk about alternative sources. An emphasis will be placed on lignocellulosic biomass usage, with a brief overview of current processes in lignocellulosic biomass valorization and leading on to present routes in carboxylic acid upgrading. I will then present the objectives of my doctoral thesis, followed by two manuscripts of my work (one published and one in preparation). Finally, I will talk about the conclusions of my research with regards to my initial objectives and discuss potential research in the future.

### 1.1 Current situation with fossil fuels

Fossil fuels have been a major part of our everyday lives since the onset of the Industrial Revolution, contributing to our quality and way of life. Many daily activities would not be possible without fossil fuels, which are primarily used to feed our energy needs. Since 1850, there has been a 2.4% per year average growth rate of global energy consumption, which shows no signs of slowing down.<sup>1</sup> Amongst the global primary energy consumption of 13511.2 million tonnes of oil equivalent in 2017, 85.2% consists of fossil fuels.<sup>2</sup> There are three major categories of fossil fuels: petroleum, coal and natural gas. They serve as the raw materials and a source of energy for the production of electricity, transportation fuel, heat, chemicals and materials that we use in our daily lives. As our

quality of life improves, demand for these products increase and so does the consumption of fossil fuels.

Fossil fuels are primarily composed of hydrocarbons, meaning their energy is stored in the form of stable chemical bonds. During combustion (oxidation), oxygen is used to oxidize the carbon, releasing approximately 417 kJ of heat energy per mole of oxygen used (mainly from the conversion of weak O=O bonds to stronger C=O bonds).<sup>3</sup> This large amount of heat can then be harnessed to produce electricity or converted to mechanical energy in engines to power transportation. For example, petroleum-derived car gasoline has an energy density around 46.4 MJ/kg (34.2 MJ/L). These high values for both gravimetric and volumetric energy density makes gasoline an ideal energy carrier. Furthermore, the dense liquid form of most fossil fuels makes it easy to transport or handle. Fossil fuels as hydrocarbons are also a convenient source of carbon for the petrochemicals industry because they are already concentrated, volatile, and also have interesting properties like double bonds and aromatics which can be easily functionalized. This serves as the basis for all the carbon-based products that we use. Plastics, for example, are mainly made from olefins produced by petroleum cracking.

However, our relentless use of fossil fuels is becoming increasingly unsustainable. The severe climate change around the world has been attributed to mankind's usage of fossil fuels. Burning of fossil fuels releases carbon dioxide into the atmosphere that was previously locked up underground. Atmospheric carbon dioxide acts as a greenhouse gas, trapping heat within the atmosphere, resulting in global warming. The National Oceanic & Atmospheric Administration has reported that current global carbon dioxide concentrations are above 400 ppm (Figure 1.1),<sup>4</sup> up from about 260 ppm<sup>5</sup> prior to the Industrial Revolution, which was the period when fossil fuel use began to skyrocket. This

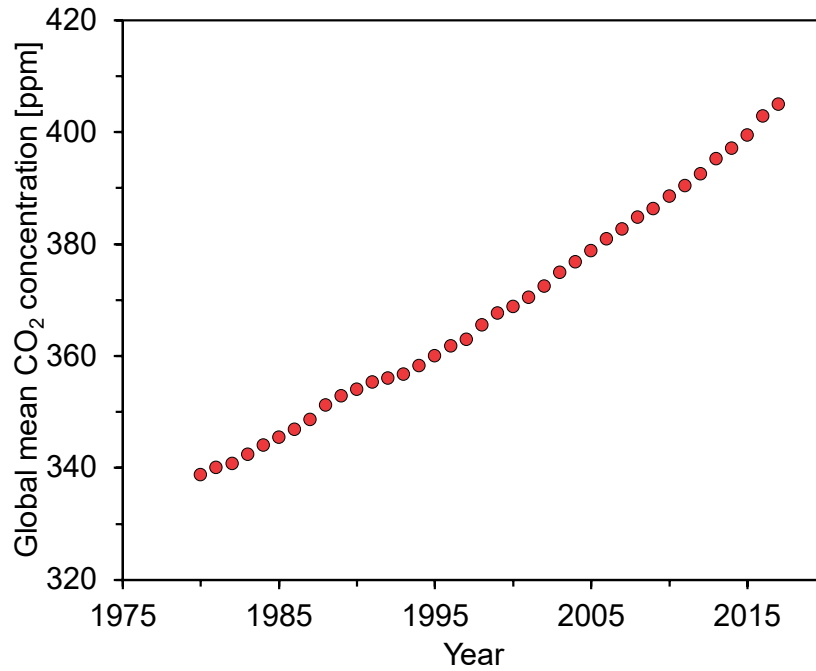


**Figure 1.1.** Global mean CO<sub>2</sub> concentration from 1980 to 2017. Data from NOAA/ESRL.<sup>4</sup>

has already caused an increase in global mean temperatures of about 1 °C compared to pre-industrial levels,<sup>6</sup> very close to the 1.5 °C limit stipulated by the Paris Agreement.<sup>7</sup>

Furthermore, fossil fuels are finite, with remaining sources becoming increasingly dangerous, expensive, and more environmentally burdensome to mine. Fossil fuel extraction has notably resulted in numerous ecological disasters, the most recent being the Deepwater Horizon oil spill in the Gulf of Mexico. These environmental and economic issues, coupled with geopolitical issues stemming from unequal geographical distribution of fossil fuels, has led the global community to search for alternative and sustainable options.

## 1.2 Alternatives to fossil fuels

Most forms of energy we use comes from the sun (with a few exceptions), as even the energy that is contained within fossil fuels was originally formed photosynthetically

from solar energy. On average,  $341 \text{ W/m}^2$  of solar radiation reaches the Earth, with  $161 \text{ W/m}^2$  reaching the surface.<sup>8</sup> This translates to about 82 PW, or about 2600000 EJ per year. In comparison, the total energy consumption of the world in 2017 was calculated to be 567 EJ.<sup>2</sup> Merely harnessing 2% of solar energy would fulfil our yearly energy needs. Therefore, sustainably capturing solar energy, whether directly or indirectly after having undergone other transformations (e.g. photosynthesis), has been the main thrust of renewable energy research.

Furthermore, it is important to realize that fossil fuels are not only used as an energy source, but also as a source of carbon to make commodity chemicals. Therefore, any solutions towards reducing our dependence on fossil fuels would have to identify and exploit alternative sources for both energy and carbon.

### **1.2.1 Alternative energy sources**

#### **Direct solar energy**

Direct solar energy utilization refers to capturing the energy in the photons emitted from the sun directly into a form of usable energy. The foremost example of direct solar energy use is photovoltaics. Within solar cells, usually made with silicon, cadmium telluride, copper indium gallium selenide, or more recently perovskites or organic dyes, solar energy is directly converted to electrical energy, with efficiencies in laboratory settings of up to 44.7%.<sup>9</sup> More commonly, installed solar cells have functional yearly efficiencies between 7% and 8%.<sup>10</sup> The generated electricity can be used directly, or stored in batteries for future use. A less established method of storage transforms this electrical energy to chemical energy by performing water splitting to generate hydrogen and oxygen during

so-called artificial photosynthesis.<sup>11</sup> Rather than solar cells, it's also possible to collect thermal solar energy through the use of mirrors, concentrate it to a localized position to heat up molten salts as a heating fluid, and then generate electricity in a manner akin to traditional fossil fuel power plants.<sup>12</sup>

However, there are several challenges associated with direct solar energy use. In particular, because solar energy is intermittent, direct usage of solar energy is highly dependent on the weather and time of day. Differences in rain and cloud coverage change the amount of solar radiation reaching the surface of the Earth throughout the day, causing intermittent generation of heat and electricity. Seasonal changes for both the northern and southern hemisphere also affects the amount of solar energy available throughout the year. Most importantly, there is no solar energy available during the night, which is when electricity demand can be the highest. Current battery energy capacities and lifetimes do not yet enable large scale electricity storage to ensure a constant electricity distribution, and certainly not dense enough to be put on an airplane for air transportation.

### **Indirect solar energy or other sources**

Instead of directly utilizing solar energy, we can also harness solar energy that has been transformed into other forms by nature. A prominent example is hydroelectric energy, where the gravitational potential energy of water at a higher spatial location is used to drive a turbine to generate electricity. This method is very prevalent in mountainous regions, so much so that in 2017, about 60% of domestic electricity production in Switzerland came from hydroelectricity.<sup>13</sup> Another source of energy is wind energy, which harnesses the kinetic energy of wind to spin turbines for electricity. Biomass is another potential source of indirect solar energy, which is solar energy that has been stored in

chemical bonds via photosynthesis. Specifically, chlorophyll in leaves absorb solar energy and use it to reduce carbon dioxide to glucose, hence storing chemical energy in the form of chemical bonds within the plant.

Energy can also be generated by sources other than the sun. The foremost example of this is nuclear energy, where nuclear fission splits heavy elements into lighter fragments. These fragments contain less mass than the original heavy element, with the lost mass transformed into large amounts of energy. Additionally, geothermal energy from the Earth's crust can be used as a source of heat or to power turbines for electricity generation.

Unfortunately, these methods also entail many problems and challenges. Hydroelectric energy has very limited downsides during electricity generation, but is restricted to areas with large water bodies preferably in mountainous regions. Furthermore, the building of dams for hydroelectric power plants has been associated with ecological problems and the destruction of local habitats. Wind energy suffers from the same unpredictable behavior as solar energy, and also require construction of large wind turbines over big open areas. Biomass is still considered expensive to produce and transport for relatively low value applications like power and heat. However, it is still often used as a heat source for individual homes. Nuclear energy, while being able to provide large amounts of energy continuously relative to the other sources, encounters problems with disposal of radioactive waste, in addition to potentially catastrophic power plant failures that can endanger a large area. Geothermal energy suffers from the same drawbacks of hydroelectric energy, as it can only be economically extracted from regions with high tectonic or volcanic activity.



### 1.2.2 Alternative carbon sources

In contrast to alternative energy sources, where energy in any form can be used, alternative carbon sources must actually contain carbon atoms in order to produce the vast amounts of carbon-based products that we use. Additionally, the majority of liquid fuels that we know of is made up of hydrocarbons (with the exception of liquid hydrogen in rocket fuel). In fact, there are only two major sources of renewable carbon on this planet, namely atmospheric carbon dioxide and biomass. Utilizing either of these would result in a net zero change in the amount of carbon in the atmosphere, provided biomass can be exploited without leading to significant deforestation (Figure 1.2).

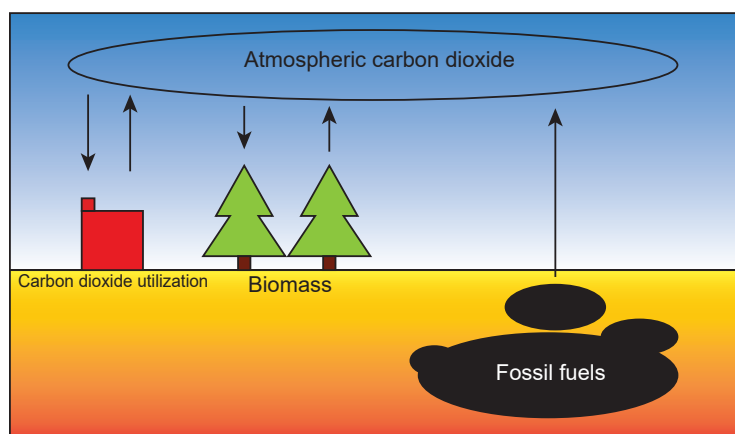


**Figure 1.2.** Atmospheric and terrestrial carbon cycle.

#### Atmospheric carbon dioxide

While atmospheric carbon dioxide would seem like the ideal source of carbon to replace fossil fuels, carbon dioxide represents the highest oxidation state of carbon, with an enthalpy of formation of  $-393.92 \text{ kJ/mol}$ .<sup>14</sup> Any process using carbon dioxide has to start with an input of energy to reduce it to a lower oxidation state, thus resulting in a high energy consumption (at least  $393.92 \text{ kJ/mol}$  to transform it to elemental carbon). Further

exacerbating this issue is the low concentration of carbon dioxide in the atmosphere, which causes the capture of carbon dioxide to be entropically unfavorable. There are attempts to consolidate carbon dioxide utilization with solar energy and water splitting,<sup>15</sup> but it still does not address the issue of carbon dioxide concentration. An interesting and practical approach to this is by capturing carbon dioxide from the flue gas of power plants, where the concentration would be much higher (15% vs 400 ppm).<sup>16</sup>

## **Biomass**

In addition to directly converting carbon dioxide and/or reducing it with solar-derived hydrogen, we can use biomass. Biomass uses solar energy to convert carbon dioxide into usable carbon compounds that form the plant meaning that concentration issues are not present. Furthermore, the well distributed nature of plants on the planet reduces geopolitical instabilities caused by resource imbalances. Because we require both alternative sources of energy and carbon to complement other sustainable sources, biomass could provide an interesting feedstock due to its ability to meet both of those needs. In the shift to using renewable energy in the future, biomass could be used to produce renewable liquid carbon-based fuels to replace fossil fuels in sectors where a change to an alternate form of energy carrier is not feasible (aviation or maritime industry). The International Energy Agency (IEA) projects that by 2050, 27 % of the energy demand in the transportation sector will be met by biofuels.<sup>17</sup> Biomass could also be a source of carbon for chemical production in biorefineries, replacing petrochemicals with biochemicals.

## 1.3 Biomass as a renewable source of carbon and energy

Biomass refers to all available carbon-based organic material that was biologically grown. This includes a wide range of materials such as all plants, animals, food and other microorganisms. It was estimated that for plant biomass alone, there was a global production of  $200 \times 10^9$  tons/year, of which  $8 - 20 \times 10^9$  tons/year is potentially accessible.<sup>18</sup> Currently, in terms of energy, biomass contributes about 45 EJ per year,<sup>19</sup> compared to the worldwide energy consumption of 567 EJ.

The carbon contained in these materials originates from atmospheric carbon dioxide, therefore any release of carbon from biomass utilization is net carbon neutral, provided no significant amounts of fossil carbon or energy were used to facilitate photosynthesis or conversion. The same applies to the energy of these materials, as they all originate from sunlight. This means that biomass utilization could be sustainable both in terms of carbon as well as energy.

Feedstocks for biomass utilization can be broadly categorized into first, second and third generation feedstocks, which refers to their consecutive adoption into mainstream usage (Figure 1.3).

### 1.3.1 First-generation biomass

First-generation biomass feedstocks are biomass with significant amounts of edible components, such as corn, palm oil, sugar cane and beetroot. These forms of biomass

## Types of biomass:

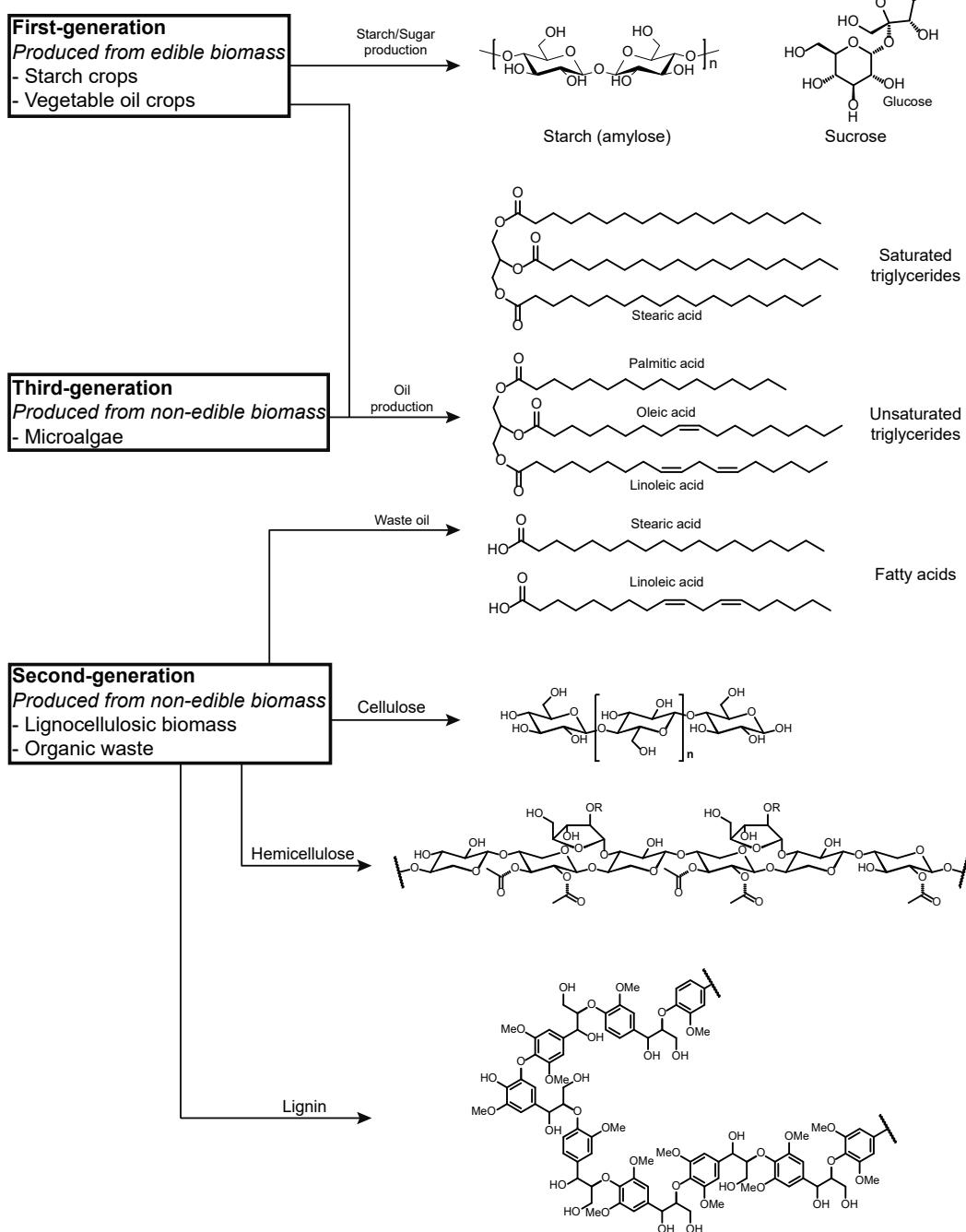


**Figure 1.3.** Three generations of biomass feedstock and their components. Adapted from Questell-Santiago and Luterbacher<sup>20</sup> with permission from The Royal Society of Chemistry.

contain high amounts of mono or disaccharides, starch and/or triglycerides, which are highly ideal to convert to biofuels due to their high energy content as well as their easy depolymerization. For example, corn and sugarcane are widely grown for their high starch

and sugar content which can be fermented with minimal modification into bioethanol, the most prominent biofuel around the world. Biodiesel is also a very popular biofuel that is produced primarily from the transesterification of vegetable oil such as palm oil and rapeseed oil.

However, first-generation biomass feedstocks face several roadblocks to widespread implementation. First, these biomass feedstocks are also food sources. Their high energy content and ease of depolymerization is also the reason why the human body can easily digest these biomass fractions for sustenance. As such, the competition between food and fuels can lead to price increases and food shortages, generally threatening food security.<sup>21</sup>

Furthermore, food crops can usually only be grown in regions with a suitable climate and soil type, further reducing their availability. To obtain high yields of the crop, large amounts of fertilizers are also required, which are currently still being produced from fossil resources.<sup>22</sup> This had led to the argument that using food crops as energy sources only provides minimal carbon and energy savings as compared to fossil fuels, due to the important fossil input associated with growing these plants as well as the negative impacts of agriculture (eutrophication, soil loss, greenhouse gas emissions). For example, the energy yield of corn ethanol is about 63 - 76 GJ/ha (1.52 - 1.82 tonnes of oil equivalent/ha), whereas for switchgrass ethanol, a second-generation biomass feedstock (discussed below), the energy yield is about 228 - 407 GJ/ha (5.56 - 10 tonnes of oil equivalent/ha).<sup>23</sup>

As such, while first generation feedstocks remain popular, the future of biomass valorization is expected to be focused on non-food biomass.<sup>24</sup>

### 1.3.2 Second-generation biomass

Second-generation biomass feedstocks arose out of the challenges associated with the first-generation feedstocks, and generally include terrestrial biomass that are considered non-edible. Lignocellulosic biomass, which include woody plants, agricultural and forestry wastes, as well as specifically grown energy crops fall under this category. Organic wastes such as food waste and animal waste are also included as second-generation feedstocks.

Out of all these, lignocellulosic biomass comprises the majority, and is in fact the largest category (90 %) of all plant biomass.<sup>18</sup> In contrast to the easily digested starches of the first-generation feedstocks, lignocellulosic biomass in general comprises three natural polymers: cellulose, hemicellulose and lignin, which are much harder to depolymerize than starch (which leads to the hardness and structural integrity of these plants). However, they are rarely considered edible, thus eliminating the main problem that plagues first-generation feedstocks. Of all the available lignocellulosic biomass sources, agricultural and forestry wastes are ideal sources of renewable carbon and energy, as part of the wastes left on the fields or forests can be removed with no detrimental effects on soil quality. However, they are usually not available in large quantities (only  $\sim 30$  % can be removed), which would adversely affect the scale of biorefineries. Energy crops (crops specifically cultivated for their high growth rate and energy content, such as switchgrass) are more likely to fulfil the amounts needed for realistic production of energy and carbon. However, this would have to be done in such a way that minimizes deforestation or intrusion into farmland, possibly by growing energy crops on non-arable land (where available, such as in Southeastern USA).<sup>25</sup>

A less prominent source of second-generation biomass are organic wastes. This is

in large due to their inconsistent structure, limited availability as well as being more dispersed geographically. Nevertheless, there are still routes which use these sources. For example, cooking oil waste is a good source of biomass for the production of biodiesel, rather than using virgin vegetable oil.<sup>26</sup> The used oil is usually discarded, which can be a major source of environmental pollution, as well as still containing a high amount of usable energy.

### 1.3.3 Third-generation biomass

Third generation biomass generally refers to algae. As algae is grown in water, they do not take up arable land space, which is one of the main arguments against growing energy crops. Importantly, fast growing algae which can have a high oil content is often seen as a very interesting biomass source as this oil can be then extracted to be used as a biofuel. Algae's high theoretical photosynthetic efficiency (10 – 20% depending on bioreactor design) compared to lignocellulosic plants (0.5% for switchgrass),<sup>27</sup> which leads to a rapid growth and associated carbon dioxide uptake, presents a major advantage over second generation feedstocks, which require more (often higher quality) land. Additionally, the oil produced has a high carbon and energy content, as well as a low oxygen content, making subsequent upgrading to biofuels much easier.

However, with current technologies, production and harvesting of algae oil is still not economically competitive with fossil fuels and even other sources of biomass.<sup>28</sup> Practical yields of algae in open ponds remain low (0.1 kg/m<sup>3</sup>/day), with high yields only achieved in expensive photobioreactors (1.5 kg/m<sup>3</sup>/day).<sup>29</sup> Equipment costs, as well as operating costs for electricity and fertilizer also contribute to the high costs of production. These

reasons have hampered the commercial adoption of algae as a biomass feedstock, with only a handful of production plants operating worldwide.

Of these three generations, second generation biomass remains the most researched and, at present, advantageous feedstock for the sustainable production of fuels and carbon-based chemicals. More specifically, lignocellulosic biomass is especially advantageous for upgrading due to its widespread availability and well defined structure. Nevertheless, there are various challenges in the use of lignocellulosic biomass, namely the recalcitrance of lignocellulosic biomass towards degradation as well as its high oxygen content, which are further detailed below.

## 1.4 Lignocellulosic biomass as a feedstock for the production of fuels and chemicals

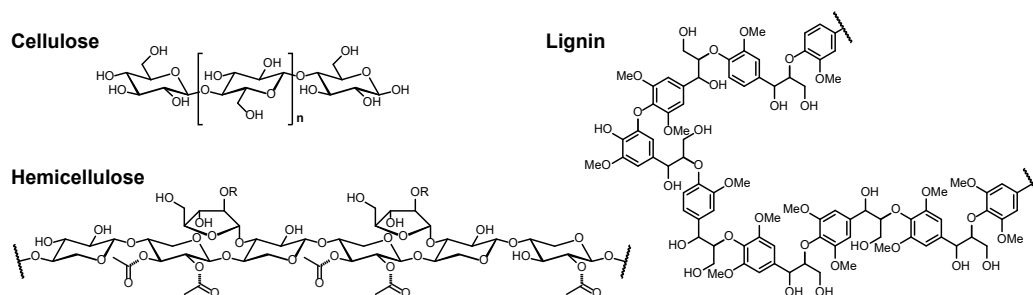


**Figure 1.4.** Three main fractions of lignocellulosic biomass.

Lignocellulosic biomass is mainly composed of 3 natural polymers (Figure 1.4). Cellulose constitutes around 40 - 50% of lignocellulosic biomass. It is a crystalline straight-chained polymer of pure cellobiose units, which are also linked via hydrogen bonding to the neighboring chains due to the presence of multiple hydroxyl side chains, which results in arrangements of straight bundles called fibrils. This rigid and straight bonding confers



structural strength to lignocellulosic-based plants, which contributes to their size.

The second fraction, hemicellulose, is approximately 25 - 35% of lignocellulosic biomass. It is an amorphous branched heteropolymer of predominantly xylose units, although there also various other sugars present in hemicellulose such as mannose, arabinose and galactose. Large amounts of acetyl side chains are also present in hemicellulose. This, along with the branched and flexible nature of hemicellulose, allows it to act as a glue that binds multiple bundles of cellulose fibrils together with lignin. Along with cellulose, these two polysaccharide fractions are the main sources of 6 and 5-carbon (hexose and pentose) sugars in lignocellulosic biomass.

The last major biopolymer is lignin, which comprises 15 - 30% of lignocellulosic biomass. In contrast with the polysaccharide fractions, lignin is a complex heteropolymer of aromatic propanoid monomer units, which results from a radical polymerization during biosynthesis. It forms a sheath around the bundles of cellulose fibrils, and is covalently linked to hemicellulose via ferulic and coumaric acid units. This protects the cellulose from degradation as well as imparting additional structural strength to the plant.

The structural nature of lignocellulosic biomass that protects it from the elements also poses challenges in its utilization as a source of carbon and energy.<sup>30</sup> The lignin sheath is resistant to biological and chemical attack, thus restricting accessibility towards the polysaccharide fractions, where the majority of carbon and energy is. Furthermore, the crystallinity of cellulose makes both biological and chemical depolymerization more challenging. Finally, each fraction of lignocellulosic biomass reacts at a different rate, with hemicellulose being the easiest to deconstruct. At the harsher conditions required to depolymerize cellulose and/or fully extract lignin, the monomers of hemicellulose have

typically already degraded to undesired products such as humins. At typical reaction conditions, it is not uncommon to find that the degradation rate of the sugar monomers are higher or the same as the depolymerization rates, which further limit the attainable yields and concentrations of the desired products.<sup>31</sup>

Beyond deconstruction, there is also the issue that lignocellulosic biomass is a highly oxygenated compound. An elemental analysis of different feedstocks show that lignocellulosic biomass generally has around 40% oxygen, far higher than the 1% present in petroleum.<sup>32</sup> This means the carbon in biomass is already partially oxidized and highly functionalized, reducing the overall energy density and thus requiring defunctionalization, which is opposite of what is usually done with fossil fuel feedstocks. Furthermore, the length of continuous carbon-carbon bonds in lignocellulosic biomass are short (only 6 carbons in cellulose) compared to fossil fuels (ranging from 5 to 40 carbons in petroleum), which affects its compatibility with various engines that require fuels with a longer C-C chain (e.g. diesel and jet fuels).

## 1.5 Valorization of lignocellulosic biomass

Based on the challenges outlined above, most scientific research in this area has focused on effective lignocellulosic biomass fractionation into their respective monomers, followed by conversion into platform molecules, and finally upgrading to fuels and chemicals. A short overview of the current state of research in biomass valorization is presented below (Figure 1.5).

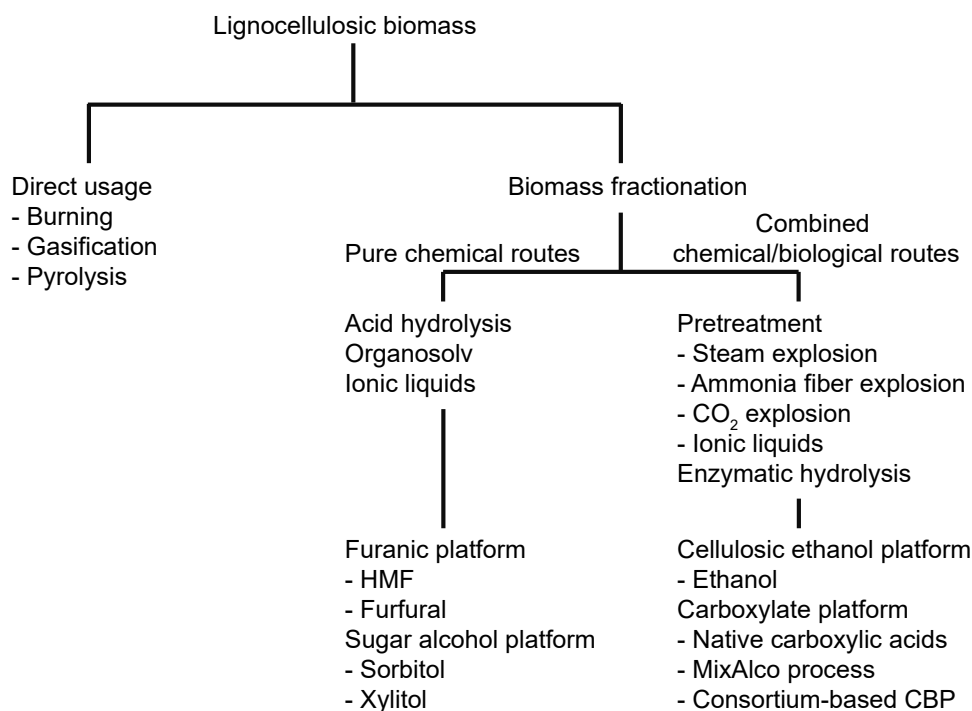


**Figure 1.5.** An overview of lignocellulosic biomass valorization routes.

### 1.5.1 Direct usage

Within this category, lignocellulosic biomass is usually regarded as a single entity. The whole biomass is treated as such, and all 3 fractions are used at the same step. The classical way of illustrating this is the direct burning of wood to produce heat. While this remains popular in certain regions for heating homes and cooking, it does not represent the best usage of lignocellulosic biomass, mainly due to particulate formation during combustion and poor use of the fixed carbon that biomass represents, as the carbon could have been upgraded to chemicals or fuels rather than just burnt. Two other direct process routes fall within this classification: gasification and pyrolysis.

## Gasification

Gasification of lignocellulosic biomass refers to the process of converting all fractions of the solid biomass into gaseous products.<sup>33</sup> This can be done at very high temperatures ( $> 700\text{ }^{\circ}\text{C}$ ) and a controlled amount of oxygen and steam. Care must be taken to not have combustion occur. The main goal is to break the C-C bonds within the biomass so that the resulting product is volatile. By this process, syngas ( $\text{CO}/\text{H}_2$ ) is obtained predominantly, with  $\text{CO}_2$  as a side product due to overoxidation. The obtained syngas can be burnt for its heating value, or more ideally, be upgraded further to fuels and chemicals. For example, syngas can be converted to methanol or dimethyl ether,<sup>34</sup> or to diesel fuel via Fischer-Tropsch synthesis.<sup>35</sup> However, gasification is highly energy intensive, and char formation as well as overoxidation to  $\text{CO}_2$  limits syngas yields.

## Pyrolysis

Rather than feeding in oxygen, heating lignocellulosic biomass in the absence of oxygen and at a lower temperature ( $300 - 650\text{ }^{\circ}\text{C}$ ) is called pyrolysis.<sup>36</sup> Due to the milder conditions involved, the end product is liquid pyrolysis bio-oil rather than gaseous products. The heat drives away volatile substances within the biomass, improving its heating value, while inducing numerous chemical reactions which transform solid biomass into liquid bio-oil. This bio-oil can then be further purified to be used as a fuel or as a replacement for petroleum in petrochemical refineries. The production of charcoal utilizes the principles of pyrolysis, although the aim is to produce a solid product rather than a liquid. However, when the target is liquid bio-oil, char production significantly limits yields as well as posing problems with reactor operation. A variant of pyrolysis is hy-

drothermal liquefaction, which is pyrolysis performed in the presence of water at lower temperatures (200 – 350 °C) and higher pressures (20 – 200 bar).<sup>37</sup> Liquefaction has the added benefit of being able to process high moisture feedstock at lower temperatures, and also produces less char.<sup>38</sup>

### **1.5.2 Fractionation and subsequent upgrading**

More commonly, the three major fractions within lignocellulosic biomass are separated (or used at different stages of the process), as they each have different properties and reactivities, thus different and possibly more useful end products can be obtained. This enables more targeted upgrading towards fuels and chemicals once the sugars and lignin are purified into separate or more concentrated streams. Traditional routes have largely ignored the valorization of lignin in favor of the more easily upgraded sugars, frequently leaving lignin to be burnt for heat. However, recent studies have shown that for economical utilization of lignocellulosic biomass, all three fractions must be considered, as lignin could be a source of high value specialty phenolics that can greatly facilitate the economics of a biorefinery.<sup>39</sup> As the technologies for targeted lignin valorization were only developed quite recently, the fractionation and upgrading routes discussed below are focused on the recovery of the sugars.

#### **Depolymerization of lignocellulosic biomass to sugars**

Biomass fractionation usually starts with the depolymerization of the polysaccharide fractions into soluble and more reactive sugar monomers. Below, I discuss various methods to depolymerize cellulose and hemicellulose.

**Pure chemical routes** Chemical or catalytic routes involve the addition of chemical reagents or catalysts to lignocellulosic biomass. Chemical reactions are the major force driving the depolymerization process, usually at elevated temperatures and pressures. This route can depolymerize both polysaccharide fractions, but can involve significant sugar degradation at the same reaction conditions.

**Acid hydrolysis** Acid catalyzed hydrolysis of lignocellulosic biomass can be carried out either using concentrated acids or dilute acid solutions.<sup>40</sup> Sulfuric acid, hydrochloric acid or phosphoric acid have all been investigated as catalysts for this process. By using concentrated acids at room temperature, both cellulose and hemicellulose can be solubilized at the same time into oligomers. Dilute acid conditions at higher temperatures (e.g. 120 °C for 1 hour) can then hydrolyze all oligomers into carbohydrate monomers at relatively high yields.<sup>41</sup> Biomass can also be directly hydrolyzed by dilute acids at high temperatures (167 – 297 °C). However, the higher temperatures required rapidly degrades the glucose into furans which repolymerizes to form humins. This is due to the lower activation energy for glucose decomposition (130 – 140 kJ/mol) compared to the considerably higher activation energy for cellulose hydrolysis (171 – 189 kJ/mol) at these conditions.<sup>42</sup>

**Organosolv methods** Rather than purely aqueous systems, using organic solvents as a co-solvent with water is also a popular way to depolymerize lignocellulosic biomass. The introduction of organic solvents into the system changes the solubility of biomass in the reaction media. For instance, lignin is soluble in  $\gamma$ -valerolactone (GVL) but not in pure water. Furthermore, different solvent effects can aid in depolymerizing polysaccharides.<sup>43,44</sup> For example, using a mixture of  $\gamma$ -valerolactone (GVL) with water and dilute

sulfuric acid in a flow through system to depolymerize biomass led to monomer yields of 70% for both C<sub>5</sub> and C<sub>6</sub> sugars.<sup>45</sup> The presence of GVL lowers the activation energy for polysaccharide depolymerization, enabling the use of dilute acid catalysts. This increases the rate of polysaccharide depolymerization compared to degradation which minimizes subsequent degradation to humins (which was the problem with aqueous dilute acid hydrolysis, as mentioned above). Similar solvent effects were also seen in other polar aprotic solvents such as THF or dioxane.<sup>42,46</sup> GVL completely solubilizes lignin, and can be easily separated by addition of liquid CO<sub>2</sub> to form a gas-expanded GVL phase which spontaneously separates from the sugar-rich water phase, or by using phenolic solvents.<sup>47</sup>

More recently, a novel organosolv method using dioxane has been developed, whereby aldehydes are added to the reaction.<sup>48</sup> This aldehyde-protection method traps the solubilized xylose by forming acetal rings on the free hydroxyl groups, which protects xylose from degrading.<sup>31</sup> Lignin is also protected in a similar manner, preventing it from condensing and facilitating its subsequent depolymerization at high yields.

**Ionic liquids** The high ionic strength environment in ionic liquids presents similar solvent effects as in organic solvents, which can be exploited to produce sugars directly from the polysaccharides.<sup>42</sup> However, despite lowering the activation energy for polysaccharide depolymerization, the low water content in ionic liquids accelerates sugar degradation.<sup>40</sup> Addition of water (as is with organosolv methods) can mitigate this, but it causes cellulose precipitation. This can be prevented with progressive addition of water, which both stabilizes the soluble sugars and prevents early precipitation of cellulose. With corn stover and a 1 wt % HCl solution in 1-ethyl-3-methylimidazolium chloride, overall yields of 70% and 79% glucose and xylose can be obtained, respectively.<sup>49</sup>

**Combined chemical/biological routes** In this route, lignocellulosic biomass is usually subjected to an initial pretreatment process. These pretreatments are typically used only in biological routes, where their goal is increasing the digestibility of the biomass in preparation for subsequent enzymatic hydrolysis and biological upgrading. Typically, pressure/temperature is used together with a reactive substance inside the biomass. An explosive change in pressure breaks apart the structure of the biomass, enhancing the digestibility of the remaining solids while solubilizing some of the more reactive fractions. After pretreatment, cellulose usually remains as a solid, albeit with much higher surface area. This cellulose is then hydrolyzed by enzymes to soluble glucose.

**Steam explosion** In steam explosion, lignocellulosic biomass is mixed with high-pressure steam for a short amount of time without any additional reagents.<sup>50</sup> During this time, hemicellulose hydrolysis occurs, catalyzed by the protons present in water, which occur at a higher concentration at higher temperatures. The acetyl side chains connected to hemicellulose are also cleaved at this stage, and the released acetic acid could also catalyze the hydrolysis of hemicellulose. Subsequently, the biomass steam mixture is explosively decompressed. The reduction in pressure cools down the biomass, quenching any hydrolysis reactions. This short heating period hydrolyzes hemicellulose and the acetyl groups into a liquid stream, but minimizes the formation of degradation products. The explosive decompression also disrupts the structural integrity of the remaining cellulose and lignin solids, which when coupled with the removal of hemicellulose, increases the accessible surface area and decreases the crystallinity of cellulose.<sup>51</sup>

**Ammonia fiber explosion (AFEX)** AFEX is similar to steam explosion, in that a rapid decrease in pressure breaks apart the structure of lignocellulosic biomass.<sup>52</sup> Instead



of steam, an anhydrous liquid stream of ammonia is used. In addition to hemicellulose removal, the presence of ammonia solubilizes lignin into the liquid stream. The ammonia swells the leftover cellulose solids and also changes the crystal structure from cellulose I to cellulose III,<sup>53</sup> which is more easily hydrolyzable by enzymes.<sup>54</sup>

**CO<sub>2</sub> explosion** In CO<sub>2</sub> explosion, lignocellulosic biomass is subjected to supercritical CO<sub>2</sub>.<sup>20</sup> The mass transfer and solvating properties of supercritical CO<sub>2</sub> allow the CO<sub>2</sub> molecules to easily penetrate the cellulose fraction. The mixture is then explosively decompressed, leading to an autohydrolysis of the liquor and a complete solubilization of the hemicellulose. The remaining solid residue consists of lignin and cellulose with increased accessible surface area due to the explosive action. The low temperatures in CO<sub>2</sub> explosion also minimizes sugar degradation.

**Ionic liquids** Ionic liquids can also be used to pretreat lignocellulosic biomass. In this case, rather than producing monomeric sugars (with an acid catalyst as mentioned above), ionic liquids (pure or mixed with water) is used purely to pretreat the biomass in preparation for enzymatic hydrolysis. Ionic liquids are able to completely solubilize cellulose, which can then be recovered by the addition of water.<sup>55</sup> Furthermore, the recovered cellulose has high surface area, is amorphous (improving enzyme accessibility) , and the whole process can be done essentially at room temperature.<sup>56</sup>

**Enzymatic hydrolysis** After pretreatment, depending on the route used, the polysaccharide fractions of lignocellulosic biomass are transformed into a solid cellulose stream (with higher surface area and digestibility) and solubilized hemicellulose. The cellulose has to be hydrolyzed to obtain the monomeric glucose units, which can be done

at mild conditions (45 – 50 °C). This is usually accomplished by cellulolytic enzymes, produced by either bacteria (anaerobic) or fungi (aerobic).<sup>57</sup> Normally, these cellulases are produced *ex situ* (in the case of fungal cellulases) and then added to the reaction media, with the exception of consolidated bioprocessing (discussed below). However, the production of these enzymes are expensive, and they are hard to recover/recycle after hydrolysis is complete.

### **Upgrading of sugars to platform molecules**

Once the polysaccharides are successfully depolymerized into liquid monomeric streams, upgrading to fuels and chemicals can occur. While many individual routes exist, each with a targeted end product in mind, most processes go through a certain family of compounds called platform molecules. These platform molecules serve as an intermediate valorization step after sugars, and are referred to as such because of the large variety of end products that can be produced from them. Thus, sugar upgrading routes can be categorized based on the platform molecules produced. Note that while direct production of platform molecules from lignocellulosic biomass is possible without isolating the sugar monomers, the reaction conditions usually (with a few exceptions) degrades these platform molecules faster than their formation, in addition to frequently sacrificing the other fractions of lignocellulosic biomass (lignin usually reacts with itself, and the resulting condensed lignin is not easily upgradable with current technologies). Broadly speaking, technologies that aim to transform lignocellulosic biomass to fuels and chemicals can be classified into two different production platforms, each based on a similar type of process.

**Chemically produced platform molecules** These platform molecules are produced via chemical or catalytic conversion of sugars, and leads off from the chemical routes of biomass fractionation. The furanic and sugar alcohol platforms belong to this family, and entails the use platform molecules that are sugar-derived furans and polyols.

**Furanic platform** In this route, monomeric hexoses and pentoses are dehydrated to their respective furanic platform molecules, 5-hydroxymethylfurfural (HMF) and furfural, either separately or in tandem. Dilute mineral acids are usually employed as catalysts, although there have been several studies on using solid acid catalysts.<sup>58,59</sup>

The main challenge in this route is the low stability of the furanic platform molecules, which limit their yield. To combat this, biphasic systems have been used to continuously extract the furans to the organic phase as soon as they are produced, thus lowering degradation due to the acid catalysts present in the aqueous phase.<sup>60,61</sup>

Once HMF and furfural are produced, they then serve as platform molecules for subsequent upgrading (Figure 1.6A and 1.6B), in addition to being used as specialty chemicals themselves. HMF/furfural can be rehydrated to form levulinic acid and formic acid, both stable end products in their own right. Levulinic acid can also be converted into GVL (Figure 1.6C), which can serve as a renewable fuel/chemical precursor<sup>62,63</sup> or further converted to butene,<sup>64,65</sup> an industrially important olefin. Butene oligomerization can be used to valorize it to a jet fuel.<sup>66</sup> HMF can also be oxidized to 2,5-furandicarboxylic acid (FDCA),<sup>67</sup> a potential replacement for terephthalic acid in the production of polyethylene terephthalate (PET) bottles. Furfural itself is a specialized solvent, but it can also be hydrogenated to furfuryl alcohol, which is used as a precursor for resins and adhesives. Aldol condensation of furfural with acetone and subsequent hydrodeoxygenation could

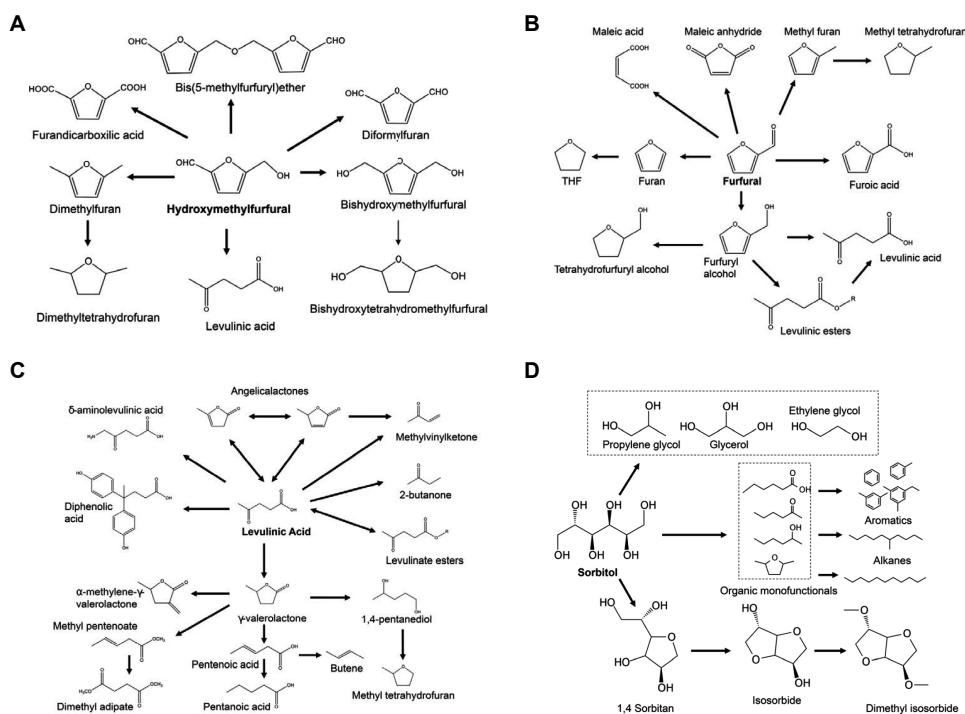


**Figure 1.6.** The furanic and sugar alcohol platform with their subsequent upgrading routes. A) Upgrading of HMF. B) Upgrading of furfural. C) Upgrading of levulinic acid and GVL. D) Upgrading of sorbitol. Reproduced from Luterbacher et al.<sup>40</sup> with permission from The Royal Society of Chemistry.

also lead to jet fuels.<sup>68</sup>

**Sugar alcohol platform** Hydrogenation of hexoses and pentoses produce sorbitol and xylitol, the corresponding polyol platform molecules. Both sorbitol and xylitol are heavily used as sweeteners in the food and flavor industry, but can also be upgraded further (Figure 1.6D). For example, they can be converted to alkanes or aromatics.<sup>69</sup> These polyols also have uses in the production of polyurethane.<sup>70</sup>

**Biologically produced platform molecules** After pretreatment and enzymatic hydrolysis, the isolated sugars are usually converted via biological routes to either ethanol (the major biofuel currently in use) or carboxylic acids.

**Cellulosic ethanol platform** The most direct route in this case skips over any platform molecule in favor of directly producing cellulosic ethanol as a fuel.<sup>71</sup> Glucose can be fermented to ethanol, similarly to corn grain-based ethanol, but without the disadvantages of using a food crop. Different strains of fermenting yeast have also been developed to ferment xylose, further increasing conversion efficiencies.<sup>72</sup>

A more advanced approach called simultaneous saccharification and co-fermentation (SSCF) combines both depolymerization of polysaccharides and subsequent fermentation to ethanol.<sup>73</sup> By having enzymes which depolymerize the polysaccharide to monomers in the same reactor as fermenting microorganisms, pretreated lignocellulosic biomass can be upgraded to ethanol in one step. Consolidated bioprocessing (CBP) (discussed below in the context of the carboxylate platform) operates on a similar principle, except that the production of the hydrolytic enzymes also takes place in the same reactor, either using a different species of microorganism or the same microorganism engineered to also produce enzymes.

**Carboxylate platform** In the carboxylate platform, sugars are further fermented to carboxylic acids, which are then used as platform molecules to produce fuels and chemicals. This biological route contrasts with the chemical route of the furanic and sugar alcohol platforms.

**Native carboxylic acids** Short chain carboxylic acids are natively present in almost all lignocellulosic biomass. The acetyl side chains of hemicellulose represent 1 - 5 wt % of lignocellulosic biomass,<sup>74</sup> and are easily cleaved during pretreatment.<sup>50</sup> While they may only be a small fraction of lignocellulosic biomass, at large scale biorefiner-

ies they represent a potential source of carbon and energy. Furthermore, several alternative second-generation biomass feedstocks like waste cooking oil, which are basically triglycerides, also contain significant amount of long chain carboxylic acids. Therefore, carboxylic acids are naturally present in several biomass sources and are an interesting starting material for further valorization.

**MixAlco process** The most prominent example of commercial developments around the carboxylate platform is the MixAlco process developed at Texas A&M University.<sup>75,76</sup> In the MixAlco process, all non-lignin fractions of lignocellulosic biomass are fed to a naturally occurring mixed culture of microorganisms to be fermented via consolidated bioprocessing into a mixture of C<sub>2</sub> to C<sub>7</sub> aliphatic carboxylate salts (0.3 g carboxylic acids/g biomass digested). These salts are then dewatered, and thermally converted to ketones (400 °C, 3 h, 61% conversion). The ketones are subsequently hydrogenated to alcohols (155 °C, Raney nickel, 24 h, 100% conversion), dehydrated and oligomerized using zeolites to higher alkanes (410 °C, H-ZSM-5, 100% conversion) for use as fuel. In 2010, an 11 month production campaign produced 100 L of jet fuel and 100 L of gasoline at a yield of 5.5 kg liquid hydrocarbons per 100 kg of paper and chicken manure, with plans to scale up to 6000 L of jet fuel production.<sup>76</sup> More recently, a commercial plant is planned to be built in 2019.<sup>77</sup> The main limitation to the MixAlco process is that the carboxylic acids produced are a mixture of different acids, which is disadvantageous for targeted upgrading to specific chemicals.

**Synthetic consortium-based consolidated bioprocessing** More recently, a novel type of consolidated bioprocessing (CBP) has been developed, based on a synthetic consortia of microorganisms.<sup>78</sup> This is in contrast with the naturally occurring microor-

ganism cultures that the MixAlco process uses. By employing a synthetic consortium of different microorganisms (even from different kingdoms), different processes which do not naturally occur can be combined in a single reactor. The reaction conditions for each microorganism can be identified and spatially isolated within different parts of the reactor. To accomplish this, a membrane biofilm reactor was employed. An aerobic fungal biofilm was grown on an oxygen permeable membrane, while anaerobic bacteria are grown in the bulk of the reactor (Figure 1.7). All oxygen is consumed by the fungal biofilm, so the bulk of the reactor is anaerobic. This physical separation of the two different cross-kingdom microorganisms allow them to survive in the same reactor based on the decreasing oxygen concentration from the membrane. The fungus releases cellulolytic enzymes to hydrolyze lignocellulosic biomass, while the bacteria ferments the released sugars into carboxylic acids, with a targeted single carboxylic acid product possible by careful selection of the consortium (up to 85% yield of lactic acid from steam-pretreated beech wood after 200 h in a fed-batch reactor).<sup>79</sup> This process is chosen as the production route for the carboxylic acid feedstocks that will be discussed in Chapters 2 and 3, mainly because of the ability to target a single type of carboxylic acid rather than mixtures.

## **1.6 Carboxylic acids as platform molecules to fuels and chemicals**

The brief introduction presented above on current technologies in lignocellulosic biomass valorization highlights several key points. Past efforts on lignocellulosic biomass utilization have focused on fuels, with relatively small amount of research on chemicals production. Specifically, bioethanol and biodiesel production has been the main thrust for

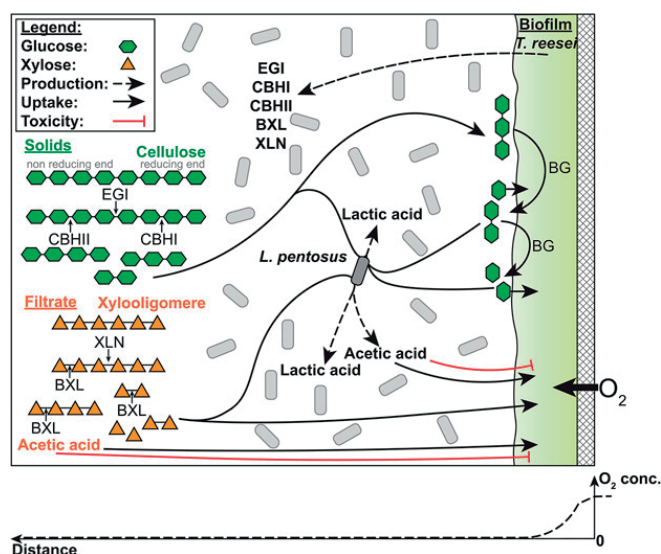


**Figure 1.7.** Consolidated bioprocessing of steam-pretreated beech wood to lactic acid in a membrane biofilm reactor by a cross-kingdom consortia of *T. reesei*/*L. pentosus*. The dissolved oxygen concentration in the reactor as a function of distance from the membrane is shown in the lower part of the figure. Reproduced from Shahab et al.<sup>79</sup> with permission from John Wiley and Sons.

scientific research. However, the rise of electric cars and electricity production via solar energy has somewhat reduced the need for these technologies, and refocused the majority of scientific research towards solar energy production. Nevertheless, liquid carbon-based fuels are still necessary in key transportation areas where switching to electric-based propulsion is not feasible. Notably, the air transportation sector still relies on liquid jet fuel as the main source of energy and, given the low energy density of current batteries, will likely not be able to substitute these fuels with electricity in the near to medium term. The physical and energy requirements of jet fuel can only currently be met by liquid carbon fuels. In addition, carbon-based chemicals still need a sustainable alternative.

Looking at current technologies, the furanic and sugar alcohol platforms present the highest variety of sustainable chemicals production. However, some key features are still missing. Most notably is the constraint of only being able to produce products of 6 or 5 carbon molecules absent additional chain lengthening reactions. This prevents production



of some key compounds. For example, the only olefin available via this platform is butene production from GVL decarboxylation. This limitation can also be seen in fuel production, where routes in C-C coupling towards high carbon numbers are needed. Only two methods so far have achieved this, namely butene oligomerization from GVL, and aldol condensation of furfural with acetone, which restricts our choice of starting feed. It is clear that more research in expanding the variety and carbon chain lengths of the fuels and chemicals produced is needed.

These limitations can be addressed by utilizing carboxylic acids as platform molecules for the production of fuels and chemicals. The carboxylate platform has not been as widely explored as the furanic and sugar alcohol platforms. Targeted production of specific carboxylic acids can allow different carbon chain lengths to be produced ( $C_1$  up to  $C_6$ ). Furthermore, the carboxyl functionality could introduce different methods for C-C coupling. Further research in upgrading carboxylic acids could complement the furanic and sugar alcohol platforms in expanding the portfolio of fuels and chemicals that can be produced from lignocellulosic biomass.

## 1.7 Current upgrading routes with carboxylic acids

The valorization of carboxylic acids has always been a challenge due to the stability of the carboxyl group. Additionally, aliphatic carboxylic acids, which are common in biomass feedstocks, lack any electron withdrawing groups (e.g. phenyl groups) or neighboring hydroxyl functionalities ( $\alpha$ -hydroxy acids). Aliphatic carboxylic acids are typically weak acids with low dissociation constants ( $pK_a$  of hexanoic acid = 4.85). Furthermore, dissociated carboxylate anions are resonance-stabilized, which also lowers their

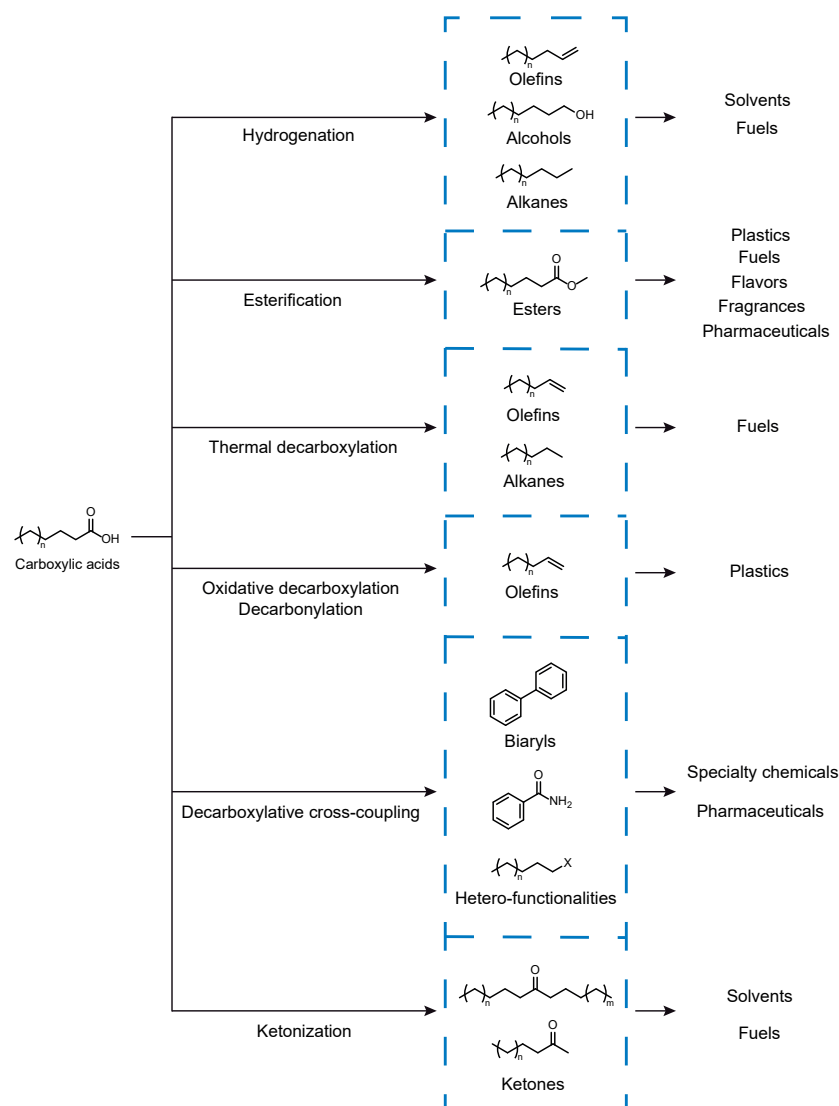


**Figure 1.8.** Common upgrading routes for carboxylic acids towards building block molecules (in the blue box) and subsequently their family of end products.

reactivity. The straight chain carbon backbone also limits any reactions to carbon-carbon bond scissions. Thus, the upgrading process, whether by deoxygenation, changing the functionality, or extending the carbon chain length, must start by targeting the carboxyl group. In this section, a brief overview of selected carboxylic acid upgrading routes will be discussed (Figure 1.8).

### 1.7.1 Addition/substitution reactions

#### Hydrogenation

The simplest and most straightforward way to upgrade carboxylic acids is to perform hydrogenation. This maintains the carbon chain length, which is especially important in the context of biomass conversion due to the importance of maximizing carbon conversion. Platinum supported on titania can be used to hydrogenate carboxylic acids to either alkanes or alcohols.<sup>80</sup> The selectivity can be tuned depending on reaction conditions as well as the addition of Re as a co-catalyst. Re as a catalyst itself supported on titania was also shown to selectively hydrogenate carboxylic acids to alcohols.<sup>81</sup> Cortright et al. has also investigated the hydrogenation of lactic acid to 1,2-propanediol using copper supported on silica.<sup>82</sup> Alcohols formed from carboxylic acid hydrogenation can be dehydrated to form olefins, as is the case with the MixAlco process,<sup>75</sup> which can be subsequently oligomerized to higher alkanes.

#### Esterification

Carboxylic acids can be condensed to esters in the presence of alcohols, which is extremely important in the flavors and fragrances industry. Esterification transforms the often foul-smelling carboxylic acids into esters which have pleasant and fruity smells, which are then used in flavoring foods and the production of perfumes. Additionally esterification is used extensively in the synthesis of pharmaceuticals and specialty chemicals. Soaps are produced from esters, or from the direct neutralization of carboxylic acids using a base. Typically, a homogeneous acid catalyst such as sulfuric acid is employed,

with an excess of alcohol.<sup>83</sup> It is also possible to use a homogeneous basic catalyst such as NaOH to catalyze esterification, but such conditions can also lead to soaps via saponification depending on the water content.<sup>84</sup> Other more unconventional routes involve the use of solid acid catalysts such as Amberlyst-15<sup>85</sup> or acid-functionalized carbon.<sup>86,87</sup>

A subset of esterification reactions of carboxylic acids is transesterification, whereby an ester is converted into another ester by changing the alcoholate group. Transesterification is extremely important as most carboxylic acids found in plant oils or waste cooking oil are in the form of triglycerides, a triester of glycerol and 3 long-chain carboxylic acids. Rather than hydrolyzing the triglycerides into free carboxylic acids and then functionalizing it, an alcoholysis of the ester takes place, which replaces the original alcohol with another alcohol.

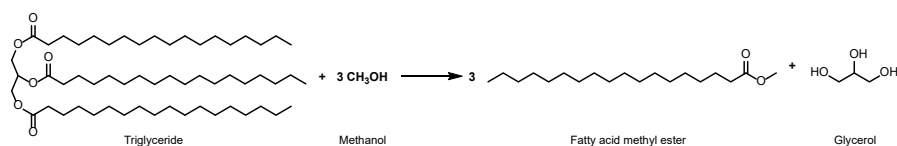


**Figure 1.9.** Transesterification of triglycerides to fatty acid methyl esters (FAME).

Transesterification has found application in the production of biodiesel. Triglycerides are transesterified to fatty acid methyl esters (FAME) using methanol, which are suitable to be used as biodiesel (Figure 1.9).<sup>88</sup> Similarly to esterification, both acid and base catalysts can be used, but in this case, the water content of the starting feed must be closely controlled in order to prevent saponification to soaps or hydrolysis to free carboxylic acids.<sup>89,90</sup>

Both esterification and transesterification are also employed industrially in the plastics industry for the production of polyesters. The most prominent example is in the production of polyethylene terephthalate (PET), where terephthalic acid or dimethyl

terephthalate is reacted with ethylene glycol in esterification or transesterification, respectively.<sup>91</sup> Similar approaches are used in the biomass-derived analog of PET, polyethylene furanoate (PEF), made from 2,5-furandicarboxylic acid.<sup>92,93</sup>

## 1.7.2 Decarboxylative reactions

### Thermal decarboxylation

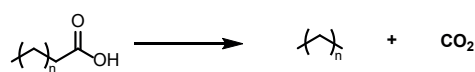


**Figure 1.10.** Thermal decarboxylation of carboxylic acids to alkanes.

Rather than using an external source of hydrogen to deoxygenate carboxylic acids, an alternate route can feature the decarboxylation of carboxylic acids (Figure 1.10). In this method, the carboxyl group is removed as carbon dioxide. Traditional thermal decarboxylation processes primarily result in alkanes as the end product. Commonly, palladium supported on carbon is used as the catalyst, with which both lauric acid<sup>94</sup> and stearic acid<sup>95</sup> have been shown to decarboxylate to form their corresponding alkanes with 1 less carbon. Thermal decarboxylation has also been applied to convert GVL to butenes via pentenoic acid decarboxylation, as mentioned above.<sup>64–66</sup> However, this is a rare case of olefin production from thermal decarboxylation, as it is only due to the fact that pentenoic acid has a double bond already present.

Decarboxylation does result in a loss of one carbon atom. In the context where thermal decarboxylation is typically used to transform long chain carboxylic acids to fuels, this might not be a major concern. But for short chain carboxylic acids that are derived from lignocellulosic biomass, this represents a big loss in carbon economy. Additionally, most

thermal decarboxylation routes result in alkanes, which are not that attractive as short chain alkanes have low energy densities due to their gaseous form.

## Oxidative decarboxylation

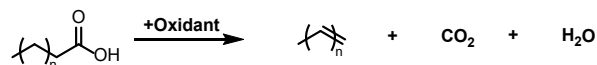


**Figure 1.11.** Oxidative decarboxylation of carboxylic acids to olefins.

A variant of decarboxylation, termed oxidative decarboxylation, has been developed to valorize carboxylic acids. In oxidative decarboxylation, an oxidant is employed to convert carboxylic acids to olefins, with the loss of one molecule of carbon dioxide and the production of one water molecule (Figure 1.11). Kochi and co-workers showed that using lead(IV) tetraacetate, manganese(III) acetate or ammonium peroxydisulfate as the oxidant with catalytic copper(II) acetate or silver yielded terminal olefins from primary aliphatic acids.<sup>96–99</sup> However, these reactions always required the use of stoichiometric oxidants or metals to function, which is unsustainable and expensive in the context of bulk chemical production.

It is possible to substitute these stoichiometric oxidants in favor of environmental friendly oxidants such as  $H_2O_2$  or  $O_2$  in enzymatic oxidative decarboxylation.<sup>100–103</sup> However, these systems use specifically engineered strains of bacteria and also require additional sacrificial reagents, thus negating the benefit of using environmental friendly oxidants.

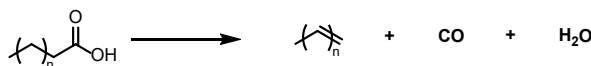


**Figure 1.12.** Decarbonylation of carboxylic acids to olefins.

## Decarbonylation

The carboxyl group of carboxylic acids can be removed as carbon monoxide and water, instead of carbon dioxide. This reaction, called decarbonylation, has been demonstrated to form olefins from carboxylic acids (Figure 1.12). Foglia and Barr studied the decarbonylation of stearic acid into a mixture of heptadecenes over rhodium trichloride and triphenylphosphine at 280 °C.<sup>104</sup> Using iridium or iron as a catalyst lowers the reaction temperature, but an equivalent amount of acid anhydride must be added to activate the carboxylic acid.<sup>105,106</sup> While resulting in primarily olefins and producing valuable carbon monoxide, decarbonylation seems to only work with additional activators, similarly to oxidative decarboxylation.

## Decarboxylative coupling reactions

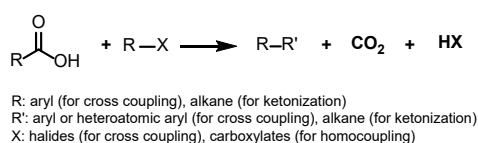


**Figure 1.13.** Decarboxylative coupling reactions.

During metal-catalyzed decarboxylations, if the protonolysis of the organometallic species can be avoided, there is the possibility of coupling other substrates to the reaction. This can be exploited to introduce C-C or C-heteroatom couplings to carboxylic acids (Figure 1.13), potentially increasing the carbon chain length for fuel applications or add new functionalities for chemicals production.

## Cross-coupling reactions

**Biaryl coupling** Gooßen et al. studied the decarboxylative coupling of aryl carboxylates with aryl halides using a system of homogeneous Cu/Pd metals.<sup>107</sup> Both stoichiometric and catalytic quantities of Cu were explored, with the synthesis working on 26 biaryls with different substituents at different positions. The same researchers further refined the Cu/Pd catalyst system, resulting in a procedure that was applicable to a wide range of aryl carboxylates and aryl halides.<sup>108–110</sup> Ag/Pd-based systems has also been studied, but they usually require stoichiometric amounts of Ag to function.<sup>111–114</sup> Rather than bimetallic systems, single metal complexes are preferable as catalysts due to their lower metal usage. Thus, protocols employing only Pd or Cu have been developed.<sup>115–120</sup>

**Other functionalities**  $\alpha$ -ketocarboxylic acids, meaning carboxylic acids having a keto group in the  $\alpha$  position, have been used as substrate to perform cross coupling with aryl halides to obtain aryl or biaryl ketones using the aforementioned Cu/Pd catalyst system.<sup>121</sup> Addition of amines to the reaction changes the selectivity, resulting in aryl azomethines instead.<sup>122</sup> Other functionalities explored with aromatic decarboxylative cross coupling include, oxalic acid monoesters, which have been shown to decarboxylatively cross couple with aryl halides to produce aromatic esters,<sup>123</sup> and the synthesis of azaarenes.<sup>124</sup> There have also been reports on C-heteroatom cross couplings with the production of aryl amides,<sup>125</sup> aryl sulfides<sup>126</sup> and aryl vinyl sulfides.<sup>127</sup>

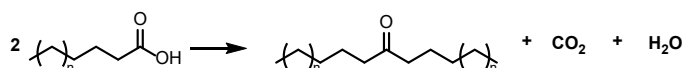


**Figure 1.14.** Ketonization of carboxylic acids to ketones. Homo-ketonization is shown here.



**Ketonization with subsequent aldol condensation** The methods discussed above only discuss cross-coupling of carboxylic acids to other functionalities. In addition, these studies have mainly focused on aromatic carboxylic acids in organic synthesis, with little to no investigation on other types of carboxylic acids, which makes it not that applicable to biomass upgrading as aromatic carboxylic acids are not common in the carboxylate platform. Ketonization seems to be the only route towards homocoupling of aliphatic carboxylic acids. In this context, ketonization refers to the conversion of 2 molecules of carboxylic acids to a ketone, with the loss of 1 molecule each of carbon dioxide and water (Figure 1.14). This allows for deoxygenation without need for external hydrogen, similar to decarboxylation/decarbonylation, while introducing C-C coupling to the reaction. Both homo and cross-ketonizations are possible,<sup>128,129</sup> resulting in symmetrical or asymmetrical ketones, respectively.

Ketonization is typically catalyzed by metal oxides at high temperatures ( $> 300\text{ }^{\circ}\text{C}$ ). Pham et al. provided insight into the reaction mechanisms, intermediates and catalysts in the ketonization of acetic acids.<sup>130</sup> They elucidated, based on previous studies by other groups,<sup>131–133</sup> that there are two different mechanisms for acetone formation from acetic acid. Using basic oxides with low lattice energies (such as MgO or CaO), acetic acid interacts strongly with the bulk of the oxides to form acetate salts, which then decompose at high temperatures to form acetone. This bulk ketonization method is reminiscent of the MixAlco process, where calcium carboxylate salts are decomposed to form ketones.<sup>75</sup> This method requires higher temperatures than surface ketonization, fundamentally alters the structure of the oxides, as well as only forming ketones despite the presence of external hydrogen. On the other hand, on oxides with high lattice energies such as  $\text{CeO}_2$  or  $\text{ZrO}_2$ , ketonization is confined to the surface of the oxides. In this case, the role and presence

of the  $\alpha$ -hydrogen on at least one of the carboxylic acids is crucial. The  $\alpha$ -hydrogen is first abstracted, and the resulting nucleophilic carbon can attack another carboxylic acid to form a ketone. Carboxylic acids with no  $\alpha$ -hydrogen are unable to undergo ketonization.<sup>128</sup> They further performed ketonization of acetic acid over Ru/TiO<sub>2</sub>/C at 180 °C, and showed high acetone yields in both aqueous and organic phase reactions.<sup>134</sup>

Gliński et al. tested the ketonization of acetic acid on 20 different metal oxides supported on silica, titania, and alumina at temperatures ranging from 300 to 450 °C.<sup>135</sup> They found that ceria and mangania exhibited the highest activity for the conversion of acetic acid to acetone. Furthermore, they tried carboxylic acids with longer carbon chain lengths and found similar performance. It would seem that amphoteric metal oxides such as CeO<sub>2</sub> or ZrO<sub>2</sub> are the most active catalysts for ketonization, which is corroborated by other studies.<sup>136,137</sup> This has been suggested to be due to the synergetic effect of adjacent Bronsted basic and Lewis acid sites, which coordinates the primary carboxylate and abstracts the  $\alpha$ -hydrogen, and stabilizes another carboxylic acid for the coupling reaction, respectively.<sup>130</sup> Mixed oxides such as CeO<sub>2</sub>-ZrO<sub>2</sub> also exhibit higher activity due to this effect, as they have higher amounts of coordinatively unsaturated cation sites (oxygen vacancies), which behave similarly to Lewis acid sites. Specifically, Gaertner et al. used CeO<sub>2</sub>-ZrO<sub>2</sub> to perform both homo and cross-ketonization on a variety of different carboxylic acids.<sup>129</sup>

While biomass-derived ketones such as acetone are valuable as solvents, there is still a possibility for further upgrading them. Crisci et al. used a zinc-zirconia mixed oxide to introduce two extra steps in the reaction, namely aldol condensation of 2 acetone molecules to form mesityl oxide, followed by C-C hydrolytic bond cleavage to isobutene, an important olefin.<sup>138</sup> They reported a 75% yield based on the theoretical maximum

for the direct production of isobutene from acetic acid. The same research group also investigated the hydrodeoxygenation of acetone using  $\text{MoO}_3$  to propylene.<sup>139</sup> It is also well known that acetone can be successively condensed to form higher aromatics and cyclohexenes over acid and base catalysts.<sup>140,141</sup> This concept can be applied to ketones other than acetone. Sacia et al. performed successive condensations on methyl ketones to form trimers, which they then separately hydrogenate to form cycloalkanes.<sup>142</sup>

## 1.8 Challenges in upgrading carboxylic acids

In the introduction, while reviewing lignocellulosic biomass valorization, I presented two different platforms on carbohydrate upgrading. While the furanic and sugar alcohol platforms have been thoroughly studied and more widely implemented, several drawbacks remain, notably the lack of upgrading routes towards other olefin varieties, as well as the limitation towards 6 or 5 carbon molecules (with only a few C-C coupling routes available). These issues can be potentially addressed by upgrading the carboxylate platform, which remains relatively unexplored by researchers mainly because biological routes have traditionally focused on ethanol production. However, upgrading carboxylic acids does come with some challenges. Based on current studies in carboxylic acid valorization, I have identified several important issues that need to be addressed.

Decarboxylative reactions, which are the bulk of carboxylic acid conversion routes, reduce the overall carbon efficiency of the reaction. For long chain carboxylic acids found in vegetable oil or waste cooking oil, the loss of one carbon during decarboxylation is not significant. However, for short chain carboxylic acids derived from fermentation, this is extremely important as it represents a big loss in carbon efficiency (75% for butanoic

acid).

There is also a lack of C-C coupling routes towards liquid transportation fuels. Most existing processes can only couple aryl carboxylates, with ketonization followed by aldol condensation as only route that has potential for aliphatic carboxylic acids. Currently, that requires multiple steps, thus not feasible economically, and has never been explored in one-pot systems.

Furthermore, especially in coupling routes, not enough research has been done on upgrading short chain aliphatic carboxylic acids. Most upgrading routes either utilize long chain carboxylic acids, or aromatic carboxylic acids, neither which are the most ubiquitous in biomass-derived streams. There is also lack of focus on real biomass-derived carboxylic acid upgrading, with most studies performed using model compounds or for organic synthesis purposes only. This lack of knowledge hinders the use of the carboxylate platform, as reactions carried out with model compounds frequently do not translate well into real biomass-derived feed.

Finally, there seems to be frequent usage of stoichiometric reagents or homogeneous catalytic systems in current upgrading processes, which seems to be the only way to convert carboxylic acids directly to olefins. Stoichiometric reagents are not feasible both in terms of economics or sustainability for the production of a bulk chemical such as olefins. This is also true for homogeneous catalysts, which can hamper downstream separations or scale up to continuous processes.

## 1.9 Objectives

In light of this, the overall goal of my thesis is to study the catalytic upgrading of biomass-derived carboxylic acids to fuels and chemicals. To address the issues highlighted above in Section 1.8, I have formulated 4 objectives for my thesis.

### 1.9.1 Objective 1: To study the direct conversion of carboxylic acids to olefins via tandem hydrogenation/dehydration

I plan to investigate an alternate route of carboxylic acid upgrading to olefins by performing both hydrogenation and dehydration in one process. In doing so, short chain olefins can be produced, which are valuable precursors for the petrochemical industry, especially if the carbon chain length is odd numbered. By avoiding decarboxylation and using hydrogenation, the carbon efficiency can be maximized, and there will be no use of expensive stoichiometric reagents/oxidants.

### 1.9.2 Objective 2: To investigate the conversion of carboxylic acids to liquid transportation fuels via ketonization/aldol condensation

I intend to design a process where ketonization of carboxylic acids and the subsequent aldol condensation of the resulting ketones occurs in the presence of a single catalytic system. By inducing cascade aldol condensation reactions, high carbon chain length liquid fuels can be obtained in a single reactor. In this case, the initial loss of one carbon

dioxide in the ketonization step would not be as problematic. Furthermore, this would enable the direct valorization of short chain carboxylic acids to liquid fuels, which usually requires multiples steps, thus driving down process costs.

### **1.9.3 Objective 3: To use real biomass-derived carboxylic acids**

Frequently, research in biomass upgrading focuses on model compounds and do not translate their work to real biomass-derived feedstock. I intend to avoid that. To that end, I am collaborating with the research group of Professor Michael Studer from the Bern University of Applied Sciences to obtain carboxylic acids produced from a novel consortium-based consolidated bioprocessing of beech wood.

### **1.9.4 Objective 4: To understand the fundamental surface reaction phenomena occurring during catalytic upgrading of carboxylic acids**

For industrial production of fuels and chemicals, heterogeneous catalysts are still the preferred catalyst. I will focus on heterogeneous catalysis, with an emphasis on oxide-supported metal nanoparticles. Additionally, I plan to thoroughly investigate the upgrading routes using techniques such as Fourier-transform infrared (FTIR) spectroscopy, temperature-programmed desorption/reduction (TPD/TPR), acid/basic site titration via chemisorption, and N<sub>2</sub> physisorption, in order to understand the fundamental surface reaction phenomena that occurs during carboxylic acid upgrading, with an emphasis on catalyst-substrate interactions. Throughout my investigations, I will consolidate chemical process engineering principles with fundamental surface chemistry phenomena.

## Chapter 2

# Selectivity control during the single-step conversion of aliphatic carboxylic acids to linear olefins

This chapter was published as a letter in *ACS Catalysis* as **Yeap, J. H.**; Héroguel, F.; Shahab, R. L.; Rozmysłowicz, B.; Studer, M. H.; Luterbacher, J. S. Selectivity Control during the Single-Step Conversion of Aliphatic Carboxylic Acids to Linear Olefins. *ACS Catal.* **2018**, 8, 10769–10773. DOI: 10.1021/acscatal.8b03370.<sup>143</sup> The full manuscript, minus the introduction and with minor formatting changes, is reproduced here with permission from the American Chemical Society. The supplementary information for this chapter can be found in Appendix A.

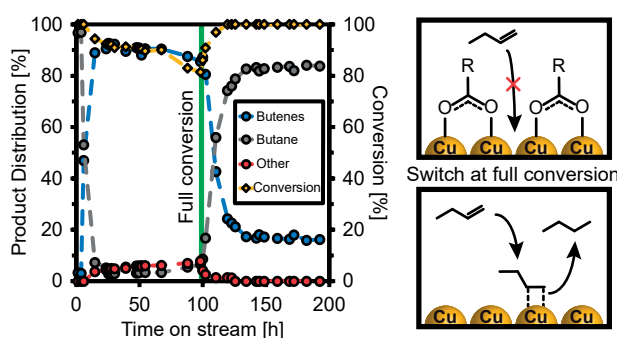
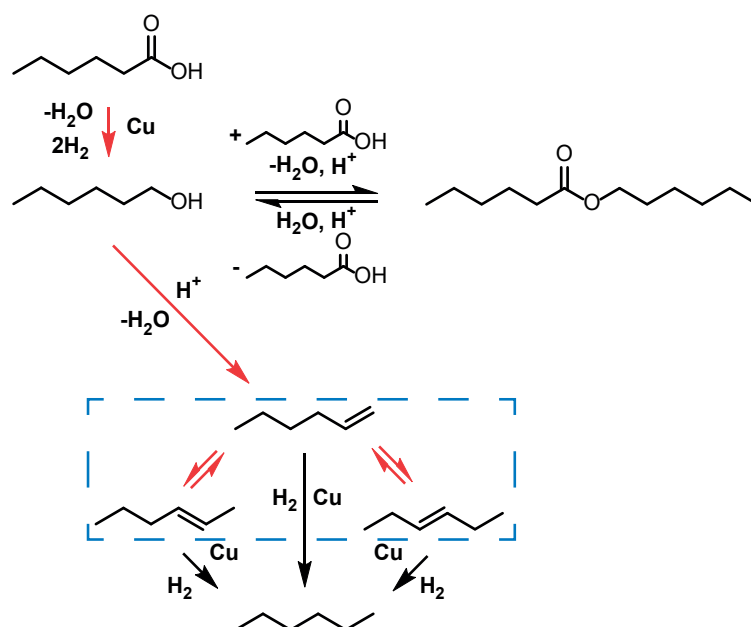


Figure 2.1. Graphical abstract

In this chapter, the aim was to devise an alternative process to convert dilute streams of carboxylic acids to olefins in one step using tandem hydrogenation/dehydration. By first hydrogenating the carboxylic acids to alcohols, followed by subsequent dehydration to olefins in the same reactor, we can avoid expensive sacrificial reagents as well as preserve

the carbon chain length of the substrate. In our investigation of using hexanoic acid and butanoic acid as substrates, we discovered a sudden switch in olefin/alkane selectivity once carboxylic acids were fully consumed. Using several catalyst surface studies, we were able to determine the nature of this selectivity switch (Figure 2.1). Finally, we demonstrate the application of this process to butanoic acid that was directly produced from pretreated beech wood in a consolidated bioprocess.

## 2.1 Results and discussion



**Figure 2.2.** Proposed reaction pathway for the tandem hydrogenation/dehydration of hexanoic acid. The main pathways are highlighted in red. The main products are enclosed in the blue dashed box

Performing tandem hydrogenation/dehydration reactions on carboxylic acids in one process required a bifunctional catalyst that had both hydrogenation and alcohol dehydration properties. We selected Cu supported on commercial silica-alumina (Cu/Si-Al), with the rationale that Cu could act as a mild hydrogenation catalyst and the acid sites on silica-alumina could perform dehydration reactions. Partial hydrogenation of hexanoic



acid resulted in 1-hexanol, which could partially esterify with unreacted hexanoic acid to form hexyl hexanoate (Figure 2.2). This is an undesired side reaction that occurs mainly on Brønsted acid sites, but it is reversible.<sup>144</sup> As an intermediate, 1-hexanol then underwent dehydration to form hexenes. As a primary alcohol, the reaction likely occurred through the E2 mechanism (single step elimination with no carbocationic intermediate), resulting in 1-hexene. However, at high temperatures and acidic conditions, double bond migration was favorable, resulting in formation of internal hexenes. Finally, undesired overhydrogenation of the hexenes to hexane also occurred, and, as discussed below, was highly dependent on reaction conditions.

We carried out the tandem hydrogenation/dehydration of hexanoic acid in an upflow fixed-bed reactor at 210 °C and 5 bar H<sub>2</sub>, using Cu/Si-Al with a copper loading of 6 wt % and a metal dispersion of 5%. At first, hexane was the major product indicating almost complete overhydrogenation of olefins (Figure 2.3A), likely due to an abundance of hydrogen present on the fresh catalyst bed. After this initial induction period, the reaction stabilized and selectivity to hexenes increased significantly until they were the major product. At a weight hourly space velocity (WHSV) of 0.99 h<sup>-1</sup>, we obtained 96.7% conversion and a molar product distribution of 92.0% hexenes and 7.3% hexane at steady state. The hexenes consisted of predominantly 2-hexene and 3-hexene (95 mol % of total olefins), indicating a high degree of double bond migration after the dehydration step. Skeletal rearrangement was not significant (3 mol % of total olefins). There was a slight overhydrogenation of the olefins to hexane under those reaction conditions, along with a small production of hexyl hexanoate. The conversion and product distribution were constant over 80 h on stream (0.8 g hexenes produced/g catalyst over 80 h in this experiment), attesting good catalyst stability. When using a higher concentration

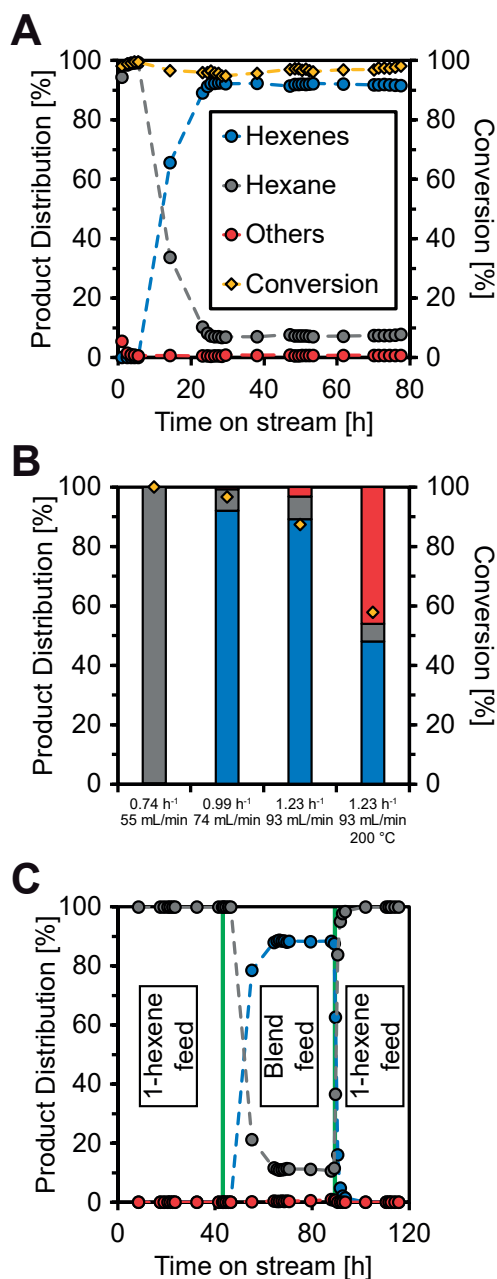


**Figure 2.3.** A) Conversion and molar product distribution of hexanoic acid tandem hydrogenation/dehydration as a function of time on stream (WHSV = 0.99 h<sup>-1</sup>, H<sub>2</sub> flow = 74 mL/min, *T* = 210 °C, *P* = 5 bar and feed = 2 wt % hexanoic acid in isooctane). B) Average steady state conversion and molar product distribution of hexanoic acid tandem hydrogenation/dehydration at different WHSV (*T* = 210 °C, *P* = 5 bar and feed = 2 wt % hexanoic acid in isooctane). C) Molar product distribution of an intermediate products study as function of time on stream (WHSV = 0.99 h<sup>-1</sup>, H<sub>2</sub> flow = 74 mL/min, *T* = 210 °C, *P* = 5 bar and initial feed = 2 wt % 1-hexene in isooctane). Green lines represent a feed switch to either 2 wt % 1-hexene/2 wt % hexanoic acid in isooctane or 2 wt % 1-hexene in isooctane. The legend for Figure 2.3B,C can be found in Figure 2.3A. The WHSV is calculated based on the total liquid feed.

(10 wt %) of hexanoic acid as feed (and adjusting the flow rate and WHSV to yield a similar ratio of incoming hexanoic acid to catalyst weight), a comparable performance to the 2 wt % feed was achieved, demonstrating that a high dilution was not necessary to obtain these results (Figure A.1, Appendix A).

Increasing the WHSV to  $1.23\text{ h}^{-1}$  lowered the conversion to 87.5% (Figure 2.3B). At these conditions, we also detected a higher amount of hexyl hexanoate in the product stream, showing that esterification was a competing side reaction when significant amounts of hexanoic acid were present. In the previous case of 96.7% conversion, the amount of unreacted hexanoic acid was low enough that most of the 1-hexanol formed proceeded to dehydrate to hexenes. We lowered the temperature of the reaction to  $200\text{ }^{\circ}\text{C}$ , thereby further lowering the conversion to 57.8%. At this conversion, large quantities of hexyl hexanoate were formed. The proportion of hexane formed was similar compared to previous conditions, implying that the slight overhydrogenation of olefins was independent of the conversion and WHSV.

Interestingly, we observed a brusque selectivity switch to 99.8% hexane at full conversion, after a decrease in WHSV from  $0.99\text{ h}^{-1}$  to  $0.74\text{ h}^{-1}$  (while maintaining the hydrogen flow to feed flow ratio constant). This contrasted with other reaction conditions where the proportion of overhydrogenation was constant.

We hypothesize that the presence of a small amount of hexanoic acid on the catalyst surface inhibited overhydrogenation of the hexenes to hexane. To ascertain the nature of this selectivity switch, we performed a study of intermediate products at  $\text{WHSV} = 0.99\text{ h}^{-1}$  (Figure 2.3C). By initially flowing only 1-hexene over the catalyst bed, complete overhydrogenation was observed. Changing the feed to a blend of hexanoic acid and

1-hexene switched the selectivity to a similar product distribution as the original hexanoic acid feed (88.3% hexenes and 11.2% hexanes) at those conditions. As the reaction temperature and pressure were constant, this switch could not have happened because of changes in vapor pressure or an unexpected phase change. We rationalized that this phenomenon occurred as a result of the interaction of the reaction species on the surface of the catalyst in the presence/absence of hexanoic acid.

The initial induction period of the reaction (shown for a WHSV of  $0.99\text{ h}^{-1}$  in Figure 2.3A) was also used to probe this phenomenon. When conducting the experiment under Ar flow for the first 24 h (instead of  $\text{H}_2$ ) and subsequently switching to  $\text{H}_2$  flow, a high selectivity of hexenes was achieved immediately (Figure A.2A, Appendix A). However, this resulted in some deactivation of the catalyst. When performing a similar experiment using an Ar flow for 1 h (Figure A.2B, Appendix A), the deactivation was not as significant (83.4% vs 96.7% conversion), and a shorter induction period was observed compared to constant  $\text{H}_2$  flow (7 h vs 24 h). These results showed that  $\text{H}_2$  was important in maintaining catalyst stability and confirmed that the initial induction period with high alkane selectivity was due to an abundance of hydrogen present on the surface of a fresh catalyst bed. Furthermore, preadsorbing the catalyst with hexanoic acid mitigated the initial overhydrogenation of the hexenes to hexane, albeit with severe catalyst deactivation under an Ar atmosphere, further confirming the important effect of adsorbed carboxylic acids on product selectivity.

To further explore the interaction of the reacting species with the catalyst surface, a temperature-programmed desorption (TPD) of 1-hexene on the catalyst surface was performed to determine its adsorbed quantity on the catalyst (Figure 2.4A).

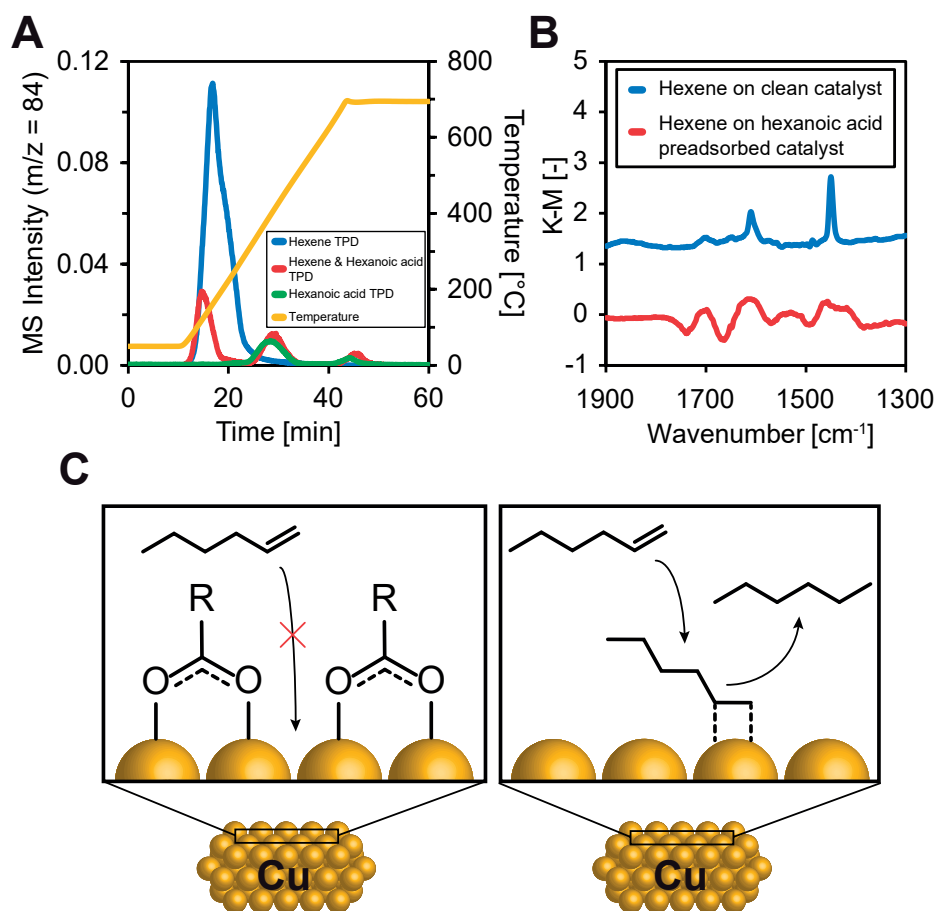


**Figure 2.4.** A) Temperature-programmed desorption (TPD) of different reaction species on the catalyst while using the MS to track mass 84 (molecular ion peak of 1-hexene). B) Subtracted FTIR spectra of different molecules adsorbed on the surface of the catalyst at 25 °C. For both spectra, the displayed spectrum is the difference between the spectra obtained before and after 1-hexene adsorption (and after hexanoic acid preadsorption for the preadsorbed catalyst). K-M stands for Kubelka-Munk. Figure A.3, Appendix A shows the subtracted FTIR spectra of 1-hexene adsorbed on the surface of KBr at 25 °C, which had no signal. C) Illustration depicting the accessibility of hydrogenation sites in the presence/absence of adsorbed hexanoic acid. The adsorption mode of carboxylic acids on copper is still debated in the literature,<sup>145–147</sup> but one mode of adsorption is shown here for illustrative purposes.

On a clean catalyst surface, we observed 234  $\mu\text{mol/g}$  of 1-hexene adsorbed on the surface of the catalyst. In contrast, by preadsorbing hexanoic acid on the catalyst (which, we estimate led to roughly the same amount of acid adsorbed as 1-hexene - measured as 285  $\mu\text{mol/g}$  with acetic acid, see Appendix A.5), the amount of 1-hexene adsorbed decreased to 10  $\mu\text{mol/g}$ . TPD of just hexanoic acid confirmed the attribution of the 2 desorption peaks at  $\sim 400$  °C and  $\sim 700$  °C to the desorption and degradation of hexanoic

acid itself (the fragmentation pattern of hexanoic acid contains mass 84), and not to more strongly adsorbed 1-hexene in the presence of hexanoic acid. These findings suggest that the presence of hexanoic acid severely limits the adsorption of 1-hexene, thus decreasing overhydrogenation.

We further confirmed this hypothesis by Fourier-transform infrared (FTIR) spectroscopy. 1-Hexene adsorbed on a clean catalyst exhibited two adsorption bands at 1608 and 1449  $\text{cm}^{-1}$ , attributed to the C=C stretching mode and the =CH<sub>2</sub> scissoring mode, respectively (Figure 2.4B). The slight red-shift of the C=C band is attributed to C=C bond weakening upon adsorption on the catalyst.<sup>148</sup> Conversely, the characteristic bands of 1-hexene were not observed upon 1-hexene adsorption after preadsorption of hexanoic acid on the catalyst. The absence of 1-hexene signals further indicated that hexanoic acid prevented 1-hexene from bonding and being overhydrogenated to hexane by occupying the hydrogenation sites of the catalyst (Figure 2.4C).

This phenomenon can be extended to other carboxylic acids. We performed tandem hydrogenation/dehydration on butanoic acid and obtained an average steady-state molar product distribution of 90.9% butenes, 3.7% butane, and 5.4% others at a conversion of 90.9% (Figure 2.5A). The increased amount of esters can be due to the lower conversion of 90.9% compared with the 96.7% obtained with our previous experiments using hexanoic acid. Nonetheless, by pushing the conversion to completion, we observed a similar selectivity switch, although there was a higher proportion of butenes (17.0%) to butane (83.0%) compared with hexanoic acid (99.8% hexane). The feed flow rate had to be reduced for butanoic acid, as there was a higher molar concentration in the feed due to the lower molar mass of butanoic acid compared with hexanoic acid.

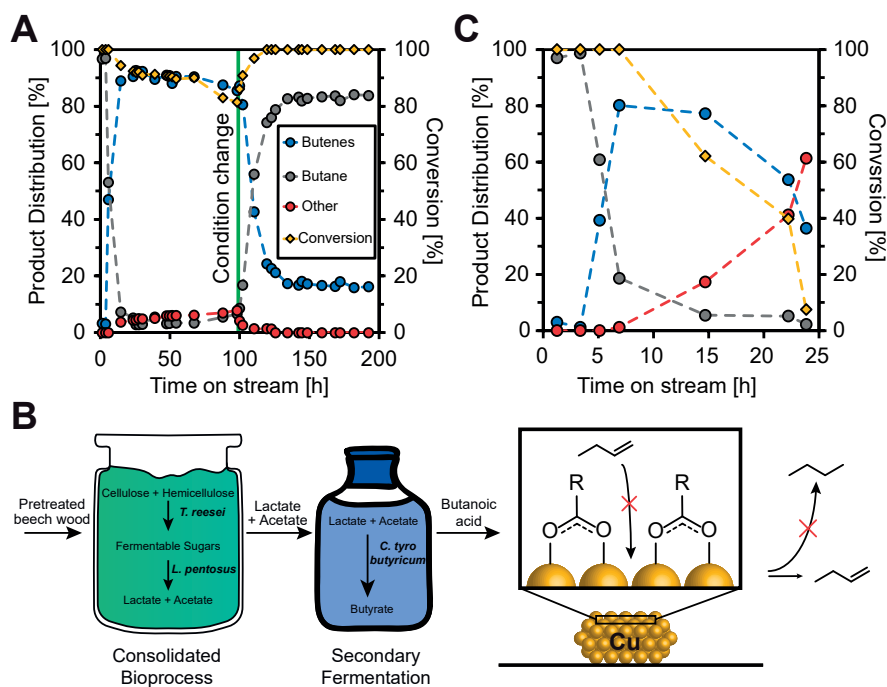


**Figure 2.5.** A) Conversion and molar product distribution of butanoic acid tandem hydrogenation/dehydration as a function of time on stream (WHSV = 0.49 h<sup>-1</sup>, H<sub>2</sub> flow = 38 mL/min, T = 210 °C, P = 5 bar, and feed = 2 wt % butanoic acid in isooctane). The green line represents a condition change to WHSV = 0.25 h<sup>-1</sup> and H<sub>2</sub> flow = 19 mL/min. B) Illustration of the consolidated bioprocessing of steam-exploded beech wood to butanoic acid, followed by tandem hydrogenation/dehydration to form butenes. The adsorption mode of carboxylic acids on copper is still debated in the literature,<sup>145–147</sup> but one mode of adsorption is shown here for illustrative purposes. C) Conversion and molar product distribution of biomass-derived butanoic acid tandem hydrogenation/dehydration as a function of time on stream (WHSV = 0.49 h<sup>-1</sup>, H<sub>2</sub> flow = 38 mL/min, T = 210 °C, P = 5 bar and feed = 2 wt % biomass-derived butanoic acid in isooctane). The legend for Figure 2.5C can be found in Figure 2.5A. The WHSV is calculated on the basis of the total liquid feed.

In order to demonstrate this concept for real biomass-derived products, we used our process on butanoic acid produced with a novel consolidated bioprocessing method that produced the carboxylic acid directly from steam-exploded beech wood (Figure 2.5B). Tandem hydrogenation/dehydration of biomass-derived butanoic acid initially proceeded similarly to commercial butanoic acid feed, with a peak molar product distribution of 80% butenes (Figure 2.5C). However, the catalyst suffered from significant deactivation after 8 h on stream. It is likely that the extraction process resulted in slight impurities (as we added sulfuric acid during extraction, some thiol compounds could form) that adsorbed

on the catalyst surface (separate phenomenon from the selectivity switch, as this is likely irreversible), as the reaction proceeded smoothly with the commercial butanoic acid feed. Nevertheless, this shows that the use of biomass-derived carboxylic acids was possible, although optimization of the extraction process is still required.

## 2.2 Conclusion

In summary, we demonstrate that biomass-derived streams of carboxylic acids (produced from beech wood) can be converted into mixtures of olefins in a single step. Using Cu/SiO<sub>2</sub>-Al<sub>2</sub>O<sub>3</sub>, > 90% olefin selectivity was achieved at close to 99% conversion. At full conversion, an abrupt selectivity switch occurred, changing the product distribution from predominantly olefins to almost exclusively alkanes. Through TPD and FTIR catalyst surface studies, we proposed that the observed selectivity switch occurred because of the presence of a small amount of carboxylic acids on the catalyst surface, which prevented binding and subsequent overhydrogenation of the olefins. We propose that the inhibition of catalyst active sites using carboxylic acids could also be applied to hydrogenation reactions using other substrates, where selective preservation of double bond functionalities is required. By doing so, we could possibly influence the product distributions of other types of catalytic reactions by controlling the presence of carboxylic acids in the reaction media. Differences in catalyst performance when processing commercial compounds versus real biomass-derived feed in biomass upgrading reactions could also be explained; especially given the ubiquity of carboxylic acid impurities in biomass-derived mixtures, which could exhibit the same selectivity switch behavior. An improved understanding of the influence of these functionalities on catalytic reactions will be important in developing



future biorefining processes. Therefore, this phenomenon can both help better understand the catalytic processing of biomass and open new avenues for selectivity control during catalytic reactions.



## Chapter 3

# Catalytic valorization of the acetate fraction of biomass to aromatics and its integration into the carboxylate platform

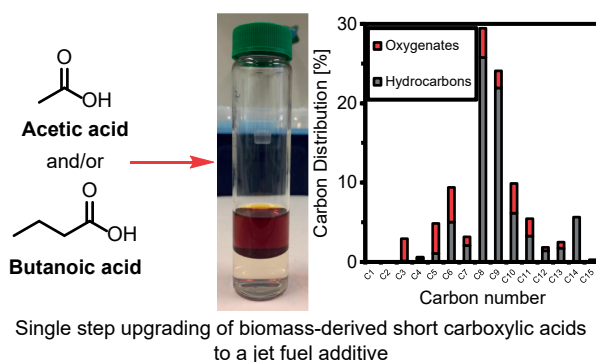


Figure 3.1. Graphical abstract

In this chapter, the aim was to upgrade an aqueous solution of acetic acid that is easily produced during biomass pretreatment through tandem ketonization and cascade aldol condensation. The direct conversion of acetic acid to deoxygenated molecules has been a significant challenge especially in the presence of water. We also propose an alternate valorization path for acetic acid in the presence of longer chain carboxylic acids. Our strategy was to use acetic acid as a reactant for cross-ketonization with longer chain carboxylic acids to create a new route to beta-ketones, which then condensed similarly to acetone. To do so, we used steam-exploded biomass (from which acetic acid was extracted) as the substrate in a novel consolidated bioprocessing approach for the direct production of butyric acid from pretreated biomass. From our process, we demonstrated that an organic oil with compositions suitable as an additive for aviation fuel can be

produced (Figure 3.1). The supplementary information for this chapter can be found in Appendix B.

## 3.1 Results and discussion

### 3.1.1 Proposed reaction pathway

In the process of upgrading short-chain carboxylic acids to potential liquid aviation fuel additives, the carbon chain length must be increased and a significant amount of oxygen removed. Ideally, chain elongation and deoxygenation should occur in a single step. Direct hydrogenation of the carboxylic acids would only result in short gas hydrocarbons. Therefore, we explored conditions that lead to the initial ketonization of the carboxylic acids, and that were conducive to subsequent aldol condensation reactions.

We chose Cu supported on  $\text{ZrO}_2$  as the catalyst for carboxylic acid upgrading. As mentioned above,  $\text{ZrO}_2$  was previously reported to catalyze the ketonization of carboxylic acids.<sup>130</sup> Separately, it has also been used to perform aldol condensation.<sup>138</sup> The combination of these two reactions could deoxygenate the substrate while increasing the carbon chain length in one step. The addition of Cu served to hydrogenate the high carbon compounds to deoxygenated hydrocarbons and maintain the catalyst's activity by promoting the formation of oxygen vacancies on  $\text{ZrO}_2$ . Without Cu, oxygenated compounds adsorbed on the active sites of the catalyst (as it was not hydrogenated) and eventually deactivated it, as we have observed with our initial experiments using only  $\text{ZrO}_2$  (Figure B.1, Appendix B). The usage of Cu, which is a relatively mild hydrogenation catalyst, also served to minimize the premature hydrogenation of carboxylic acids. Below, we

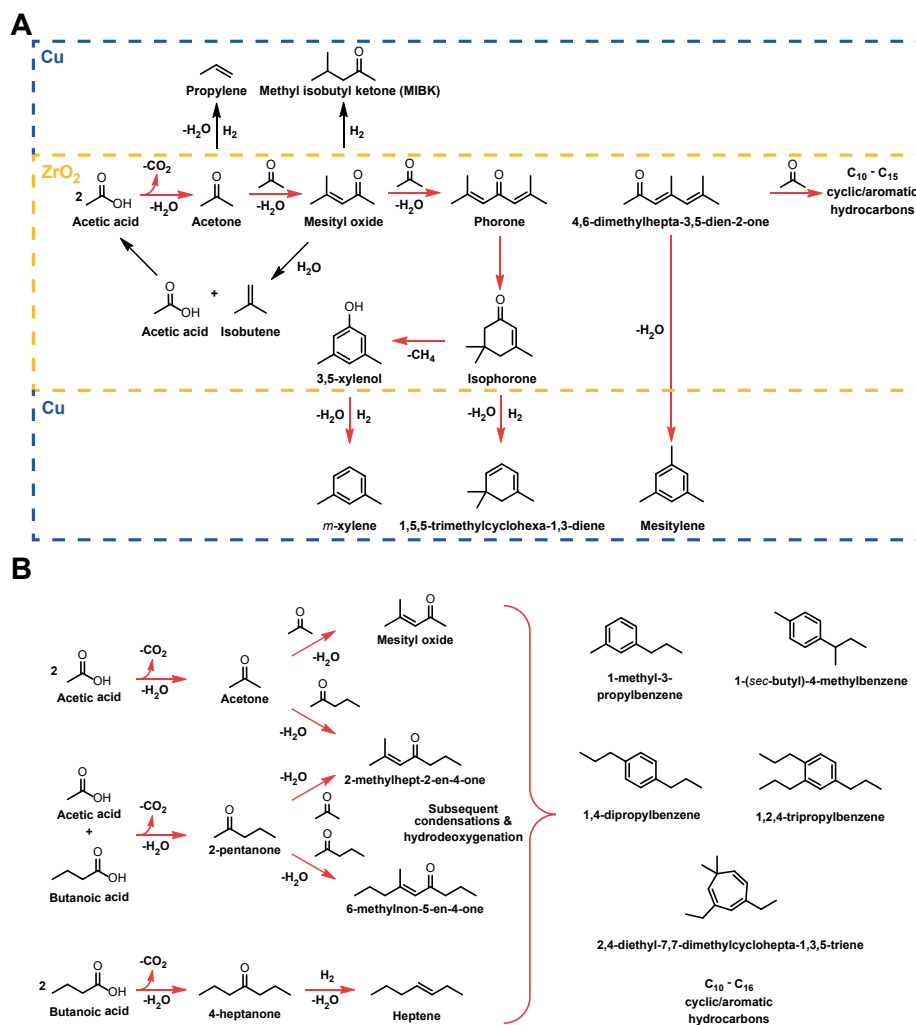


**Figure 3.2.** Proposed and simplified reaction pathway for the ketonization of carboxylic acids and subsequent cascade aldol condensation reactions to form aromatic hydrocarbons with high carbon numbers. A) Starting with pure acetic acid and performing direct ketonization. Catalytic sites are highlighted in blue and yellow. The main pathway is highlighted in red. B) Starting with a mixture of acetic and butanoic acid and performing primarily cross-ketonization. The catalytic sites are not highlighted for simplicity.

discuss the potential reaction pathways that occur on this catalyst for solutions of both pure acetic acid or mixtures of butanoic and acetic acid.

### Reaction pathway of pure acetic acid over Cu/ZrO<sub>2</sub>

Two acetic acid molecules can ketonize to form acetone (Figure 3.2A), losing 1 molecule of carbon dioxide in the process and reducing the O/C ratio from 1 to 0.33.

As the primary intermediate, acetone can react further in 2 different pathways. Hydrogenation of acetone produces isopropanol, which dehydrates over the metal oxide to form propylene. A more desirable pathway is the subsequent aldol condensation of 2 acetone molecules to form mesityl oxide. This step lengthens the carbon chain length to 6 carbons. Further cascade aldol condensations produce products with higher carbon numbers ( $C_9$  to  $C_{15}$ ). Once the carbon backbone exceeds 6 carbons, intramolecular condensations/ring-closing reactions begin to play a significant role forming aromatics and cycloalkenes. For instance, phorone ( $C_9$ ) can undergo ring-closing and hydrogenation to form isophorone or mesitylene. Importantly, although Cu is a mild hydrogenation catalyst, some hydrogenation could still occur at all steps. A small proportion of acetic acid may be hydrogenated before ketonization and subsequently add to the aldol condensation products, forming a plethora of compounds with carbon numbers that are not a multiple of 3. Cracking reactions could also occur, such as mesityl oxide forming acetic acid and isobutylene. As will be discussed below, through this reaction pathway, the products separated into a triphasic mixture of (i) organic oil formed by a mixture of largely deoxygenated molecules with carbon numbers  $C_8$  to  $C_{15}$ , (ii) an aqueous phase with water formed by deoxygenation reactions or any water in the feed, and unreacted oxygenates (molecules with at least 1 oxygen atom), and (iii) gas products consisting of  $CO_2$  and some short chain hydrocarbons.

### **Reaction pathway of acetic & butanoic acid over Cu/ZrO<sub>2</sub>**

Rather than ketonizing acetic acid with itself, upgrading a mixture of acetic acid and butanoic acid introduces possible cross-ketonization reactions into the reaction pathway (Figure 3.2B). Given that mixtures of acetic and longer chain carboxylic acids are com-

monly produced during the carboxylate platform, such a mixture and reaction scheme could be leveraged to increase the average carbon number of the resulting organic oil. Cross-ketonization proceeds in a similar fashion to direct ketonization, forming  $\beta$ -ketones that can then undergo cascade aldol condensation reactions. Acetone, 2-pentanone and 4-heptanone are potential intermediates, any combination of which can undergo aldol condensation. Similarly, this mechanism also led to a three phase mixture of products, with an organic oil phase containing aromatics and cycloalkenes of higher average carbon number due to the longer chain starting reactants compared to only acetic acid.

### 3.1.2 Upgrading of pure acetic acid

We first carried out the upgrading of pure acetic acid as a model feed over 2 g of 2 wt % Cu/ZrO<sub>2</sub> at a weight hourly space velocity (WHSV) of 0.3 h<sup>-1</sup>. As mentioned, the process resulted in a liquid product stream that spontaneously separated into an organic oil phase and an aqueous phase, in addition to a gas stream. Analysis of the molar carbon distribution of all 3 phases (Figure 3.3A) systematically showed complete conversion of acetic acid. The majority of carbons in the liquid phases were present in the form of C<sub>8</sub> and C<sub>9</sub> hydrocarbons. These hydrocarbons primarily consisted of both aromatics (xylenes and mesitylene) and cycloalkenes (dimethyl and trimethyl cyclohexenes). Acetone, the main intermediate in the upgrading route, represented 7.1 mol % carbon of the product stream. Since acetic acid was completely converted but acetone remained, we concluded that the cascade aldol condensation/hydrogenation reactions were rate limiting. In addition, other oxygenates, including ketones and phenols were present in both organic and aqueous phases. Methyl isobutyl ketone (MIBK) was detected, rather than mesityl oxide. The low proportion of MIBK, coupled with no observed mesityl oxide

indicated that aldol condensation of products longer than acetone had a higher rate at these reaction conditions compared to hydrogenation.

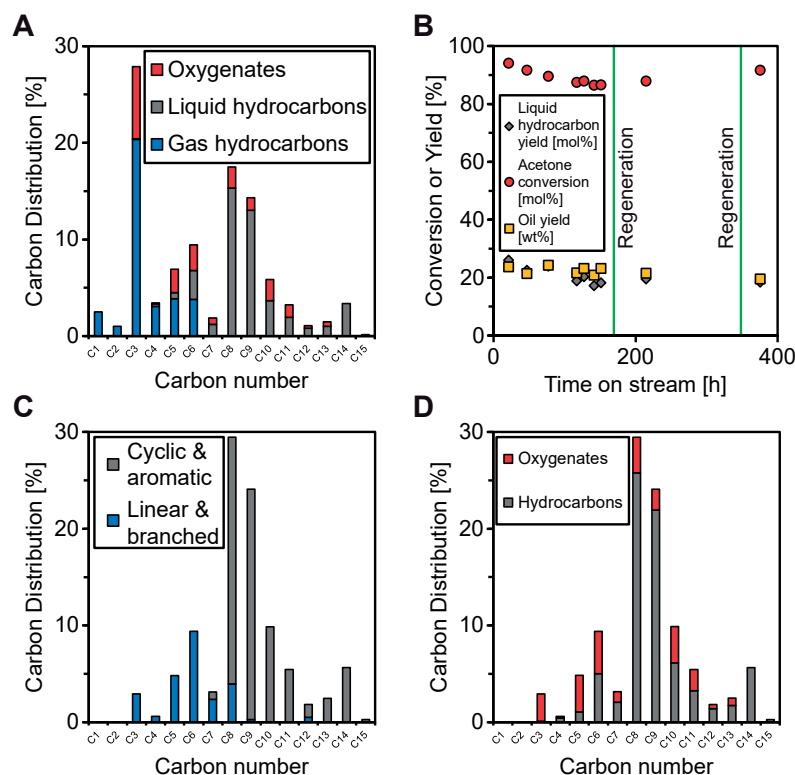


**Figure 3.3.** Upgrading of pure acetic acid over 2 g 2 wt % Cu/ZrO<sub>2</sub>. A) Molar carbon distribution of the product stream. ( $T = 400\text{ }^{\circ}\text{C}$ ,  $P = 10\text{ bar H}_2$ ,  $\text{WHSV} = 0.3\text{ h}^{-1}$ ,  $\text{H}_2\text{ flow} = 20\text{ mL/min}$ , conversion of acetone = 94.2 %, time on stream = 21.3 h) Oxygenates consisted of oxygenated molecules in organic, aqueous and gas phases. B) Acetone conversion, organic oil yield and liquid hydrocarbon yield as a function of time. Regeneration of the catalyst carried out at time on stream = 167.6 h and 352.4 h. C) Molar carbon distribution of linear versus cyclic and aromatic compounds in the organic oil phase. (time on stream = 21.3 h) D) Molar carbon distribution of oxygenates versus hydrocarbons in the organic oil phase. (time on stream = 21.3 h).

Over 20 mol % of carbon was converted to C<sub>3</sub> gaseous hydrocarbons, which was likely due to acetone hydrogenation by Cu at these conditions. The ratio of propylene to propane was  $\sim 20$ . Our usage of Cu mitigates catalyst deactivation, therefore the production of propylene is unavoidable. However, propylene is a valuable  $\alpha$ -olefin, making it an attractive side reaction. Moreover, the majority of gas hydrocarbons are olefins, with propylene being the majority ( $> 50\text{ mol \%}$  carbon of total gas).



Interestingly, despite the presence of Cu as a hydrogenation catalyst, the proportion of alkanes and cycloalkanes within the organic oil remained low (1.6 mol % carbon). The prevalence of double bond functionalities can also be observed in the gas phase, with propylene being the major product rather than propane. As reducible oxides such as ZrO<sub>2</sub> have high affinity towards bonding oxygenate functionalities, and since the interface between Cu and ZrO<sub>2</sub> is known to be active for hydrogenation,<sup>149</sup> we hypothesized that most hydrogenation sites were occupied by oxygenates, leading to limited double bond hydrogenation. Similar behavior was also observed in our previous study on carboxylic acid upgrading to olefins (in this case, even though acetic acid was completely converted, acetone and other oxygenates remain, which acts similarly).<sup>143</sup>

Within the carbon distribution of the product stream, 59.6 mol % were C<sub>6</sub> hydrocarbons or longer, 20.3 mol % were propylene likely produced through acetone hydrogenation, and 7.1 mol % was unreacted acetone, indicating that the main intermediate was likely acetone and subsequently mesityl oxide. Given the preponderance of aromatic molecules (Figure B.2 and Table B.1, Appendix B), ketonization/cascade aldol condensations was the primary route in the upgrading of acetic acid. However, the presence of molecules with carbon numbers that are not multiples of 3 suggests that there are other side reactions happening in addition to these simple cascade reactions. Notably, acetic acid could react in other routes (hydrogenation to acetaldehyde followed by condensation reactions with molecules of a higher carbon number) and higher hydrocarbons could also crack at high temperatures. These reactions are not necessarily detrimental, as long as the subsequent products have increased carbon chain length. Overall, a mass yield of 23.7 wt % organic oil was obtained at these conditions.

The organic oil mass yield over a course of 150 h time on stream was fairly constant

(Figure 3.3B), with minor fluctuations probably due to error when handling smaller sample sizes. Because acetic acid was completely converted, we tracked the conversion of the main intermediate, acetone, to characterize the stability of the catalyst. Over 150 h time on stream, the conversion of acetone dropped from 94.2 mol % to 86.7 mol %. However, the combined liquid hydrocarbon and oxygenates yield in the organic oil phase only decreased from 34.8 mol % to 30.8 mol %. The rest of the reduced conversion in acetone was reflected in a loss of propylene yield from 11.9 mol % to 7.4 mol %. Within the organic oil, the yield of liquid hydrocarbons decreased from 26.1 mol % to 18.2 mol %. This indicated that, not only did acetone conversion and organic oil yield slightly decrease because of poisoning on the aldol condensation sites, but the liquid hydrocarbon and propylene yield also slightly decreased due to deactivation of the hydrogenation sites of the catalyst.

Regeneration of the catalyst restored some of the liquid hydrocarbon yield and acetone conversion, with a second regeneration performing similarly. The recovery of activity indicated that the deactivation in the first run was mostly reversible, with some irreversible deactivation likely due to initial sintering, followed by reversible coking on the aldol condensation and hydrogenation sites.

The carbon distribution of the organic oil phase showed that most compounds are molecules with a carbon number of 8 or higher (79.1 mol % carbon) (Figure 3.3C). Even though it has 6 carbons, mesityl oxide only has a 5 carbon linear backbone, rendering it unlikely undergo intramolecular self-cyclization. This points to the proposed aldol condensation reaction pathway, as the majority of C<sub>6</sub> compounds detected (MIBK) are linear/branched rather than cyclic/aromatic. Overall, 75.1 mol % of the carbon in the organic oil was present as cyclic or aromatic compounds, demonstrating that cyclization

was highly favored.

An analysis of the oxygen content within the organic oil showed that the oil consisted of mostly liquid hydrocarbons (74.9 mol % carbon) rather than oxygenates (Figure 3.3D). More importantly, the O/C ratio in the oil was decreased to 0.04, compared to 1 for acetic acid and 0.33 for acetone. This 96% removal of oxygen from acetic acid indicates that our upgrading strategy is viable for producing deoxygenated oil with high carbon numbers. Using the mass fractions of C, H and O within the identified compounds of the oil to estimate the higher heating value (HHV),<sup>150</sup> we calculated that the organic oil produced from our process has a HHV of 42.5 MJ/kg. As ASTM D1655 specifications for aviation fuel stipulates a minimum net heat of combustion of 42.8 MJ/kg,<sup>151</sup> our organic oil would not affect the heat of combustion significantly if utilized as a drop-in blend. Additionally, the C<sub>8</sub> to C<sub>15</sub> range of compounds in the organic oil is similar to the carbon number distribution of kerosene-type aviation fuel (C<sub>8</sub> - C<sub>16</sub>).<sup>152</sup> The high aromatic content of the oil (Figure B.3A, Appendix B) also makes it suitable for use as an additive for conventional jet fuel, which influences critical parameters such as lubricity, density and the swelling behaviour of elastomer seals in jet turbines.<sup>153</sup> The presence of phenols in our organic oil could also be beneficial as an antioxidant additive for jet fuel.<sup>151</sup>

### 3.1.3 Upgrading of dilute & biomass-derived acetic acid

As production of glacial acetic acid is difficult in industrial processes, we explored the use of this process with a diluted acetic acid feed. To this end, we applied this upgrading route for an aqueous feed of 50 wt % acetic acid.

Because aldol condensation is a pseudo-2nd order reaction while hydrogenation is a

pseudo-1st order reaction due to the excess hydrogen that is present in this case, utilization of the same 2 wt % Cu/ZrO<sub>2</sub> catalyst resulted in a large proportion of acetone hydrogenation to propylene (Figure B.4, Appendix B). Due to this difference in kinetics, the relative rate of aldol condensation rapidly decreased with increasing water concentrations, compared to hydrogenation. This relative increase in the rate of hydrogenation could be compensated by decreasing the metal loading. Therefore, we used a catalyst for upgrading the dilute acetic acid feed that had a lower copper loading (0.5 wt %) compared to previous experiments (2 wt %). At these reaction conditions, the conversion of acetone was reduced to 59.2% (Figure 3.4A), which was due to the decrease of the aldol condensation rate that accompanied the decrease in reactant concentration with increased water content. The high amount of unreacted acetone also motivates the use of a lower copper loading, as a higher copper loading would have preferentially hydrogenated the acetone to C<sub>3</sub> gas hydrocarbons. In this case, the proportion of C<sub>3</sub> gas hydrocarbons (10.6 mol % carbon) was lower compared to 2 wt % Cu/ZrO<sub>2</sub> with pure acetic acid (20.3 mol % carbon), and much lower compared to 2 wt % Cu/ZrO<sub>2</sub> with diluted acetic acid (34.5 mol % carbon). We also performed runs with pure acetic acid with 2 wt % Cu/ZrO<sub>2</sub> and 1 bar H<sub>2</sub> partial pressure (10 vol % H<sub>2</sub> in Ar) which showed similar behavior (Figure B.5, Appendix B), but the catalyst deactivated rapidly, likely due to the insufficient regeneration of oxygen vacancies by molecular hydrogen. The decrease in the aldol condensation rate due to higher water content was also partially mitigated by the increase in total acidity and basicity of 0.5 wt % Cu/ZrO<sub>2</sub> compared to 2 wt % Cu/ZrO<sub>2</sub> (Table B.2, Appendix B), as aldol condensation reactions are catalyzed by both acid and basic sites.

Interestingly, the carbon distribution in the liquid phase hydrocarbon mixture shifted

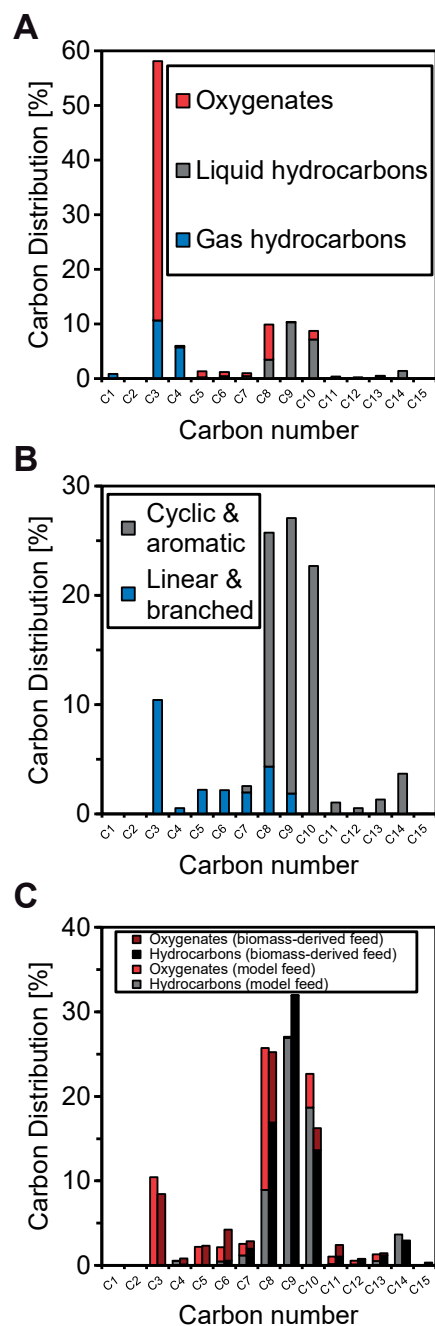


**Figure 3.4.** Upgrading of 50 wt % aqueous acetic acid over 2 g 0.5 wt % Cu/ZrO<sub>2</sub>. A) Molar carbon distribution of the product stream. ( $T = 400\text{ }^{\circ}\text{C}$ ,  $P = 10\text{ bar H}_2$ , WHSV =  $0.3\text{ h}^{-1}$ ,  $\text{H}_2$  flow =  $20\text{ mL/min}$ , conversion of acetone =  $59.2\%$ , time on stream =  $265.3\text{ h}$ ) Oxygenates consisted of oxygenated molecules in organic, aqueous and gas phases. B) Molar carbon distribution of linear versus cyclic and aromatic compounds in the organic oil phase. (time on stream =  $265.3\text{ h}$ ) C) Molar carbon distribution of oxygenates versus hydrocarbons in the organic oil phase for a 50 wt % aqueous acetic acid model feed and 40.3 wt % biomass-derived acetic acid feed. (time on stream for model feed =  $265.3\text{ h}$ , time on stream for biomass-derived feed =  $76.3\text{ h}$ ).

from primarily C<sub>8</sub> and C<sub>9</sub> to C<sub>9</sub> and C<sub>10</sub> hydrocarbons, which was also observed with 0.5 wt % Cu/ZrO<sub>2</sub> with pure acetic acid (Figure B.6, Appendix B). We attributed this phenomenon to the lower copper loading of the catalyst. Because of the lower hydrogenation rate, more oxygenated molecules underwent aldol condensation reactions to reach higher carbon numbers before being hydrogenated to liquid hydrocarbons. This is shown in our analysis of the organic oil phase (Figure 3.4B), where the majority of carbon were present as cyclic/aromatic C<sub>8</sub>, C<sub>9</sub> and C<sub>10</sub>. Aside from the higher proportion of C<sub>3</sub> linear compounds (mainly acetone) and the increase in C<sub>10</sub>, the rest of the cyclic/aromatic distribution in the organic oil remained similar to reactions with pure acetic acid and 2 wt % copper, with a cyclic/aromatic proportion of 76.5 mol % carbon. The mass yield of the organic oil was 21.2 wt %, and consisted of 61.3 mol % carbon liquid hydrocarbons (Figure 3.4C). While this is lower compared to previous experiments, further optimization on the WHSV could increase acetone conversion towards liquid hydrocarbons. Nevertheless, this indicates the possibility of upgrading aqueous acetic acid, which is important for biomass-derived feedstock.

To demonstrate this applicability to real biomass-derived streams, we used the same catalyst and conditions to upgrade 40.3 wt % aqueous acetic acid that was produced from steam-exploded beech wood (see Appendix B for detailed separation and concentration protocol). The resulting organic oil had a similar molar carbon distribution compared to the reaction with model feed (Figure 3.4C), with the only noticeable difference being a small decrease in the yield of C<sub>10</sub> hydrocarbons accompanied by a corresponding increase in the yield of C<sub>9</sub> hydrocarbons. The yield of organic oil was also reduced to 15.4 wt %. Both observations could be due to the increase in the water content of the feedstock, which might have lowered the rate of aldol condensation. Due to limited amounts of

biomass-derived acetic acid, the stability of the catalyst was not investigated. Despite these changes, these results demonstrated the possibility of upgrading biomass-derived acetic acid produced during pretreatment to liquid hydrocarbons.

The O/C content of the organic oil was reduced to 0.07 for the model acetic acid feed and 0.06 for the biomass-derived acetic acid feed. This content was slightly higher compared to the 0.04 O/C ratio of the oil from pure acetic acid upgrading, probably due to the decreased rate of hydrogenation as a result of our decision to use a lower copper loading. Nevertheless, this corresponds to a 93% and 94% removal of oxygen from model and biomass-derived acetic acid, respectively. We similarly estimated the HHV of the organic oil and found 40.6 MJ/kg for model acetic acid and 39.6 MJ/kg from biomass-derived acetic acid. These values are lower compared to the HHV of oil obtained from pure acetic acid, which could be due to the small increase in O/C ratio. Nevertheless, optimization of the reaction conditions could increase the proportion of deoxygenation which would likely increase the HHV of the oil to values similar to those obtained from pure acetic acid. Furthermore, the shift towards carbon numbers of primarily C<sub>9</sub> and C<sub>10</sub> in the upgrading of diluted acetic acid (Figure B.3B and B.3C, Appendix B) means that the resulting oil could have a higher distillation curve that would be more comparable with an aviation fuel blending agent.

### **3.1.4 Upgrading of dilute & biomass-derived acetic/butanoic acid mixtures**

We also performed cross-ketonization of acetic and butanoic acid to further increase the average carbon number of the organic oil (Figure 3.5A). An initial model feed of

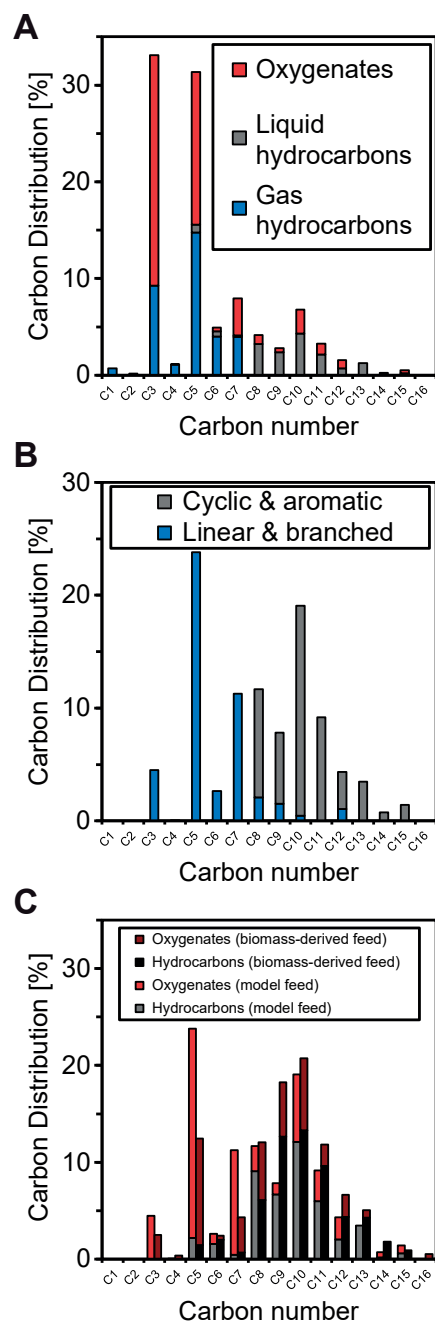


**Figure 3.5.** Upgrading of 28/12 wt % aqueous acetic/butanoic acid over 3 g 0.5 wt % Cu/ZrO<sub>2</sub>. A) Molar carbon distribution of the product stream. ( $T = 400\text{ }^{\circ}\text{C}$ ,  $P = 10\text{ bar H}_2$ , WHSV =  $0.2\text{ h}^{-1}$ ,  $\text{H}_2$  flow =  $20\text{ mL/min}$ , time on stream =  $72.1\text{ h}$ ) Oxygenates consisted of oxygenated molecules in organic, aqueous and gas phases. B) Molar carbon distribution of linear versus cyclic and aromatic compounds in the organic oil phase. (time on stream =  $72.1\text{ h}$ ) C) Molar carbon distribution of oxygenates versus hydrocarbons in the organic oil phase for 28/12 wt % aqueous acetic/butanoic acid model feed and 28/12 wt % biomass-derived acetic/butanoic acid. (time on stream for model feed =  $72.1\text{ h}$ , time on stream for biomass-derived feed =  $66.2\text{ h}$ )



28/12 wt % aqueous acetic/butanoic acid feed was used, which corresponded to a 7:3 mass ratio of acetic acid to butanoic acid.

Similarly to direct ketonization of acetic acid, full conversion of the carboxylic acids was reached. Ketonization products were once again important intermediates, with a large majority of 2-pentanone, which formed most of the oxygenated molecules in the product stream. The significant amount of this product suggested that cross-ketonization was heavily favored compared to homoketonization. This result was obtained with a reduced WHSV of  $0.2 \text{ h}^{-1}$ , because longer chain ketones were slower to condense and required longer residence time to reach reasonable conversions. As with direct ketonization of acetic acid, compounds in the organic oil that were longer than  $\text{C}_8$  were mainly cyclic/aromatic compounds (52.6 mol % carbon) (Figure 3.5B).

The mass yield of the organic oil was 17.8 wt % compared to the original acids in the feed. Within the organic oil phase, 44.5 mol % carbon were liquid hydrocarbons (Figure 3.5C). Despite a lower WHSV, the liquid hydrocarbon proportion was still lower compared to direct ketonization of acetic acid, confirming that ketones with a longer carbon chain length had a lower rate of aldol condensation. Because of their increased carbon length, a higher amount of product was retained in the organic oil rather than the aqueous phase. Importantly, liquid hydrocarbons containing 11 carbons or above constitute 12.3 mol % carbon of the organic oil, compared to 4.5 mol % carbon with direct ketonization. This larger fraction of longer carbon chain products demonstrated that cross-ketonization of acetic acid with butanoic acid can indeed increase the average carbon number of the organic oil, albeit at the expense of total liquid hydrocarbon yield. This chain lengthening showed that the products of the catalytic reactions can be tuned by the properties of the feedstock that is produced biologically.

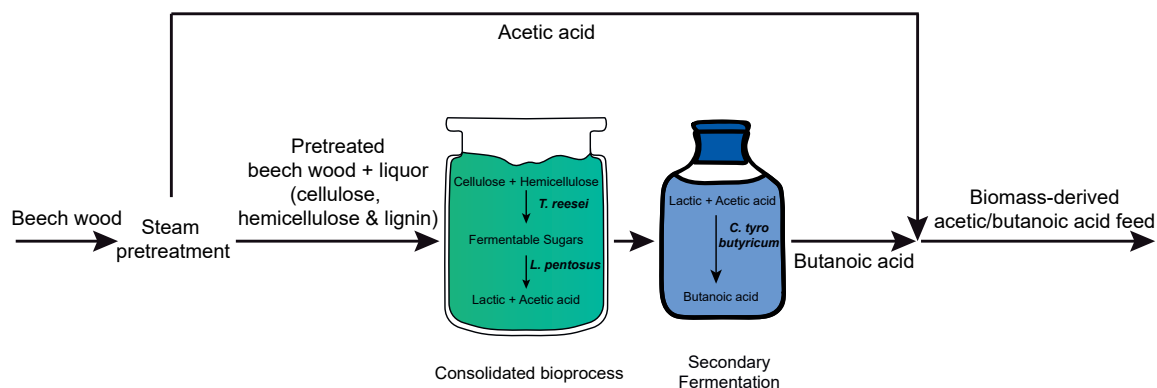


**Figure 3.6.** Steam-explosion of beech wood, followed by consolidated bioprocessing and secondary fermentation of the resulting polysaccharides to obtain biomass-derived acetic and butanoic acid.

To demonstrate this concept further, we used this cross-ketonization and aldol condensation platform to upgrade a mixture of acetic and butanoic acid produced from beech wood. The acetic acid was obtained from steam-explosion of the beech wood, similarly to our experiments above with real acetic acid feeds. After the acetate fraction was removed, the remaining polysaccharides were used to produce butanoic acid in a consolidated bioprocess based on a microbial consortium along with a secondary fermentation (Figure 3.6, see Appendix B for a description of the process). This enabled us to use 3 fractions of lignocellosic biomass (cellulose, hemicellulose and acetate) in our upgrading route.

In this case, the oil mass yield was 16.0 wt %, which was similar to the yield obtained when utilizing model feed (Figure 3.5C). However, the molar carbon distribution within the organic oil showed a higher proportion of liquid hydrocarbons (57.2 mol % carbon). We also measured a comparable amount of liquid hydrocarbons that had a carbon chain length of  $C_{11}$  or more (21.0 mol % carbon) demonstrating that our catalytic platform can be used to produce a deoxygenated oil from real bio-derived carboxylic acid mixtures.

An analysis of the compounds within the organic oil showed that the O/C content was 0.09 for the model feed and 0.07 for the biomass-derived feed. This compares favorably

with the O/C content of oil produced with pure or diluted acetic acid. From the initial O/C ratio of 0.82 (1 for acetic acid and 0.5 for butanoic acid), our upgrading process resulted in an 88% removal of oxygen for the model feed and 91% removal for the biomass-derived feed. HHV estimates indicated a value of 40.0 MJ/kg for the model feed and 40.8 MJ/kg for the biomass-derived feed, similarly to the values estimated for diluted acetic acid feeds. In the case of cross-ketonization, the larger fraction of carbon present as C<sub>11</sub> compounds and above (Fig B.3D and B.3E, Appendix B) might further benefit the properties of our oil for use as an aviation fuel blending.

### 3.1.5 Aviation fuel testing of organic oil as an additive

To demonstrate the viability of the produced organic oil as an additive for aviation fuels, the organic oil produced from pure commercial acetic acid (for highest oil yield) was tested for aviation fuel properties. The process was upscaled to 20 g of 2 wt % Cu/ZrO<sub>2</sub> at the same WHSV of 0.3 h<sup>-1</sup> in order to produce enough organic oil in a reasonable amount of time. The composition of the organic oil was verified to be similar to the organic oil that was produced at a smaller scale. Prior to fuel testing, we also performed inductively coupled plasma-mass spectrometry (ICP-MS) measurements on the organic oil, and found Cu, Fe and Cr to be below detection limits (Cu and Cr < 0.07 ppm, Fe < 0.68 ppm).

A blend of 10 vol % organic oil with Jet A-1 fuel was tested (pure organic oil not tested due to high aromatic content), in accordance with the test methods of the Aviation Fuel Quality Requirements for Jointly Operated Systems (AFQRJOS): Issue 29 – Oct 2016 for Jet A-1,<sup>154</sup> which encompasses the British Ministry of Defence Standard DEF STAN

91-091/Issue 9 and the ASTM Standard Specification D1655-16a. The test parameters include aromatic content, sulfur content, density, specific energy and the distillation curve.

**Table 3.1.** Aviation fuel testing results for a 10 vol % blend of organic oil with Jet A-1. <sup>a</sup>As established by AFQRJOS.

Limits which do not have a value are only required to report their measured values

Property	Test value	Limit <sup>a</sup>	Test method
Aromatics [vol %]	18.3	< 25.0	ASTM D1319
Sulfur, total [wt %]			
Distillation (101.3 kPa)			ASTM D86
Initial boiling point [°C]	64	-	
10 vol % recovered [°C]	165	< 205.0	
20 vol % recovered [°C]	171	-	
50 vol % recovered [°C]	189	-	
90 vol % recovered [°C]	230	-	
End point [°C]	267	< 300	
Residue [vol %]	0.8	< 1.5	
Loss [vol %]	0.2	< 1.5	
Density at 15 °C [kg/m <sup>3</sup> ]	801.1	775.0 - 840.0	ASTM D4052
Specific energy, net [MJ/kg]	43.2	> 42.8	ASTM D3338

The blended jet fuel had 18.3 vol % aromatics, showing that while the organic oil is composed predominantly of aromatics, it is still suitable to be used as an additive. The sulfur content, density and distillation curve were all within the specifications imposed by AFQRJOS (Table 3.1). More importantly, the net specific energy was 43.2 MJ/kg, demonstrating a low oxygen content. Overall, this indicated that our upgrading strategy has potential to be used for the production of an aviation fuel additive from carboxylic acids.

## 3.2 Conclusion

In summary, we presented a single step catalytic platform for valorizing the acetate and carboxylate fractions produced from lignocellulosic biomass to jet fuel additives. We notably demonstrated that real biomass-derived streams of short-chain carboxylic acids can be upgraded to aromatics and cycloalkenes of 8 carbon or higher in a single step. Specifically, aqueous streams of acetic acid and butanoic acid produced from steam pretreatment and subsequently consolidated bioprocessing of the pretreated beech wood were utilized. The resulting organic oil consisted of mainly aromatics and cycloalkenes, with compositions and heating values suitable to be used as additives for aviation fuel, which were further confirmed via aviation fuel testing. Using this method, the valorization of acetate, which is an often neglected fraction of biomass, can contribute to and expand the carboxylate platform that is based on producing carboxylic acids from biomass-derived polysaccharides. Maximizing the use of these different biomass fractions and producing drop in fuels for industries like aviation, where no other sustainable alternatives are currently available, will increase the chances of deploying efficient and profitable biorefineries.



# Chapter 4

## Conclusion

### 4.1 Summary

In Chapter 2, a process for the upgrading of hexanoic and butanoic acid to their respective olefins over Cu/SiO<sub>2</sub>-Al<sub>2</sub>O<sub>3</sub> was presented. The combination of carboxylic acid hydrogenation to alcohols followed by dehydration to olefins enabled the selective single-step production of olefins at > 90% selectivity. Throughout the study, an interesting behavior was observed. At full conversion, the selectivity abruptly switches from olefins to predominantly alkanes. This phenomenon presented an opportunity to rigorously investigate the fundamental catalyst-substrate interactions that occur on the catalyst surface during a biomass upgrading reaction. Various intermediate product studies showed that the presence/absence of carboxylic acids on the catalyst surface is key to suppressing alkane formation. By further using several in situ catalyst characterization techniques such as Fourier-transform infrared (FTIR) spectroscopy and chemisorption/desorption techniques, the observed selectivity switch phenomenon was ascertained to be due to the adsorption of carboxylic acids on the catalyst surface, blocking access of the olefins to the hydrogenation sites and thus preventing overhydrogenation to alkanes. This process allows for highly selective production of targeted olefins from their respective carboxylic acids, expanding the variety of chemicals we can produce from lignocellulosic biomass. Furthermore, the suppression of hydrogenation by the presence of carboxylic acids is a phenomenon which, to my knowledge, has not been investigated in detail by previous

studies.

In Chapter 3, I discussed the single-step conversion of short carboxylic acids to an aviation fuel additive via ketonization/cascade aldol condensation over Cu/ZrO<sub>2</sub>. Specifically, this upgrading route valorizes the existing carboxylate platform, by taking advantage of the often forgotten acetate fraction of lignocellulosic biomass, as well as using a novel consolidated bioprocessing route to produce butanoic acid from beech wood. An organic oil composed of C<sub>8</sub> to C<sub>16</sub> hydrocarbons was produced, with excellent catalyst stability and up to 96% deoxygenation of the starting material. Furthermore, by introducing cross-ketonization reactions in mixtures of biomass-derived acetic and butanoic acid, a higher carbon number can be obtained compared to just homo-ketonization of acetic acid. The produced oil was certified to meet Jet A-1 fuel standards as a 10 vol % blend, in terms of specific energy and distillation properties. As ketonization and aldol condensation reactions have traditionally been done separately, the development of the single step ketonization/cascade aldol condensation process is a novel concept, and provides a new route towards single-step production of long chain hydrocarbons from short biomass-derived carboxylic acids.

## 4.2 Outlook

The selectivity switch phenomenon that was elucidated by upgrading carboxylic acids to olefins could present new opportunities in controlling the product distribution of other catalytic reactions. A potential application could be the selective preservation of double bonds during hydrodeoxygenation of other functional groups, where a small amount of cheap carboxylic acid can be sacrificed to protect the high value olefin functionality. This



could be useful in the upgrading of guaiacyl and syringyl propanol monomers from lignin, which was only recently obtained in high yield<sup>48</sup> and purity.<sup>155</sup> Additionally, ferulic and coumaric acid, the carboxylate analogs of guaiacyl and syringyl propanol, can also be found in lignocellulosic biomass. The same tandem hydrogenation/dehydration process could be applied to selectively obtain valuable allylbenzenes from these biomass-derived aromatic compounds. Furthermore, as tandem hydrogenation/dehydration produces olefins of the same carbon length as the parent carboxylic acid, by using odd numbered carboxylic acids as feed, valuable odd numbered olefins could be obtained. Olefins produced through this route can also be oligomerized to jet fuel in a similar fashion to the butene oligomerization from GVL that was discussed in Section 1.5.

The ketonization/cascade aldol condensation process represents a new pathway to valorize short carboxylic acids. Screening studies on different carboxylic acids can be carried out to investigate the ideal mixture for jet fuel production. Lignin-derived aromatic carboxylates could even be used as feed, which might result in even higher carbon numbers or fuels with interesting properties. Furthermore, the organic oil obtained from this process can be tested at even higher blending ratios with Jet A-1 fuel, with the only limitation being the aromatic content. For this, careful optimization of reaction conditions or unique catalyst designs could result in cycloalkanes instead of aromatics, which have even better jet fuel properties.

In conclusion, the results I show in both Chapters 2 and 3 fulfil the initial objectives I have set in Section 1.9 for my doctoral thesis. The two valorization routes studied and the knowledge gained specifically addresses the shortcomings of upgrading the carboxylate platform, and presents new avenues towards sustainable fuel and chemicals production from lignocellulosic biomass.



# Appendix A

## Appendix for Chapter 2

### A.1 Chemicals and materials

All reagents and materials were used as received.  $\text{Cu}(\text{NO}_3)_2 \cdot 3\text{H}_2\text{O}$  (99.999% Cu) and silicon carbide (100 mesh) were obtained from Strem. Isooctane (99.5%), hexanoic acid (99.5%), 1-hexene (99%), 1-hexanol (99%), hexyl hexanoate (97%), dihexyl ether (97%), butanoic acid (99%), butyl butanoate (98%), dibutyl ether (99%), trioctylamine (98%), potassium bromide (99%) and concentrated nitric acid (65%) aqueous solution were obtained from Sigma-Aldrich. 1-butanol (99.5%) was obtained from Acros. Concentrated sulfuric acid (95-97%) and acetic acid (100%) was obtained from Merck. Water was purified using a Millipore Milli-Q Advantage A10 water purification system to a resistivity higher than 18  $\text{M}\Omega\cdot\text{cm}$ . Silica-alumina (Siral 70) was provided by Sasol. Quartz wool was obtained from Ohio Valley Specialty Company. Synthetic air (99.999%), hydrogen (99.999%), helium (99.9999%), nitrogen (99.999%), argon (99.9999%), 10% hydrogen (99.999%) in argon, 2%  $\text{N}_2\text{O}$  (99.998%) in helium and methane (99.9995%) were obtained from Carbagas.

For the production of butanoic acid, *Lactobacillus pentosus* (DSM-20314) and *Clostridium tyrobutyricum* (DSM-2637) were purchased from DSMZ. *Trichoderma reesei* Rut-C30 (D-86271) was purchased from VTT. MRS broth was obtained from BD Difco. Reinforced clostridial medium was obtained from VWR. Phosphoric acid, sodium hydroxide, hydrochloric acid, urea, peptone, yeast extract,  $\text{KH}_2\text{PO}_4$ ,  $(\text{NH}_4)_2\text{SO}_4$ ,  $\text{FeSO}_4 \cdot 7\text{H}_2\text{O}$ ,

MnSO<sub>4</sub>·H<sub>2</sub>O, ZnSO<sub>4</sub>·7H<sub>2</sub>O, CoCl<sub>2</sub>·6H<sub>2</sub>O, CaCl<sub>2</sub>·6H<sub>2</sub>O and MgSO<sub>4</sub>·7H<sub>2</sub>O were obtained from Sigma-Aldrich. Beech wood (*Fagus sylvatica*) was harvested in winter 2015/16 from a forest in Messen, SO, Switzerland (donated by the Forstbetrieb Bucheggberg) and chipped in April 2016 (to the size of G30 wood chips).

## A.2 Catalyst preparation

Cu supported on silica-alumina (Cu/Si-Al) was prepared via incipient wetness impregnation. The silica-alumina was calcined under a synthetic air flow (100 mL/min) at 500 °C (reached using a 5 °C/min ramp) for 6 h, treated under vacuum ( $< 10^{-2}$  mbar) at 150 °C for 2 h and stored in a nitrogen-filled glovebox prior to impregnation. The desired amount of silica-alumina was taken out of the glovebox in a round-bottom flask fitted with a rubber septum. The appropriate amount of Cu(NO<sub>3</sub>)<sub>2</sub>·3H<sub>2</sub>O was dissolved in a solution of 0.1M nitric acid to facilitate solubilization. The solution was added drop-wise to the silica-alumina support up to the incipient wetness point. The wet catalyst was dried in an oven at 110 °C for 2 h and subsequently calcined under a synthetic air flow (100 mL/min) at 400 °C (reached using a 2 °C/min ramp) for 6 h. The calcined catalyst had a light green color.

## A.3 Catalyst characterization

The loading and metal dispersion of the Cu/Si-Al catalyst was verified respectively via H<sub>2</sub> temperature-programmed reduction (TPR) and N<sub>2</sub>O pulse titration in a Micromeritics Autochem II 2920 connected to a MKS Cirrus 2 Quadrupole mass spectrometer (MS).

For each analysis, the cell was loaded with  $\sim 0.2$  g of fresh catalyst. The carrier gas was helium flowing at 50 mL/min.  $\text{H}_2$  TPR was performed by flowing 10%  $\text{H}_2$  in Ar (50 mL/min) while a temperature ramp of 10  $^\circ\text{C}/\text{min}$  was applied until reaching 300  $^\circ\text{C}$ . Subsequently,  $\text{N}_2\text{O}$  (2% in He) was sent in pulses over the catalyst at 90  $^\circ\text{C}$  until no consumption was observed as determined by monitoring the mass 44 signal on the MS. A calcination under synthetic air (50 mL/min) was performed at 400  $^\circ\text{C}$  (reached using a 5  $^\circ\text{C}/\text{min}$  ramp) for 1 h, after which a second set of  $\text{H}_2$  TPR and  $\text{N}_2\text{O}$  pulse titration experiments was carried out.

The average loading and metal dispersion of the catalyst was 6.2 wt % Cu and 4.9%, respectively. For catalysts made in different batches, the loading and dispersion was confirmed to be within 5% of the average of all the batches.

## A.4 Catalytic testing

Tandem hydrogenation/dehydration was carried out in a fixed bed tubular reactor (OD=1/4 inch) in an up flow configuration. Typically,  $\sim 3$  g of catalyst were loaded into the heated zone of the reactor supported in place by silicon carbide beds and quartz wool plugs at both ends. The catalyst was undiluted and the height of the catalyst bed was 20.5 cm. The catalyst was reduced in situ under  $\text{H}_2$  flow (100 mL/min) at 300  $^\circ\text{C}$  (reached using a 1  $^\circ\text{C}/\text{min}$  ramp) for 4 h, then cooled to the desired reaction temperature. The feed was prepared by diluting the desired carboxylic acid in isooctane to 2 wt % or 10 wt %. A SSI LS-class HPLC pump was used to deliver the feed. The pressure in the reactor was set using a Tescom back-pressure regulator, while the  $\text{H}_2$  flowrate was controlled with a Brooks mass flow controller.

Liquid samples were collected using a gas-liquid separator. Liquid phase analyses were carried out on an Agilent Technologies 7890A gas chromatograph with a flame ionization detector (FID) and a HP-5 column. Online gas phase analyses were carried out on Agilent Technologies 7890A gas chromatograph with a gas sampling valve. Depending on the feedstock, a HP-PLOT Q column or a GS-Alumina column was used for gas analysis. If the reactor was cooled down in between reaction runs, an in situ reduction was performed again prior to the next run. Most compounds were quantified using external standards of the same compound. The effective carbon number (ECN) method<sup>156</sup> was used to quantify gas phase products, with methane as the reference and applying the ideal gas molar volume at 25 °C and 1 atm. Butene/butane that remained dissolved in the liquid phase was quantified with ECN using hexene as the reference. All carbon balances were closed above 90%.

Conversion was defined as the ratio of the difference in the amount of carboxylic acid present in the product stream over the amount of carboxylic acid in the feed. The molar product distribution was defined as the moles of the individual compound divided by the total moles of products (not including carboxylic acid) in the product stream. The weight hourly space velocity (WHSV) was defined as the mass flow rate of the total liquid feed divided by the mass of the catalyst in the reactor, unless otherwise specified. In product distributions, “others” consisted of alcohols, esters and ethers. The average steady state conversion and product distribution was assumed when the standard deviation of the conversion and major product was less than 1% of the mean of the samples over a course of 50 h time on stream. In setting the reaction parameters, the pressure of the reactor is the gauge pressure. The catalyst capability was defined as the total mass of hexenes produced over the course of one experiment without changing reaction conditions divided

by the mass of the catalyst in the reactor.

## A.5 Temperature-programmed desorption (TPD) experiments

TPD experiments were performed on a Micromeritics Autochem II 2920 connected to a MKS Cirrus 2 Quadrupole mass spectrometer (MS). Typically,  $\sim 0.2$  g of fresh catalyst was loaded into the analysis cell for each experiment. The carrier gas and vapor gas was helium flowing at 50 mL/min. In situ reduction was performed at 300 °C (reached using a 10 °C/min ramp) for 30 minutes, then cooled to 50 °C. Vapors of 1-hexene at 40 °C were injected over the sample until no 1-hexene was adsorbed, as indicated by monitoring the signal of mass 84 on the MS. A helium flow was maintained for 1 h to remove physisorbed 1-hexene. Subsequently, the sample was heated to 700 °C (reached using a 10 °C/min ramp). Throughout the experiment, the MS was set to track mass 84, the molecular ion peak of hexene.

For experiments involving hexanoic acid, the analysis cell was removed after reduction and a few drops of 2 wt % hexanoic acid in isooctane were introduced. The cell was quickly reconnected to the instrument and kept at 50 °C. A helium flow was maintained for 4 h to remove bulk isooctane and hexanoic acid, followed by heating to 165 °C for 2 h to remove physisorbed hexanoic acid. After this, the sample was cooled to 50 °C and 1-hexene TPD was performed as described above.

Acetic acid was used to quantify the amount of acid that could adsorb on the catalyst surface. The use of the more volatile acetic acid (compared to longer chain carboxylic

acids) was necessary to achieve a satisfactory calibration curve. In these experiments, vapors of acetic acid at 60 °C were injected over the sample until no acetic acid was adsorbed, as indicated by monitoring the signal of mass 60 on the MS. The sample was heated to 110 °C for 2 h to remove physisorbed acetic acid. Subsequently, the sample was heated to 700 °C (reached using a 10 °C/min ramp). Throughout the experiment, the MS was set to track mass 60, the molecular ion peak of acetic acid.

The TPD of acetic acid on the catalyst showed 285  $\mu\text{mol/g}$  adsorbed. The TPD of acetic acid on just the support showed a 24% increase in acetic acid adsorbed. This increase in acetic acid adsorption was likely due to the copper nanoparticles on the catalyst blocking access to some of the pores on the support, thus decreasing the surface area available for acetic acid adsorption.

## **A.6 Fourier-Transform Infrared Spectroscopy (FTIR)**

Diffuse reflectance infrared Fourier-transform spectroscopy (DRIFTS) experiments were carried out in a Perkin Elmer Frontier FTIR spectrometer with a liquid nitrogen-cooled mercury cadmium telluride (MCT) detector using a Harrick high temperature DRIFTS cell. Each spectrum was an average of 64 scans, with a resolution of 4  $\text{cm}^{-1}$  over a range of 4000 – 400  $\text{cm}^{-1}$ . The Kubelka-Munk transform was applied to each diffuse reflectance spectrum. The catalyst was diluted in KBr at an approximate ratio of 1:10 and reduced in situ with flowing  $\text{H}_2$  (100 mL/min) at 300 °C (reached using a 1 °C/min ramp) for 4 h. The sample was cooled to 25 °C and purged with flowing He (100 mL/min)



for at least 3 h. A spectrum was taken, representing a clean catalyst surface. The cell dome was opened and a drop of 1-hexene was added. The dome was closed quickly (to minimize passivation of the catalyst due to air) and a flow of He (100 mL/min) was maintained for 3 h to remove physisorbed 1-hexene. A spectrum was taken, to which the spectrum of the clean catalyst surface was subtracted. Prior to subtraction, the entire range of the spectrum with the adsorbed 1-hexene was adjusted with a scaling factor until a least squares fit was achieved with the spectrum of the clean catalyst. For the blank experiment, only KBr was used.

For experiments involving pre-adsorbed hexanoic acid, a drop of hexanoic acid was added to the sample. The sample was dried under flowing He (100 mL/min) at 165 °C (reached using a 5 °C/min ramp) for 2 h, then cooled to 25 °C. A spectrum was taken to represent a catalyst surface with pre-adsorbed hexanoic acid. The addition of 1-hexene was done as described above. A spectrum was taken, to which the spectrum corresponding to the surface with pre-adsorbed hexanoic acid was subtracted. Prior to subtraction, the entire range of the spectrum with the adsorbed 1-hexene was adjusted with a scaling factor until a least squares fit was achieved with the spectrum of the catalyst with pre-adsorbed hexanoic acid.

## **A.7 Production of butanoic acid from beech wood**

### **A.7.1 Steam pretreatment of beech wood**

Beech wood chips (*Fagus sylvatica*) were air-dried and milled to a particle size of < 1.5 mm. The pretreatment was performed using a custom-built steam gun (Indus-

trieanlagen Planungsgesellschaft m.b.H., Austria).<sup>50</sup> Saturated steam was added to pressurize and heat the biomass to 180 °C for 25 min. The hemicellulose was hydrolyzed to yield xylose and xylooligosaccharides in the prehydrolyzate. Acetyl-side chains bound to the xylopyranose backbone of the hardwood were released into the condensate. The condensate containing the hemicellulosic sugars and the acetic acid was extracted from the reactor under pressure, prior to slowly releasing the pressure and emptying the steam-gun. The recovered biomass was pretreated again at 230 °C for 14.1 min followed by an explosive pressure release to increase the enzymatic hydrolyzability of glucan.

### A.7.2 Fungal and bacterial strains and culturing methods

*L. pentosus* precultures were grown at 30 °C in a MRS broth which contained (in g/L): peptone from casein, 10; meat extract, 10; yeast extract, 5; glucose, 20; Tween 80, 1; K<sub>2</sub>HPO<sub>4</sub>, 2; sodium acetate, 5; ammonium citrate, 2 and MgSO<sub>4</sub>·7H<sub>2</sub>O, 0.2. The pH was adjusted to 6.2 - 6.5 with hydrochloric acid. *C. tyrobutyricum* precultures were grown at 37 °C in a reinforced clostridial medium composed of (in g/L): yeast extract, 13; peptone, 10; glucose, 5; soluble starch, 1; sodium chloride, 5; sodium acetate, 3; L-cysteine-HCl, 0.5; agar, 0.5. *T. reesei* precultures were grown at 28 °C in a Mandel medium which contained (in g/L): KH<sub>2</sub>PO<sub>4</sub>, 2; (NH<sub>4</sub>)<sub>2</sub>SO<sub>4</sub>, 1.4; MgSO<sub>4</sub>·7H<sub>2</sub>O, 0.3; CaCl<sub>2</sub>·6H<sub>2</sub>O, 0.4; urea, 0.3; peptone, 0.75; yeast extract, 0.25; and 1 mL/L trace element stock. The sterile filtered trace element stock contained (in g/L): FeSO<sub>4</sub>·7H<sub>2</sub>O, 5; MnSO<sub>4</sub>·H<sub>2</sub>O, 1.6; ZnSO<sub>4</sub>·7H<sub>2</sub>O, 1.4; CoCl<sub>2</sub>·6H<sub>2</sub>O, 3.7 and 10 mL/L concentrated hydrochloric acid. To avoid precipitation, 100x CaCl<sub>2</sub> and MgSO<sub>4</sub> solutions were autoclaved separately before they were combined with the remaining ingredients.

### A.7.3 Biofilm membrane reactor

Labfors (Infors HT, Switzerland) stirred-tank reactors with a working volume of 2.7 L were modified with a polydimethylsiloxane tubular, dense membrane (Mono-Lumen Tubing 1.58 x 3.18 x 0.80 (Dow Corning, USA)). The membrane was flushed with air at a rate of 368 mL/min. The temperature was maintained at 30 °C. Mandel medium with a solid loading of 3.86 wt % pretreated beech wood solids was used. The corresponding prehydrolyzate was linearly fed in 200 h. The pH was adjusted to 6.0 using 4 N phosphoric acid and 4 M sodium hydroxide. The subsequent secondary fermentation of the obtained lactate/acetate broth was performed in serum bottles under anaerobic conditions. The serum bottles were inoculated from a two-day liquid preculture of *C. tyrobutyricum* (5 vol %). The pH was adjusted to 6.0 by the addition of 4 N phosphoric acid. The final butanoic acid concentration was 9.5 g/L.

## A.8 Extraction and purification of biomass-derived butanoic acid

The aqueous butanoic acid broths were verified to be ~1 wt % butanoic acid by high performance liquid chromatography (HPLC) using an Agilent 1260 Infinity HPLC equipped with a refractive index and UV detector. The pH of the broths were adjusted to pH 1 using concentrated sulfuric acid. Trioctylamine was contacted with the broth at a 40 wt % extractant to broth ratio, which resulted in a 75% extraction efficiency. The trioctylamine phase was removed and distilled at 230 °C to obtain butanoic acid. If the purity of the obtained butanoic acid is less than 90 wt %, a second distillation of the

butanoic acid at 180 °C was carried out. This purification method resulted in butanoic acid of over 99 wt % purity.

## A.9 Supplementary figures

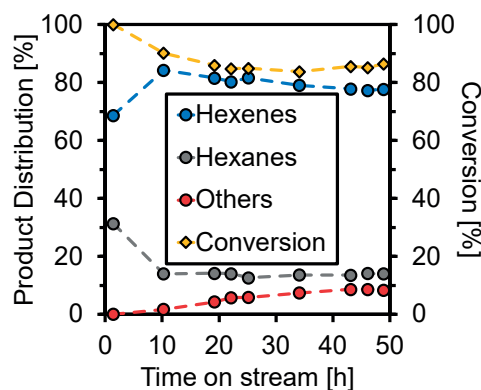


**Figure A.1.** Conversion and molar product distribution of hexanoic acid tandem hydrogenation/dehydration as a function of time on stream (WHSV = 0.25 h<sup>-1</sup>, H<sub>2</sub> flow = 74 mL/min, *T* = 210 °C, *P* = 5 bar and feed = 10 wt % hexanoic acid in isooctane). WHSV is calculated based on the total liquid feed. The WHSV that is based only on hexanoic acid (WHSV = 0.025 h<sup>-1</sup>) is similar to that used in Figure 2.3A (Total feed WHSV = 0.99 h<sup>-1</sup>, hexanoic acid feed WHSV = 0.020 h<sup>-1</sup>). The slightly reduced conversion in this more concentrated feed is likely explained by the fact that the WHSV that is based only on hexanoic acid is slightly higher here compared to Figure 2.3A (due to limited pump flow increments).

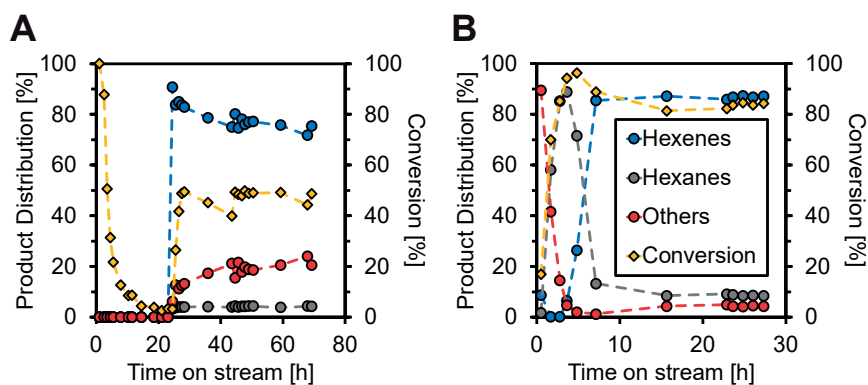


**Figure A.2.** Conversion and molar product distribution of hexanoic acid tandem hydrogenation/dehydration as a function of time on stream (WHSV = 0.99 h<sup>-1</sup>, H<sub>2</sub> or Ar flow = 74 mL/min, *T* = 210 °C, *P* = 5 bar and feed = 2 wt % hexanoic acid in isooctane). A) Ar flow was maintained initially for 24 h and subsequently switched to H<sub>2</sub> flow. B) Ar flow was maintained initially for 1 h and subsequently switched to H<sub>2</sub> flow. The legend for Figure A.2A can be found in Figure A.2B. The WHSV is calculated based on the total liquid feed.

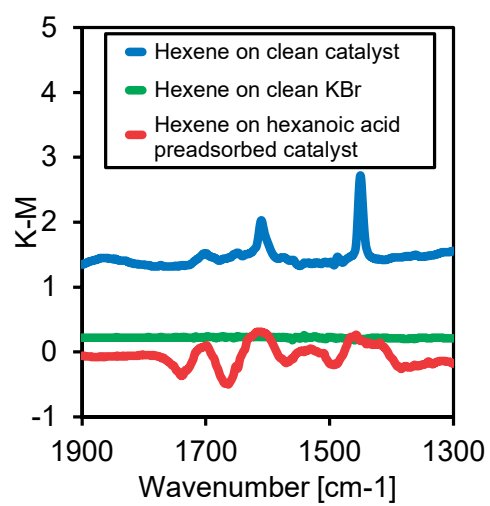


**Figure A.3.** Subtracted FTIR spectra of different molecules adsorbed on the surface of the catalyst at 25 °C. For all three spectra, the displayed spectrum is the difference between the spectra obtained before and after 1-hexene adsorption (and after hexanoic acid preadsorption for the preadsorbed catalyst). K-M stands for Kubelka-Munk.



# Appendix B

## Appendix for Chapter 3

### B.1 Chemicals and materials

All reagents and materials were used as received.  $\text{Cu}(\text{NO}_3)_2 \cdot 3\text{H}_2\text{O}$  (99.999% Cu) and silicon carbide (100 mesh) were obtained from Strem.  $\text{ZrO}(\text{NO}_3)_2 \cdot x\text{H}_2\text{O}$  (99%), urea (99-100.5%), concentrated nitric acid (65%), butanoic acid (99%), mesitylene (98%) and heptane (99%) were obtained from Sigma-Aldrich. Acetone (99.99%) was obtained from Fisher Chemical. Glacial acetic acid (100%) and concentrated sulfuric acid (95-97%) were obtained from Merck.  $\text{ZrO}_2$  was obtained from AlfaAesar. Water was purified using a Millipore Milli-Q Advantage A10 water purification system to a resistivity higher than  $18 \text{ M}\Omega \cdot \text{cm}$ . Quartz wool was obtained from Ohio Valley Specialty Company. Synthetic air (99.999%), hydrogen (99.999%), helium (99.9999%), argon (99.9999%), nitrogen (99.999%), 10% hydrogen (99.999%) in argon, 2%  $\text{N}_2\text{O}$  (99.998%) in helium and methane (99.9995%) were obtained from Carbagas.

For the production of acetic and butanoic acid, *Lactobacillus pentosus* (DSM-20314) and *Clostridium tyrobutyricum* (DSM-2637) were purchased from DSMZ, Germany. *Trichoderma reesei* Rut-C30 (D-86271) was purchased from VTT, Finland. MRS broth was obtained from BD Difco, Switzerland. Reinforced clostridial medium was obtained from VWR, Switzerland. Phosphoric acid, sodium hydroxide, hydrochloric acid, urea, peptone, yeast extract,  $\text{KH}_2\text{PO}_4$ ,  $(\text{NH}_4)_2\text{SO}_4$ ,  $\text{FeSO}_4 \cdot 7\text{H}_2\text{O}$ ,  $\text{MnSO}_4 \cdot \text{H}_2\text{O}$ ,  $\text{ZnSO}_4 \cdot 7\text{H}_2\text{O}$ ,  $\text{CoCl}_2 \cdot 6\text{H}_2\text{O}$ ,  $\text{CaCl}_2 \cdot 6\text{H}_2\text{O}$  and  $\text{MgSO}_4 \cdot 7\text{H}_2\text{O}$  were obtained from Sigma-Aldrich. Beech

wood (*Fagus sylvatica*) was harvested in winter 2015/16 from a forest in Messen, SO, Switzerland (donated by the Forstbetrieb Bucheggberg) and chipped in April 2016 to the size of G30 wood chips (max edge length: 85 mm, max cross section: 3 cm<sup>2</sup>).

## B.2 Catalyst preparation

Zirconia (ZrO<sub>2</sub>) was prepared by a modified method from Tsoncheva et al.<sup>157</sup> The ZrO<sub>2</sub> support was prepared by precipitation of ZrO(NO<sub>3</sub>)<sub>2</sub>·xH<sub>2</sub>O with urea. In a typical preparation, 5 L of water was acidified with 10 mL of concentrated nitric acid. 60 g of ZrO(NO<sub>3</sub>)<sub>2</sub>·xH<sub>2</sub>O was added and the solution was heated up to 90 °C while stirring. After the temperature stabilized, 160 g of urea were added and the solution was stirred for 15 h. The resulting precipitate was filtered and washed with water until there were no changes in the pH of the water before and after washing. The wet precipitate was dried in an oven at 110 °C overnight and subsequently calcined under flowing synthetic air at 450 °C (reached using a 2 °C/min ramp) for 3 h. The powder was stored in a nitrogen-filled glovebox prior to impregnation.

Cu supported on zirconia (Cu/ZrO<sub>2</sub>) was prepared via incipient wetness impregnation. The desired amount of zirconia was taken out of the glovebox in a round-bottom flask fitted with a rubber septum. The appropriate amount of Cu(NO<sub>3</sub>)<sub>2</sub>·3H<sub>2</sub>O was dissolved in a solution of 0.1M nitric acid to facilitate solubilization. The solution was added dropwise to the zirconia support up to the incipient wetness point. The wet catalyst was dried in an oven at 110 °C overnight.



## B.3 Catalyst characterization

The loading and dispersion of the Cu/ZrO<sub>2</sub> catalyst was verified respectively via H<sub>2</sub> temperature-programmed reduction (TPR) and N<sub>2</sub>O pulse titration in a Micromeritics Autochem II 2920 connected to an MKS Cirrus 2 Quadrupole mass spectrometer (MS). For each analysis, the cell was loaded with ~0.2 g of fresh catalyst. The carrier gas was helium flowing at 50 mL/min. H<sub>2</sub> TPR was performed by flowing 10% H<sub>2</sub> in Ar (50 mL/min) while a temperature ramp of 10 °C/min was applied until reaching 450 °C. Subsequently, N<sub>2</sub>O (2% in He) was sent in pulses over the catalyst at 90 °C until no consumption was observed as determined by monitoring the mass 44 signal on the MS. A calcination under synthetic air (50 mL/min) was performed at 500 °C (reached using a 5 °C/min ramp) for 1 h, after which a second set of H<sub>2</sub> TPR and N<sub>2</sub>O pulse titration experiments was carried out.

Subsequently, the total acid and basic sites of the Cu/ZrO<sub>2</sub> catalyst were verified respectively via NH<sub>3</sub> and CO<sub>2</sub> temperature-programmed desorption (TPD). The carrier gas was helium flowing at 50 mL/min. An initial H<sub>2</sub> TPR was performed by flowing 10% H<sub>2</sub> in Ar (50 mL/min) while a temperature ramp of 10 °C/min was applied until reaching 450 °C.

For NH<sub>3</sub> TPD, a flow of 1% NH<sub>3</sub> in He (50 mL/min) was maintained over the catalyst for 0.5 h at 50 °C, followed by a flow of He (50 mL/min) for 1 h to remove physisorbed NH<sub>3</sub>. The TPD was then carried out by heating the sample to 450 °C (reached using a 10 °C/min ramp). Throughout the experiment, the MS was set to track mass 16.

For CO<sub>2</sub> TPD, a flow of 10% CO<sub>2</sub> in He (50 mL/min) was maintained over the catalyst

for 0.5 h at 50 °C, followed by a flow of He (50 mL/min) for 1 h to remove physisorbed CO<sub>2</sub>. The TPD was then carried out by heating the sample to 450 °C (reached using a 10 °C/min ramp). Throughout the experiment, the MS was set to track mass 44.

Brunauer-Emmett-Teller (BET) surface area and Barrett-Joyner-Halenda (BJH) pore size and volume were measured using a Micromeritics 3Flex at liquid nitrogen temperature between 10<sup>-5</sup> and 0.99 relative N<sub>2</sub> pressure. For each analysis, the cell was loaded with ~0.2 g of catalyst. The samples were dried at 120 °C (reached using a 2 °C/min ramp) under vacuum (< 10<sup>-3</sup> mbar) for 4 h prior to analysis.

The catalyst characterization data is available in Table B.2.

## B.4 Catalytic testing

Upgrading of carboxylic acids was carried out in a fixed bed tubular reactor (OD=1/4 inch) in an up-flow configuration. Typically, 2 g of catalyst was diluted with silicon carbide in a 1:1 ratio by volume using a graduated cylinder, and loaded into the heated zone of the reactor supported in place by silicon carbide beds and quartz wool plugs at both ends. The height of the catalyst bed was 10 cm and started from the middle of the heated zone to enable the complete vaporization of the feed before it contacts the catalyst. The catalyst was reduced in situ under H<sub>2</sub> flow (100 mL/min) at 450 °C (reached using a 2.5 °C/min ramp) for 4 h, then cooled to the desired reaction temperature. The aqueous feeds were prepared by diluting the desired carboxylic acid in water to the appropriate concentration. An SSI LS-class HPLC pump was used to deliver the feed. The pressure in the reactor was set using a Tescom back-pressure regulator, while the H<sub>2</sub> flowrate was controlled with a Brooks mass flow controller.

For regeneration of the catalyst, the feed flow was stopped and the catalyst was dried under Ar flow (100 mL/min) for 3 h at 400 °C and 10 bar and then cooled down. The catalyst was calcined under synthetic air (100 mL/min) at 500 °C (reached using a 2 °C/min ramp) for 5 h. An in situ reduction was performed prior to the run as described above.

Liquid samples were collected using a gas-liquid separator. Liquid phase analyses were carried out on an Agilent Technologies 7890A gas chromatograph equipped with a flame ionization detector (FID) and a HP-5 column. Online gas phase analyses were carried out on Agilent Technologies 7890A gas chromatograph with a gas sampling valve and a HP-PLOT Q column. Compound identifications were carried out on an Agilent Technologies 7890A gas chromatograph equipped with an Agilent Technologies 5977A MSD and a HP-5 UI column.

Prior to analysis, organic phase samples were diluted 10 times in heptane and aqueous phase samples were diluted 10 times in water. Using the ECN method,<sup>156</sup> the response factor of a reference external standard measured using a calibration curve was used to calculate a modified response factor for each identified compound to quantify both liquid and gas phase products. We used the following ECN equation for our calculations:

$$RF_{comp} = RF_{ref} * (ECN_{ref}) / (ECN_{comp})$$

where,

$RF_{comp}$ : the modified response factor for the desired compound [mol/kg]

$RF_{ref}$ : the measured response factor for the reference external standard [mol/kg]

$ECN_{ref}$ : the effective carbon number of the reference external standard

$ECN_{comp}$ : the effective carbon number of the desired compound

Organic phase products were quantified using mesitylene as the reference external standard. Aqueous phase products were quantified using acetone as the reference external standard. Gas phase products were quantified using methane as the reference external standard and assuming the ideal gas molar volume at 25 °C and 1 atm. The effective carbon numbers of all measured compounds are given in Table B.1. All mass balances were closed above 90%, by estimating the mass of CO<sub>2</sub> formed from the 100% ketonization of the starting carboxylic acids. Carbon mole balances were closed above 80%, based on identified compounds from the chromatograms.

Conversion of acetone was defined as the ratio of the difference in the amount of acetone present in the product stream over the amount of acetone produced from acetic acid, assuming full conversion of acetic acid to acetone. The molar carbon distribution was defined as the moles of carbon of compounds with a particular carbon number divided by the total moles of carbon in the product stream. For molar carbon distributions involving the organic oil, only the carbon present in the organic oil was taken into consideration. In molar carbon distributions, “oxygenates” consisted of oxygenated molecules (molecules with at least 1 oxygen atom) in organic, aqueous and gas phases, unless specified to be only within the organic oil. “Hydrocarbons” consisted of molecules containing only carbon and hydrogen atoms.

The weight hourly space velocity (WHSV) was defined as the total mass flow rate of the feed divided by the mass of the catalyst in the reactor. The mass yield of the organic oil is defined as the mass of organic oil collected divided by the mass of carboxylic acids in the feed (not including water). The liquid hydrocarbon yield was defined as the

moles of carbon present as liquid hydrocarbon divided by the moles of carbon of acetone produced from acetic acid, assuming full conversion of acetic acid to acetone. The liquid hydrocarbon proportion within the organic oil was defined as the moles of carbon present as liquid hydrocarbons divided by the total moles of carbon in the organic oil.

For experiments with pure  $\text{ZrO}_2$  (Figure B.1), the  $\text{ZrO}_2$  used was purchased commercially from AlfaAesar.

## B.5 Estimation of higher heating values (HHV) for the organic oil

The higher heating values (HHV) for the organic oil was estimated using the mass percentages of C, H and O for all identified compounds within the oil. The molecular formula and number of moles for each identified compound were used to calculate the mass of C, H and O for each compound as well as the total mass of identified compounds. The equation for estimating the HHV for liquid fuels was based on the correlation developed by Channiwala and Parikh.<sup>150</sup> The equation is as follows:

$$HHV = 0.3491C + 1.1783H + 0.1005S - 0.1034O - 0.0151N - 0.0211A$$

where,

HHV: the higher heating value [MJ/kg]

C: carbon mass percentage [wt %]

H: hydrogen mass percentage [wt %]

S: sulfur mass percentage [wt %]

O: oxygen mass percentage [wt %]

N: nitrogen mass percentage [wt %]

A: ash content [wt %]

## **B.6 Inductively coupled plasma-mass spectrometry (ICP-MS) analysis**

ICP-MS analyses were carried out by the EPFL Central Environmental Laboratory with an Agilent 8900 Triple Quadrupole ICP-MS. Around 300 mg of the organic oil was added into a Teflon tube, along with 8 mL of 65% nitric acid and 1 mL of 30% hydrochloric acid. The sample was subsequently digested in a microwave oven. The resulting liquid was filtered (0.45  $\mu\text{m}$ ) and diluted to 50 mL with water. The sample was again diluted by half with water prior to analysis.

## **B.7 Aviation fuel testing**

The organic oil was tested without any purification/work up as a 10 vol % blend with Jet A-1 fuel using standard methods specified by the Aviation Fuel Quality Requirements for Jointly Operated Systems (AFQRJOS): Issue 29 – Oct 2016.

## **B.8 Production of acetic and butanoic acid from beech wood**

## **B.9 Steam pretreatment of beech wood**

Beech wood chips (*Fagus sylvatica*) were air-dried and milled to a particle size of < 1.5 mm. The pretreatment was performed using a custom-built steam gun (Industrieanlagen Planungsgesellschaft m.b.H., Austria).<sup>50</sup> Saturated steam was added to pressurize and heat the biomass to 180 °C for 25 min. The hemicellulose was hydrolyzed to yield xylose and xylooligosaccharides in the prehydrolyzate. Acetyl-side chains bound to the xylopyranose backbone of the hardwood were released into the condensate. The condensate containing the hemicellulosic sugars and the acetic acid was extracted from the reactor under pressure, prior to slowly releasing the pressure and emptying the steam-gun. The recovered biomass was pretreated again at 230 °C for 14.1 min followed by an explosive pressure release to increase the enzymatic hydrolyzability of glucan. Following this procedure, the acetic acid concentration was 10 g/L.

## **B.10 Fungal and bacterial strains and culturing methods**

*L. pentosus* precultures were grown at 30 °C in a MRS broth which contained (in g/L): peptone from casein, 10; meat extract, 10; yeast extract, 5; glucose, 20; Tween 80, 1; K<sub>2</sub>HPO<sub>4</sub>, 2; sodium acetate, 5; ammonium citrate, 2 and MgSO<sub>4</sub>·7H<sub>2</sub>O, 0.2. The pH was

adjusted to 6.2 - 6.5 with hydrochloric acid. *C. tyrobutyricum* precultures were grown at 37 °C in a reinforced clostridial medium composed of (in g/L): yeast extract, 13; peptone, 10; glucose, 5; soluble starch, 1; sodium chloride, 5; sodium acetate, 3; L-cysteine-HCl, 0.5; agar, 0.5. *T. reesei* precultures were grown at 28 °C in a Mandel medium which contained (in g/L): KH<sub>2</sub>PO<sub>4</sub>, 2; (NH<sub>4</sub>)<sub>2</sub>SO<sub>4</sub>, 1.4; MgSO<sub>4</sub>·7H<sub>2</sub>O, 0.3; CaCl<sub>2</sub>·6H<sub>2</sub>O, 0.4; urea, 0.3; peptone, 0.75; yeast extract, 0.25; and 1 mL/L trace element stock. The sterile filtered trace element stock contained (in g/L): FeSO<sub>4</sub>·7H<sub>2</sub>O, 5; MnSO<sub>4</sub>·H<sub>2</sub>O, 1.6; ZnSO<sub>4</sub>·7H<sub>2</sub>O, 1.4; CoCl<sub>2</sub>·6H<sub>2</sub>O, 3.7 and 10 mL/L concentrated hydrochloric acid. To avoid precipitation, 100x CaCl<sub>2</sub> and MgSO<sub>2</sub> solutions were autoclaved separately before they were combined with the remaining ingredients.

## B.11 Biofilm membrane reactor

Labfors (Infors HT, Switzerland) stirred-tank reactors with a working volume of 2.7 L were modified with a polydimethylsiloxane tubular, dense membrane (Mono-Lumen Tubing 1.58 x 3.18 x 0.80 (Dow Corning, USA)) (Figure B.7). The membrane was flushed with air at a rate of 368 mL/min. The temperature was maintained at 30 °C. Mandel medium with a solid loading of 3.86 wt % pretreated beech wood solids was used. The corresponding prehydrolyzate was linearly fed in 200 h. The pH was adjusted to 6.0 using 4 N phosphoric acid and 4 M sodium hydroxide. The subsequent secondary fermentation of the obtained lactate/acetate broth was performed in serum bottles under anaerobic conditions. The serum bottles were inoculated from a two-day liquid preculture of *C. tyrobutyricum* (5 vol %). The pH was adjusted to 6.0 by the addition of 4 N phosphoric acid. The final butanoic acid concentration was 9.5 g/L.



## **B.12 Purification of biomass-derived acetic and butanoic acid in water**

The concentration of the aqueous acetic and butanoic acid broths were verified by high performance liquid chromatography (HPLC) using an Agilent 1260 Infinity HPLC equipped with a refractive index and UV detector.

## **B.13 Purification of acetic acid**

The acetic acid solution was distilled to separate the acetic acid and water from any residual organic wood matter. The mixture was then neutralized with excess sodium carbonate. Subsequently, water was removed under vacuum using a rotary evaporator. The resulting salts were acidified with excess sulfuric acid. The mixture was then distilled at 125 °C to recover the acetic acid. A second purification of the acetic acid mixture was carried out with the same protocol. This purification method resulted in acetic acid with a purity of 40 wt % in water with a final recovery yield of 83 wt %.

## **B.14 Purification of butanoic acid**

The fermentation broth contained butanoic acid partly in solution and partly in salt form. The butanoic acid in solution was purified with the same method as acetic acid. The residual solids from the initial distillation contained some butanoate salts. Excess water and sulfuric acid were added to the solids to convert the salts to butanoic acid.

The solution was then distilled at 180 ° C to recover the butanoic acid. This purification method resulted in butanoic acid with a purity of 40.3 wt % in water for a final recovery yield of 82 wt %.

## B.15 Supplementary figures and tables

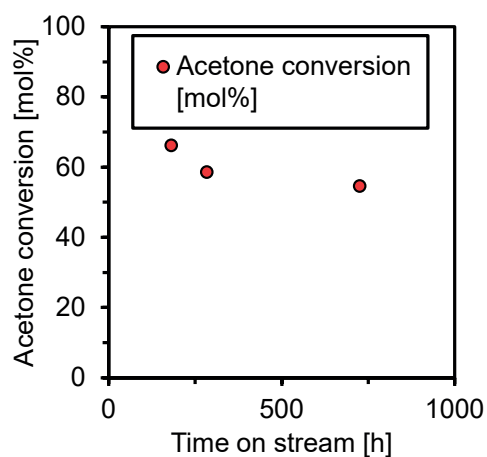


**Figure B.1.** Conversion of acetone as a function of time on stream during the upgrading of pure acetic acid over 2 g commercial  $\text{ZrO}_2$ . ( $T = 400\text{ }^\circ\text{C}$ ,  $P = 10\text{ bar H}_2$ ,  $\text{WHSV} = 0.3\text{ h}^{-1}$ ,  $\text{H}_2\text{ flow} = 20\text{ mL/min}$ )

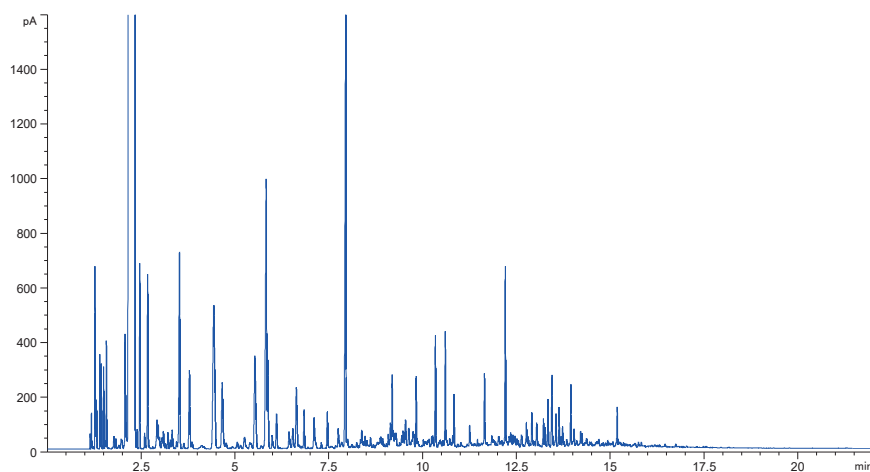


**Figure B.2.** Gas chromatogram of the organic oil during the upgrading of pure acetic acid ( $T = 400\text{ }^\circ\text{C}$ ,  $P = 10\text{ bar H}_2$ ,  $\text{H}_2\text{ flow} = 20\text{ mL/min}$  time on stream = 21.3 h, corresponding to Figure 3.3D).

**Table B.1.** List of identified compounds from the gas chromatogram (Figure B.1) of the organic oil during the upgrading of pure acetic acid ( $T = 400\text{ }^{\circ}\text{C}$ ,  $P = 10\text{ bar H}_2$ ,  $\text{H}_2\text{ flow} = 20\text{ mL/min}$  time on stream = 21.3 h, corresponding to Figure 3.3D).

Compound name	Retention time [min]	Area	ECN
Propene	1.135	29.5858	2.9
Isobutylene	1.169	110.944	3.9
1-butene, 3-methyl	1.222	7.1959	4.9
Acetone	1.265	481.76	2
2-pentene	1.291	110.842	4.9
2-pentene	1.305	151.006	4.9
1-pentene, 4-methyl	1.394	260.223	5.9
2-butene, 2,3-dimethyl	1.431	344.384	5.9
1-pentene, 2-methyl	1.494	258.71	5.9
2-butanone	1.531	32.5655	3
2-pentene, 4-methyl	1.567	392.129	4.9
1,3-pentadiene, 2-methyl	1.72	4.9874	5.8
1,3-pentadiene, 2-methyl	1.743	7.5053	5.8
1-pentene, 2,4-dimethyl	1.768	66.7508	6.9
2-pentene, 3,4-dimethyl	1.818	63.2588	6.9
Hexane, 2-methyl	1.869	4.6911	7
Hexane, 2-methyl	1.898	32.0685	7
Hexane, 3-methyl	1.966	100.87	7
2-pentanone	2.064	763.818	4
1,3-pentadiene, 2,4-dimethyl	2.369	1.1792	6.8
2-heptene	2.395	57.1681	6.9
ethyl cyclopentane	2.597	62.1754	7
1-butanol, 3-methyl	2.624	12.9618	4.4
MIBK	2.678	820.255	5
3-hexene, 2,5-dimethyl	2.81	10.3455	7.9

1-heptene, 6-methyl	2.928	197.506	7.9
2-pentanol, 4-methyl	2.96	122.893	5.25
2-methyl, 2-heptene	2.993	67.1094	7.9
2-methyl heptane	3.064	58.6998	8
Toluene	3.097	108.376	7
cyclohexene, 1-methyl	3.154	27.3365	6.9
2-heptene, 6-methyl	3.219	93.848	7.9
cyclohexane, 1,3-dimethyl	3.284	48.5985	8
2-heptene, 6-methyl	3.332	124.96	7.9
cyclohexene, 4,4-dimethyl	3.449	43.2184	7.9
Cyclohexene, 3,5-dimethyl	3.525	1257.99	7.9
3-heptene, 4-methyl	3.643	40.5617	7.9
cyclopentene, 1,2,3-trimethyl	3.713	4.7957	7.9
Cyclohexene, 3,5-dimethyl	3.791	555.18	7.9
Cyclohexane, 1,3-dimethyl	3.862	57.7369	8
trans-2-methyl, 3-octene	4.127	22.0201	8.9
Cyclohexene, 3,5-dimethyl	4.439	1841.39	7.9
Cyclohexene, 3,5,5-trimethyl	4.665	643.293	8.9
Cyclohexane, 1,1,3-trimethyl	4.769	48.9398	9
2-pentanone, 3-ethyl	4.935	17.4872	6
1,3-cyclopentadiene, 5,5dimethyl-1-ethyl	5.067	56.7648	8.8
2,3-dimethyl-3-heptene	5.152	29.7884	8.9
1,1-dimethyl-4-methylenecyclohexane	5.257	128.87	8.9
1,3-cyclopentadiene, 5,5dimethyl-1-ethyl	5.402	37.6723	8.8
2,3-dimethyl cyclohexa-1,3-diene	5.436	33.539	7.8
Cyclohexene, 3,5,5-trimethyl	5.536	937.218	8.9
2-methyl 2-octene	5.704	20.236	8.9
m-xylene	5.826	2142.33	8
Cyclohexene, 3,3,5-trimethyl	5.874	560.924	8.9

4-heptanone	5.985	93.9678	6
Cyclohexene, 3,3,5-trimethyl	6.102	233.871	8.9
2-heptanone	6.434	129.95	6
1,3-cyclopentadiene, 5,5dimethyl-1-ethyl	6.536	139.836	8.8
Cyclopentane, 1,3-dimethyl-2-(1-methylethylidene)	6.63	483.808	9.9
Cyclohexanone, 2-ethyl-2-propyl	6.693	19.0575	10
Cyclohexanone, 2-ethyl-2-propyl	6.777	8.6005	10
1,3-cyclohexadiene, 1,3,5,5-tetramethyl	6.837	228.932	9.8
4-heptanone, 2-methyl	7.104	256.694	7
1,4-cyclohexadiene, 3,3,6,6-tetramethyl	7.296	31.1503	9.8
Cyclohexene, 1,5,5-trimethyl-3-methylene	7.457	211.607	9.8
6-methyl 2-heptanone	7.746	112.178	7
Benzene 1-methylethyl	7.837	45.4742	9
Mesitylene	7.945	2706.33	9
Cyclohexane, 1-methyl-3-(1-methylethylidene)	8.376	101.178	9.9
Benzene 1-methyl-3-propyl	9.184	335.165	10
Benzene 1-ethyl-2,4-dimethyl	9.539	174.585	10
4,4-dimethyl-2-propenylcyclopentanone	9.625	112.764	9
3,5-decadiene, 2,2-dimethyl-, (Z,Z)-	9.739	129.16	11.8
Benzene, 1-methyl-4-(2-methylpropyl)-	9.824	314.579	11
Benzene, 1-methyl-4-(1-methylpropyl)-	10.337	527.378	11
3,5-xlenol	10.6	489.437	7.4
Benzene 1,4-dimethyl-2-(2-methylpropyl)	10.834	225.625	12
Phenol 2-ethyl-5-methyl	11.248	140.273	8.4
Phenol 2,4,6-trimethyl	11.644	377.404	8.4
Phenol, 2-ethyl-4,5-dimethyl	12.201	783.784	9.4
Benzene, 1,3-dimethyl-2-propoxy	12.762	161.957	10
Phenol, 2-(1,1-dimethylethyl)-3-methyl-	12.908	198.823	10.4
1,1,6,8-tetramethyl-1,2-dihydronaphthalene	13.036	161.097	14

2,5,8-trimethyltetralin	13.216	148.208	13
-------------------------	--------	---------	----

**Table B.2.** Characterization data for the two catalysts utilized in this study

Catalyst	Cu loading [wt %]	Cu disper- sion [%]	BET sur- face area [m <sup>2</sup> /g]	BJH pore size [nm]	BJH pore volume [cm <sup>3</sup> /g]	Total acid- ity [ $\mu$ mol/g]	Total basic- ity [ $\mu$ mol/g]
2 wt% Cu/ZrO <sub>2</sub>	1.92	9.28	106.97	3.4	0.072	200	275
0.5 wt% Cu/ZrO <sub>2</sub>	0.52	7.00	102.37	3.4	0.081	290	296

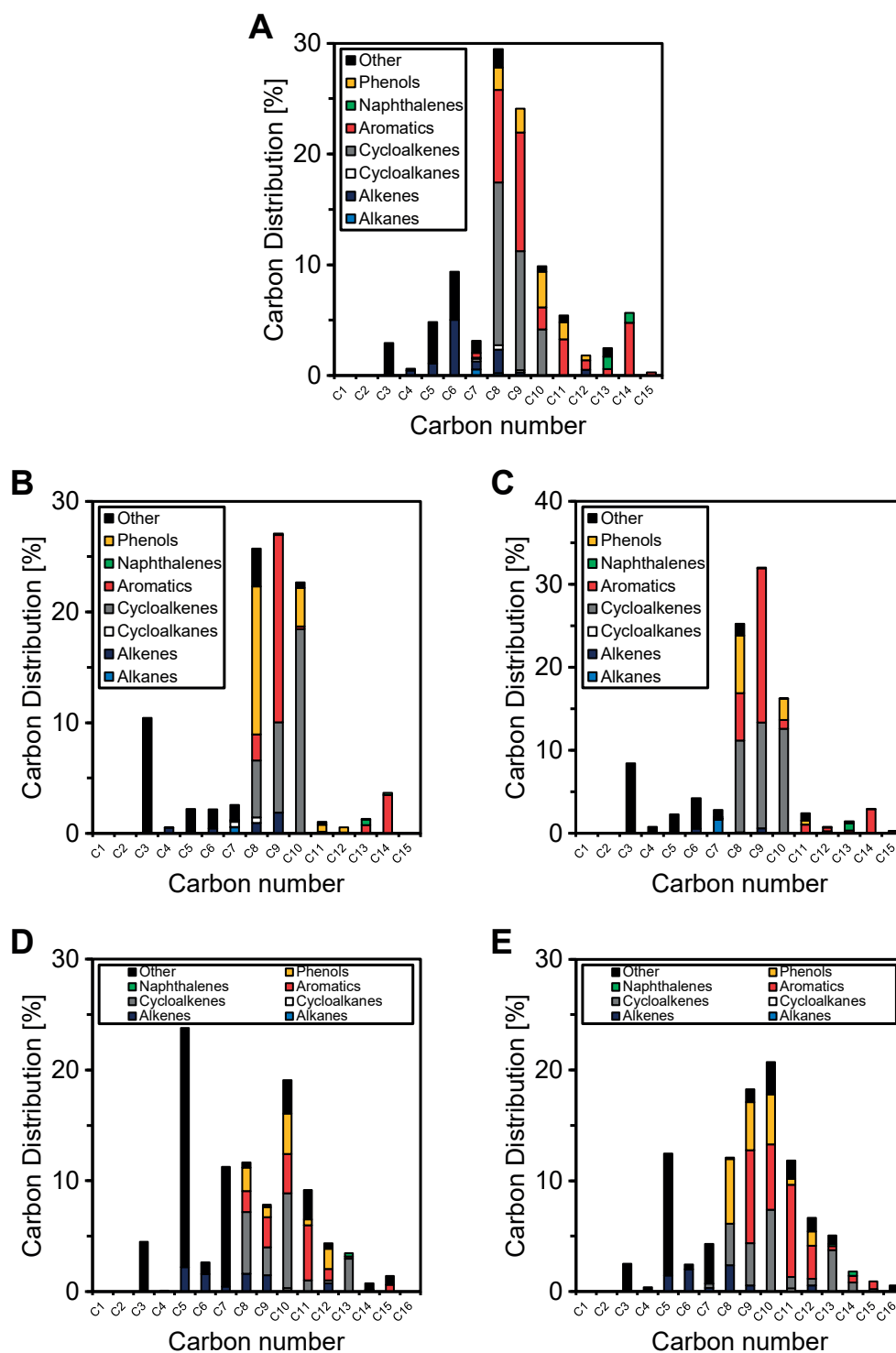


**Figure B.3.** Molar carbon distribution of the organic oil during the upgrading of: A) Pure acetic acid (time on stream = 21.3 h, corresponding to Figure 3.3D), B) 50 wt % aqueous acetic acid (time on stream = 265.3 h, corresponding to Figure 3.4C), C) 40.3 wt % biomass-derived acetic acid (time on stream = 76.3 h, corresponding to Figure 3.4C), D) 28/12 wt % aqueous acetic/butanoic acid (time on stream = 72.1 h, corresponding to Figure 3.5C) and E) 28/12 wt % biomass-derived acetic/butanoic acid (time on stream = 66.2 h, corresponding to Figure 3.5C) ( $T = 400\text{ }^{\circ}\text{C}$ ,  $P = 10\text{ bar H}_2$ ,  $\text{H}_2\text{ flow} = 20\text{ mL/min}$ ). “Others” consisted of oxygenates that are not phenols.

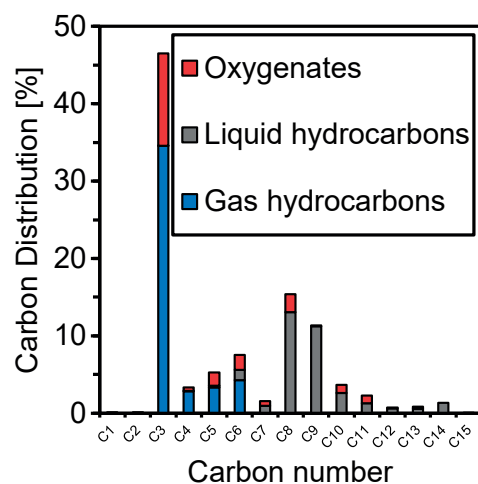


**Figure B.4.** Molar carbon distribution of the product stream during the upgrading of 50 wt % aqueous acetic acid over 2 g of 2 wt % Cu/ZrO<sub>2</sub> ( $T = 400\text{ }^{\circ}\text{C}$ ,  $P = 10\text{ bar H}_2$ , WHSV = 0.3 h<sup>-1</sup>, H<sub>2</sub> flow = 20 mL/min, conversion of acetone = 87.8 %, time on stream = 61.4 h). Oxygenates refers to oxygenated molecules in organic, aqueous and gas phases.

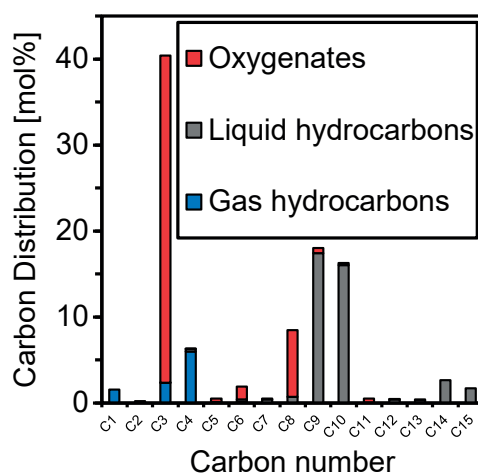


**Figure B.5.** Molar carbon distribution of the product stream during the upgrading of pure acetic acid over 2 g of 2 wt % Cu/ZrO<sub>2</sub> at 1 bar H<sub>2</sub> partial pressure ( $T = 400\text{ }^{\circ}\text{C}$ ,  $P = 10\text{ bar 10% H}_2$  in argon, WHSV = 0.3 h<sup>-1</sup>, 10% H<sub>2</sub> in argon flow = 20 mL/min, conversion of acetone = 70.6 %, time on stream = 34.3 h). Oxygenates refers to oxygenated molecules in organic, aqueous and gas phases.



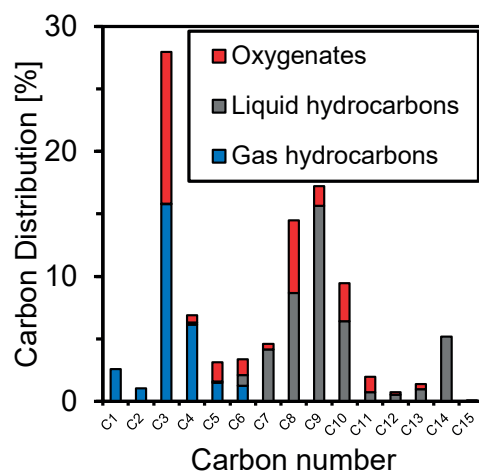


**Figure B.6.** Molar carbon distribution of the product stream during the upgrading of pure acetic acid over 2 g of 0.5 wt % Cu/ZrO<sub>2</sub> ( $T = 400\text{ }^{\circ}\text{C}$ ,  $P = 10\text{ bar H}_2$ , WHSV =  $0.3\text{ h}^{-1}$ , H<sub>2</sub> flow = 20 mL/min, conversion of acetone = 91.2 %, time on stream = 42.7 h). Oxygenates refers to oxygenated molecules in organic, aqueous and gas phases.

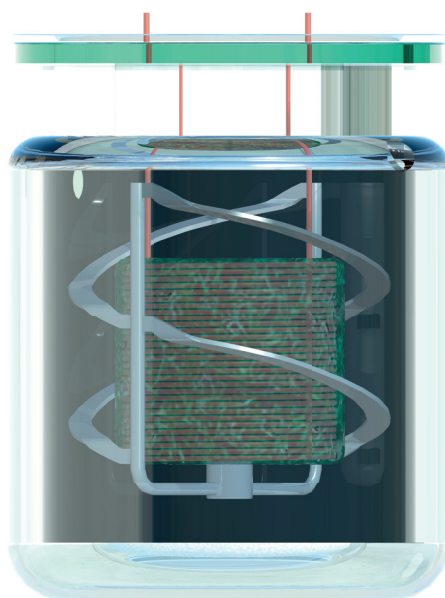


**Figure B.7.** Biofilm membrane reactor used to produce butanoic acid from pretreated beech wood.



# References

- (1) Sorrell, S. Reducing energy demand: A review of issues, challenges and approaches. *Renewable Sustainable Energy Rev.* **2015**, *47*, 74–82.
- (2) *BP Statistical Review of World Energy 2018*; BP: 2018.
- (3) Schmidt-Rohr, K. Why Combustions Are Always Exothermic, Yielding About 418 kJ per Mole of O<sub>2</sub>. *J. Chem. Educ.* **2015**, *92*, 2094–2099.
- (4) Dlugokencky, E.; Tans, P. Trends in Atmospheric Carbon Dioxide., EN-US, 2018.
- (5) Wigley, T. M. L. The pre-industrial carbon dioxide level. *Clim. Change* **1983**, *5*, 315–320.
- (6) Team, C. W.; Pachauri, R. K.; Meyer, L. In, IPCC: Geneva, Switzerland, 2014, p 151.
- (7) In *Paris Agreement*, United Nations: Paris, France, 2015.
- (8) Trenberth, K. E.; Fasullo, J. T.; Kiehl, J. Earth’s Global Energy Budget. *Bull. Am. Meteorol. Soc.* **2009**, *90*, 311–324.
- (9) Dimroth, F. et al. Wafer bonded four-junction GaInP/GaAs//GaInAsP/GaInAs concentrator solar cells with 44.7% efficiency. *Prog. Photovoltaics* **2014**, *22*, 277–282.
- (10) Cueto, J. A. d. Review of the field performance of one cadmium telluride module. *Prog. Photovoltaics* **1998**, *6*, 433–446.
- (11) Bard, A. J.; Fox, M. A. Artificial Photosynthesis: Solar Splitting of Water to Hydrogen and Oxygen. *Acc. Chem. Res.* **1995**, *28*, 141–145.

- (12) Montes, M. J.; Abánades, A.; Martínez-Val, J. M. Performance of a direct steam generation solar thermal power plant for electricity production as a function of the solar multiple. *Sol. Energy* **2009**, *83*, 679–689.
- (13) *Energy Consumption in Switzerland 2017*; Swiss Federal Office of Energy SFOE: Bern, Switzerland, 2018.
- (14) Chase, M. W. NIST-JANAF Thermochemical Tables, Fourth Edition. *J. Phys. Chem. Ref. Data, Monograph 9* **1998**, 1–1951.
- (15) Liu, C.; Colón, B. C.; Ziesack, M.; Silver, P. A.; Nocera, D. G. Water splitting–biosynthetic system with CO<sub>2</sub> reduction efficiencies exceeding photosynthesis. *Science* **2016**, *352*, 1210–1213.
- (16) D’Alessandro, D. M.; Smit, B.; Long, J. R. Carbon Dioxide Capture: Prospects for New Materials. *Angew. Chem., Int. Ed.* **2010**, *49*, 6058–6082.
- (17) *Technology Roadmap - Biofuels for Transport*; tech. rep.; Paris, France: International Energy Agency, 2011.
- (18) Saini, J. K.; Saini, R.; Tewari, L. Lignocellulosic agriculture wastes as biomass feedstocks for second-generation bioethanol production: concepts and recent developments. *3 Biotech* **2015**, *5*, 337–353.
- (19) Hoogwijk, M.; Faaij, A.; van den Broek, R.; Berndes, G.; Gielen, D.; Turkenburg, W. Exploration of the ranges of the global potential of biomass for energy. *Biomass Bioenergy* **2003**, *25*, 119–133.
- (20) Questell-Santiago, Y. M.; Luterbacher, J. S., Chapter 2: Introduction to High Pressure CO<sub>2</sub> and H<sub>2</sub>O Technologies in Sustainable Biomass Processing. In *High Pressure Technologies in Biomass Conversion*, 2017, pp 9–36.

- (21) Rosegrant, M. W. Biofuels and Grain Prices: Impacts and Policy Responses., Washington, D.C., 2008.
- (22) Mohr, A.; Raman, S. Lessons from first generation biofuels and implications for the sustainability appraisal of second generation biofuels. *Energy Policy* **2013**, *63*, 114–122.
- (23) Escobar, J. C.; Lora, E. S.; Venturini, O. J.; Yáñez, E. E.; Castillo, E. F.; Almazan, O. Biofuels: Environment, technology and food security. *Renewable Sustainable Energy Rev.* **2009**, *13*, 1275–1287.
- (24) Hammond, G. P.; Li, B. Environmental and resource burdens associated with world biofuel production out to 2050: footprint components from carbon emissions and land use to waste arisings and water consumption. *GCB Bioenergy* **2016**, *8*, 894–908.
- (25) Mitchell, R. B.; Schmer, M. R.; Anderson, W. F.; Jin, V.; Balkcom, K. S.; Kiniry, J.; Coffin, A.; White, P. Dedicated Energy Crops and Crop Residues for Bioenergy Feedstocks in the Central and Eastern USA. *BioEnergy Res.* **2016**, *9*, 384–398.
- (26) Zhang, Y.; Dubé, M. A.; McLean, D. D.; Kates, M. Biodiesel production from waste cooking oil: 1. Process design and technological assessment. *Bioresour. Technol.* **2003**, *89*, 1–16.
- (27) Li, Y.; Horsman, M.; Wu, N.; Lan, C. Q.; Dubois-Calero, N. Biofuels from Microalgae. *Biotechnol. Prog.* **2008**, *24*, 815–820.
- (28) Williams, P. J. l. B.; Laurens, L. M. L. Microalgae as biodiesel & biomass feedstocks: Review & analysis of the biochemistry, energetics & economics. *Energy Environ. Sci.* **2010**, *3*, 554–590.

- (29) Chisti, Y. Biodiesel from microalgae. *Biotechnol. Adv.* **2007**, *25*, 294–306.
- (30) Himmel, M. E.; Ding, S.-Y.; Johnson, D. K.; Adney, W. S.; Nimlos, M. R.; Brady, J. W.; Foust, T. D. Biomass Recalcitrance: Engineering Plants and Enzymes for Biofuels Production. *Science* **2007**, *315*, 804–807.
- (31) Questell-Santiago, Y. M.; Zambrano-Varela, R.; Amiri, M. T.; Luterbacher, J. S. Carbohydrate stabilization extends the kinetic limits of chemical polysaccharide depolymerization. *Nat. Chem.* **2018**, *1*.
- (32) Cherubini, F. The biorefinery concept: Using biomass instead of oil for producing energy and chemicals. *Energy Convers. Manage.* **2010**, *51*, 1412–1421.
- (33) Rapagnà, S.; Jand, N.; Foscolo, P. U. Catalytic gasification of biomass to produce hydrogen rich gas. *Int. J. Hydrogen Energy* **1998**, *23*, 551–557.
- (34) Adachi, Y.; Komoto, M.; Watanabe, I.; Ohno, Y.; Fujimoto, K. Effective utilization of remote coal through dimethyl ether synthesis. *Fuel* **2000**, *79*, 229–234.
- (35) Jun, K.-W.; Roh, H.-S.; Kim, K.-S.; Ryu, J.-S.; Lee, K.-W. Catalytic investigation for Fischer-Tropsch synthesis from bio-mass derived syngas. *Appl. Catal., A* **2004**, *259*, 221–226.
- (36) Basu, P., *Biomass Gasification and Pyrolysis: Practical Design and Theory*, Google-Books-ID: QSypbUSdkikC; Academic Press: 2010.
- (37) Hognon, C.; Delrue, F.; Texier, J.; Grateau, M.; Thiery, S.; Miller, H.; Roubaud, A. Comparison of pyrolysis and hydrothermal liquefaction of *Chlamydomonas reinhardtii*. Growth studies on the recovered hydrothermal aqueous phase. *Biomass Bioenergy* **2015**, *73*, 23–31.

- (38) Gollakota, A. R. K.; Kishore, N.; Gu, S. A review on hydrothermal liquefaction of biomass. *Renewable Sustainable Energy Rev.* **2018**, *81*, 1378–1392.
- (39) Luterbacher, J.; Azarpira, A.; Motagamwala, A. H.; Lu, F.; Ralph, J.; Dumesic, J. Lignin monomer production integrated into the  $\gamma$ -valerolactone sugar platform. *Energy Environ. Sci.* **2015**, *8*, 2657–2663.
- (40) Luterbacher, J. S.; Alonso, D. M.; Dumesic, J. A. Targeted chemical upgrading of lignocellulosic biomass to platform molecules. *Green Chem.* **2014**, *16*, 4816–4838.
- (41) Sluiter, A.; Hames, B.; Ruiz, R.; Scarlata, C.; Sluiter, J.; Templeton, D.; Crocker, D., *Determination of Structural Carbohydrates and Lignin in Biomass*; NREL: Golden, Colorado, 2012.
- (42) Shuai, L.; Luterbacher, J. Organic Solvent Effects in Biomass Conversion Reactions. *ChemSusChem* **2016**, *9*, 133–155.
- (43) Walker, T. W.; Chew, A. K.; Li, H.; Demir, B.; Zhang, Z. C.; Huber, G. W.; Lehn, R. C. V.; Dumesic, J. A. Universal kinetic solvent effects in acid-catalyzed reactions of biomass-derived oxygenates. *Energy Environ. Sci.* **2018**, *11*, 617–628.
- (44) Mellmer, M. A.; Sanpitakseree, C.; Demir, B.; Bai, P.; Ma, K.; Neurock, M.; Dumesic, J. A. Solvent-enabled control of reactivity for liquid-phase reactions of biomass-derived compounds. *Nat. Catal.* **2018**, *1*, 199.
- (45) Luterbacher, J. S.; Rand, J. M.; Alonso, D. M.; Han, J.; Youngquist, J. T.; Marvelias, C. T.; Pfleger, B. F.; Dumesic, J. A. Nonenzymatic Sugar Production from Biomass Using Biomass-Derived  $\gamma$ -Valerolactone. *Science* **2014**, *343*, 277–280.

- (46) Mellmer, M. A.; Sener, C.; Gallo, J. M. R.; Luterbacher, J. S.; Alonso, D. M.; Dumesic, J. A. Solvent Effects in Acid-Catalyzed Biomass Conversion Reactions. *Angew. Chem., Int. Ed.* **2014**, *53*, 11872–11875.
- (47) Luterbacher, J. S.; Alonso, D. M.; Rand, J. M.; Questell-Santiago, Y. M.; Yeap, J. H.; Pfleger, B. F.; Dumesic, J. A. Solvent-Enabled Nonenzymatic Sugar Production from Biomass for Chemical and Biological Upgrading. *ChemSusChem* **2015**, *8*, 1317–1322.
- (48) Shuai, L.; Amiri, M. T.; Questell-Santiago, Y. M.; Héroguel, F.; Li, Y.; Kim, H.; Meilan, R.; Chapple, C.; Ralph, J.; Luterbacher, J. S. Formaldehyde stabilization facilitates lignin monomer production during biomass depolymerization. *Science* **2016**, *354*, 329–333.
- (49) Binder, J. B.; Raines, R. T. Fermentable sugars by chemical hydrolysis of biomass. *PNAS* **2010**, *107*, 4516–4521.
- (50) Pielhop, T.; Amgarten, J.; von Rohr, P. R.; Studer, M. H. Steam explosion pretreatment of softwood: the effect of the explosive decompression on enzymatic digestibility. *Biotechnol. Biofuels* **2016**, *9*, 152.
- (51) Kumar, P.; Barrett, D. M.; Delwiche, M. J.; Stroeve, P. Methods for Pretreatment of Lignocellulosic Biomass for Efficient Hydrolysis and Biofuel Production. *Ind. Eng. Chem. Res.* **2009**, *48*, 3713–3729.
- (52) Alizadeh, H.; Teymouri, F.; Gilbert, T. I.; Dale, B. E. Pretreatment of switchgrass by ammonia fiber explosion (AFEX). *Appl. Biochem. Biotechnol.* **2005**, *124*, 1133–1141.



- (53) Mosier, N.; Wyman, C.; Dale, B.; Elander, R.; Lee, Y. Y.; Holtzapple, M.; Ladisch, M. Features of promising technologies for pretreatment of lignocellulosic biomass. *Bioresour. Technol.* **2005**, *96*, 673–686.
- (54) Gao, D.; Chundawat, S. P. S.; Sethi, A.; Balan, V.; Gnanakaran, S.; Dale, B. E. Increased enzyme binding to substrate is not necessary for more efficient cellulose hydrolysis. *PNAS* **2013**, *110*, 10922–10927.
- (55) Hou, Q.; Ju, M.; Li, W.; Liu, L.; Chen, Y.; Yang, Q. Pretreatment of Lignocellulosic Biomass with Ionic Liquids and Ionic Liquid-Based Solvent Systems. *Molecules* **2017**, *22*, 490.
- (56) Li, C.; Knierim, B.; Manisseri, C.; Arora, R.; Scheller, H. V.; Auer, M.; Vogel, K. P.; Simmons, B. A.; Singh, S. Comparison of dilute acid and ionic liquid pretreatment of switchgrass: Biomass recalcitrance, delignification and enzymatic saccharification. *Bioresour. Technol.* **2010**, *101*, 4900–4906.
- (57) Sun, Y.; Cheng, J. Hydrolysis of lignocellulosic materials for ethanol production: a review. *Bioresour. Technol.* **2002**, *83*, 1–11.
- (58) Gallo, J. M. R.; Alonso, D. M.; Mellmer, M. A.; Yeap, J. H.; Wong, H. C.; Dumesic, J. A. Production of Furfural from Lignocellulosic Biomass Using Beta Zeolite and Biomass-Derived Solvent. *Top. Catal.* **2013**, *56*, 1775–1781.
- (59) Gallo, J. M. R.; Alonso, D. M.; Mellmer, M. A.; Dumesic, J. A. Production and upgrading of 5-hydroxymethylfurfural using heterogeneous catalysts and biomass-derived solvents. *Green Chem.* **2012**, *15*, 85–90.

- (60) Román-Leshkov, Y.; Dumesic, J. A. Solvent Effects on Fructose Dehydration to 5-Hydroxymethylfurfural in Biphasic Systems Saturated with Inorganic Salts. *Top. Catal.* **2009**, *52*, 297–303.
- (61) Román-Leshkov, Y.; Chheda, J. N.; Dumesic, J. A. Phase Modifiers Promote Efficient Production of Hydroxymethylfurfural from Fructose. *Science* **2006**, *312*, 1933–1937.
- (62) Wettstein, S. G.; Alonso, D. M.; Chong, Y.; Dumesic, J. A. Production of levulinic acid and gamma-valerolactone (GVL) from cellulose using GVL as a solvent in biphasic systems. *Energy Environ. Sci.* **2012**, *5*, 8199–8203.
- (63) Alonso, D. M.; Wettstein, S. G.; Dumesic, J. A. Gamma-valerolactone, a sustainable platform molecule derived from lignocellulosic biomass. *Green Chem.* **2013**, *15*, 584–595.
- (64) Bond, J. Q.; Jungong, C. S.; Chatzidimitriou, A. Microkinetic analysis of ring opening and decarboxylation of  $\gamma$ -valerolactone over silica alumina. *J. Catal.* **2016**, *344*, 640–656.
- (65) Bond, J. Q.; Wang, D.; Alonso, D. M.; Dumesic, J. A. Interconversion between  $\gamma$ -valerolactone and pentenoic acid combined with decarboxylation to form butene over silica/alumina. *J. Catal.* **2011**, *281*, 290–299.
- (66) Bond, J. Q.; Alonso, D. M.; Wang, D.; West, R. M.; Dumesic, J. A. Integrated Catalytic Conversion of  $\gamma$ -Valerolactone to Liquid Alkenes for Transportation Fuels. *Science* **2010**, *327*, 1110–1114.

- (67) Motagamwala, A. H.; Won, W.; Sener, C.; Alonso, D. M.; Maravelias, C. T.; Dumesic, J. A. Toward biomass-derived renewable plastics: Production of 2,5-furandicarboxylic acid from fructose. *Sci. Adv.* **2018**, *4*, eaap9722.
- (68) Bond, J. Q. et al. Production of renewable jet fuel range alkanes and commodity chemicals from integrated catalytic processing of biomass. *Energy Environ. Sci.* **2014**, *7*, 1500–1523.
- (69) Kunkes, E. L.; Simonetti, D. A.; West, R. M.; Serrano-Ruiz, J. C.; Gärtner, C. A.; Dumesic, J. A. Catalytic Conversion of Biomass to Monofunctional Hydrocarbons and Targeted Liquid-Fuel Classes. *Science* **2008**, *322*, 417–421.
- (70) Anand, A.; Kulkarni, R. D.; Gite, V. V. Preparation and properties of eco-friendly two pack PU coatings based on renewable source (sorbitol) and its property improvement by nano ZnO. *Prog. Org. Coat.* **2012**, *74*, 764–767.
- (71) Wyman, C. E. What is (and is not) vital to advancing cellulosic ethanol. *Trends Biotechnol.* **2007**, *25*, 153–157.
- (72) Kötter, P.; Ciriacy, M. Xylose fermentation by *Saccharomyces cerevisiae*. *Appl. Microbiol. Biotechnol.* **1993**, *38*, 776–783.
- (73) Holtzapple, M. T.; Granda, C. B. Carboxylate Platform: The MixAlco Process Part 1: Comparison of Three Biomass Conversion Platforms. *Appl. Biochem. Biotechnol.* **2009**, *156*, 95–106.
- (74) Johnson, A. M.; Kim, H.; Ralph, J.; Mansfield, S. D. Natural acetylation impacts carbohydrate recovery during deconstruction of *Populus trichocarpa* wood. *Biotechnol. Biofuels* **2017**, *10*, 48.

- (75) Holtzapple, M. T.; Davison, R. R.; Ross, M. K.; Aldrett-Lee, S.; Nagwani, M.; Lee, C.-M.; Lee, C.; Adelson, S.; Kaar, W.; Gaskin, D.; Shirage, H.; Chang, N.-S.; Chang, V. S.; Loescher, M. E. Biomass conversion to mixed alcohol fuels using the MixAlco process. *Appl. Biochem. Biotechnol.* **1999**, *79*, 609–631.
- (76) Taco Vasquez, S.; Dunkleman, J.; Chaudhuri, S. K.; Bond, A.; Holtzapple, M. T. Biomass conversion to hydrocarbon fuels using the MixAlco<sup>TM</sup> process at a pilot-plant scale. *Biomass Bioenergy* **2014**, *62*, 138–148.
- (77) McDowell, M. The MixAlco process: Green energy for the future., en.
- (78) Brethauer, S.; Studer, M. H. Consolidated bioprocessing of lignocellulose by a microbial consortium. *Energy Environ. Sci.* **2014**, *7*, 1446–1453.
- (79) Shahab, R. L.; Luterbacher, J. S.; Brethauer, S.; Studer, M. H. Consolidated bioprocessing of lignocellulosic biomass to lactic acid by a synthetic fungal-bacterial consortium. *Biotechnol. Bioeng.* **2018**, *115*, 1207–1215.
- (80) Manyar, H. G.; Paun, C.; Pilus, R.; Rooney, D. W.; Thompson, J. M.; Hardacre, C. Highly selective and efficient hydrogenation of carboxylic acids to alcohols using titania supported Pt catalysts. *Chem. Commun.* **2010**, *46*, 6279–6281.
- (81) Rozmysłowicz, B.; Kirilin, A.; Aho, A.; Manyar, H.; Hardacre, C.; Wärnå, J.; Salmi, T.; Murzin, D. Y. Selective hydrogenation of fatty acids to alcohols over highly dispersed ReOx/TiO<sub>2</sub> catalyst. *J. Catal.* **2015**, *328*, 197–207.
- (82) Cortright, R. D.; Sanchez-Castillo, M.; Dumesic, J. A. Conversion of biomass to 1,2-propanediol by selective catalytic hydrogenation of lactic acid over silica-supported copper. *Appl. Catal., B* **2002**, *39*, 353–359.

- (83) Marchetti, J. M.; Errazu, A. F. Esterification of free fatty acids using sulfuric acid as catalyst in the presence of triglycerides. *Biomass Bioenergy* **2008**, *32*, 892–895.
- (84) Marchetti, J. M.; Miguel, V. U.; Errazu, A. F. Possible methods for biodiesel production. *Renewable Sustainable Energy Rev.* **2007**, *11*, 1300–1311.
- (85) Park, J.-Y.; Wang, Z.-M.; Kim, D.-K.; Lee, J.-S. Effects of water on the esterification of free fatty acids by acid catalysts. *Renewable Energy* **2010**, *35*, 614–618.
- (86) Mazumder, N. A.; Rano, R.; Sarmah, G. A green and efficient solid acid catalyst from coal fly ash for Fischer esterification reaction. *J. Ind. Eng. Chem.* **2015**, *32*, 211–217.
- (87) Takagaki, A.; Toda, M.; Okamura, M.; Kondo, J. N.; Hayashi, S.; Domen, K.; Hara, M. Esterification of higher fatty acids by a novel strong solid acid. *Catal. Today* **2006**, *116*, 157–161.
- (88) Fukuda, H.; Kondo, A.; Noda, H. Biodiesel fuel production by transesterification of oils. *J. Biosci. Bioeng.* **2001**, *92*, 405–416.
- (89) Meher, L. C.; Vidya Sagar, D.; Naik, S. N. Technical aspects of biodiesel production by transesterification—a review. *Renewable Sustainable Energy Rev.* **2006**, *10*, 248–268.
- (90) Leung, D. Y. C.; Wu, X.; Leung, M. K. H. A review on biodiesel production using catalyzed transesterification. *Appl. Energy* **2010**, *87*, 1083–1095.
- (91) Di Serio, M.; Tesser, R.; Ferrara, A.; Santacesaria, E. Heterogeneous basic catalysts for the transesterification and the polycondensation reactions in PET production from DMT. *J. Mol. Catal. A: Chem.* **2004**, *212*, 251–257.

- (92) Knoop, R. J. I.; Vogelzang, W.; Haveren, J. v.; Es, D. S. v. High molecular weight poly(ethylene-2,5-furanoate); critical aspects in synthesis and mechanical property determination. *J. Polym. Sci., Part A: Polym. Chem.* **2013**, *51*, 4191–4199.
- (93) Terzopoulou, Z.; Karakatsianopoulou, E.; Kasmi, N.; Tsanaktsis, V.; Nikolaidis, N.; Kostoglou, M.; Z. Papageorgiou, G.; A. Lambropoulou, D.; N. Bikiaris, D. Effect of catalyst type on molecular weight increase and coloration of poly(ethylene furanoate) biobased polyester during melt polycondensation. *Polym. Chem.* **2017**, *8*, 6895–6908.
- (94) Mäki-Arvela, P.; Snåre, M.; Eränen, K.; Myllyoja, J.; Murzin, D. Y. Continuous decarboxylation of lauric acid over Pd/C catalyst. *Fuel* **2008**, *87*, 3543–3549.
- (95) Snåre, M.; Kubičková, I.; Mäki-Arvela, P.; Eränen, K.; Murzin, D. Y. Heterogeneous Catalytic Deoxygenation of Stearic Acid for Production of Biodiesel. *Ind. Eng. Chem. Res.* **2006**, *45*, 5708–5715.
- (96) Bacha, J. D.; Kochi, J. K. Alkenes from acids by oxidative decarboxylation. *Tetrahedron* **1968**, *24*, 2215–2226.
- (97) Anderson, J. M.; Kochi, J. K. Silver(I)-catalyzed oxidative decarboxylation of acids by peroxydisulfate. Role of silver(II). *J. Am. Chem. Soc.* **1970**, *92*, 1651–1659.
- (98) Anderson, J. M.; Kochi, J. K. Silver(II) complexes in oxidative decarboxylation of acids. *J. Org. Chem.* **1970**, *35*, 986–989.
- (99) Anderson, J. M.; Kochi, J. K. Manganese(III) complexes in oxidative decarboxylation of acids. *J. Am. Chem. Soc.* **1970**, *92*, 2450–2460.

- (100) Grant, J. L.; Hsieh, C. H.; Makris, T. M. Decarboxylation of Fatty Acids to Terminal Alkenes by Cytochrome P450 Compound I. *J. Am. Chem. Soc.* **2015**, *137*, 4940–4943.
- (101) Rui, Z.; Harris, N. C.; Zhu, X.; Huang, W.; Zhang, W. Discovery of a Family of Desaturase-Like Enzymes for 1-Alkene Biosynthesis. *ACS Catal.* **2015**, *5*, 7091–7094.
- (102) Rui, Z.; Li, X.; Zhu, X.; Liu, J.; Domigan, B.; Barr, I.; Cate, J. H. D.; Zhang, W. Microbial biosynthesis of medium-chain 1-alkenes by a nonheme iron oxidase. *PNAS* **2014**, *111*, 18237–18242.
- (103) Dennig, A.; Kuhn, M.; Tassoti, S.; Thiessenhusen, A.; Gilch, S.; Bültner, T.; Haas, T.; Hall, M.; Faber, K. Oxidative Decarboxylation of Short-Chain Fatty Acids to 1-Alkenes. *Angew. Chem., Int. Ed.* **2015**, *54*, 8819–8822.
- (104) Foglia, T. A.; Barr, P. A. Decarbonylation dehydration of fatty acids to alkenes in the presence of transition metal complexes. *J. Am. Oil Chem. Soc.* **1976**, *53*, 737–741.
- (105) Maetani, S.; Fukuyama, T.; Suzuki, N.; Ishihara, D.; Ryu, I. Iron-catalyzed decarbonylation reaction of aliphatic carboxylic acids leading to  $\alpha$ -olefins. *Chem. Commun.* **2012**, *48*, 2552–2554.
- (106) Maetani, S.; Fukuyama, T.; Suzuki, N.; Ishihara, D.; Ryu, I. Efficient Iridium-Catalyzed Decarbonylation Reaction of Aliphatic Carboxylic Acids Leading to Internal or Terminal Alkenes. *Organometallics* **2011**, *30*, 1389–1394.
- (107) Gooßen, L. J.; Deng, G.; Levy, L. M. Synthesis of Biaryls via Catalytic Decarboxylative Coupling. *Science* **2006**, *313*, 662–664.

- (108) Goossen, L. J.; Rodríguez, N.; Melzer, B.; Linder, C.; Deng, G.; Levy, L. M. Biaryl Synthesis via Pd-Catalyzed Decarboxylative Coupling of Aromatic Carboxylates with Aryl Halides. *J. Am. Chem. Soc.* **2007**, *129*, 4824–4833.
- (109) Gooßen, L. J.; Zimmermann, B.; Knauber, T. Palladium/Copper-Catalyzed Decarboxylative Cross-Coupling of Aryl Chlorides with Potassium Carboxylates. *Angew. Chem., Int. Ed.* **2008**, *47*, 7103–7106.
- (110) Gooßen, L. J.; Zimmermann, B.; Linder, C.; Rodríguez, N.; Lange, P. P.; Hartung, J. Synthesis of Biaryls and Aryl Ketones via Microwave-Assisted Decarboxylative Cross-Couplings. *Adv. Synth. Catal.* **2009**, *351*, 2667–2674.
- (111) Becht, J.-M.; Drian, C. L. Biaryl Synthesis via Decarboxylative Pd-Catalyzed Reactions of Arenecarboxylic Acids and Diaryliodonium Triflates. *Org. Lett.* **2008**, *10*, 3161–3164.
- (112) Becht, J.-M.; Catala, C.; Le Drian, C.; Wagner, A. Synthesis of Biaryls via Decarboxylative Pd-Catalyzed Cross-Coupling Reaction. *Org. Lett.* **2007**, *9*, 1781–1783.
- (113) Wang, Z.; Ding, Q.; He, X.; Wu, J. Pd-catalyzed decarboxylative couplings of arenecarboxylic acids with aryl iodides. *Tetrahedron* **2009**, *65*, 4635–4638.
- (114) Zhang, F.; Greaney, M. F. Decarboxylative Cross-Coupling of Azoyl Carboxylic Acids with Aryl Halides. *Org. Lett.* **2010**, *12*, 4745–4747.
- (115) Forgione, P.; Brochu, M.-C.; St-Onge, M.; Thesen, K. H.; Bailey, M. D.; Bilodeau, F. Unexpected Intermolecular Pd-Catalyzed Cross-Coupling Reaction Employing Heteroaromatic Carboxylic Acids as Coupling Partners. *J. Am. Chem. Soc.* **2006**, *128*, 11350–11351.



- (116) Bilodeau, F.; Brochu, M.-C.; Guimond, N.; Thesen, K. H.; Forgione, P. Palladium-Catalyzed Decarboxylative Cross-Coupling Reaction Between Heteroaromatic Carboxylic Acids and Aryl Halides. *J. Org. Chem.* **2010**, *75*, 1550–1560.
- (117) Shang, R.; Xu, Q.; Jiang, Y.-Y.; Wang, Y.; Liu, L. Pd-Catalyzed Decarboxylative Cross Coupling of Potassium Polyfluorobenzoates with Aryl Bromides, Chlorides, and Triflates. *Org. Lett.* **2010**, *12*, 1000–1003.
- (118) Arroyave, F. A.; Reynolds, J. R. 3,4-Propylenedioxyproline-Based Conjugated Oligomers via Pd-Mediated Decarboxylative Cross Coupling. *Org. Lett.* **2010**, *12*, 1328–1331.
- (119) Miyasaka, M.; Hirano, K.; Satoh, T.; Miura, M. Synthesis of 2,3-Diarylbenzo[b]thiophenes via Nickel-Catalyzed Suzuki–Miyaura Cross-Coupling and Palladium-Catalyzed Decarboxylative Arylation. *Adv. Synth. Catal.* **2009**, *351*, 2683–2688.
- (120) Shang, R.; Fu, Y.; Wang, Y.; Xu, Q.; Yu, H.-Z.; Liu, L. Copper-Catalyzed Decarboxylative Cross-Coupling of Potassium Polyfluorobenzoates with Aryl Iodides and Bromides. *Angew. Chem., Int. Ed.* **2009**, *48*, 9350–9354.
- (121) Gooßen, L. J.; Rudolphi, F.; Oppel, C.; Rodríguez, N. Synthesis of Ketones from  $\alpha$ -Oxocarboxylates and Aryl Bromides by Cu/Pd-Catalyzed Decarboxylative Cross-Coupling. *Angew. Chem., Int. Ed.* **2008**, *47*, 3043–3045.
- (122) Rudolphi, F.; Song, B.; Gooßen, L. J. Synthesis of Azomethines from  $\alpha$ -Oxocarboxylates, Amines and Aryl Bromides via One-Pot Three-Component Decarboxylative Coupling. *Adv. Synth. Catal.* **2011**, *353*, 337–342.

- (123) Shang, R.; Fu, Y.; Li, J.-B.; Zhang, S.-L.; Guo, Q.-X.; Liu, L. Synthesis of Aromatic Esters via Pd-Catalyzed Decarboxylative Coupling of Potassium Oxalate Monoesters with Aryl Bromides and Chlorides. *J. Am. Chem. Soc.* **2009**, *131*, 5738–5739.
- (124) Shang, R.; Yang, Z.-W.; Wang, Y.; Zhang, S.-L.; Liu, L. Palladium-Catalyzed Decarboxylative Couplings of 2-(2-Azaaryl)acetates with Aryl Halides and Triflates. *J. Am. Chem. Soc.* **2010**, *132*, 14391–14393.
- (125) Jia, W.; Jiao, N. Cu-Catalyzed Oxidative Amidation of Propiolic Acids Under Air via Decarboxylative Coupling. *Org. Lett.* **2010**, *12*, 2000–2003.
- (126) Duan, Z.; Ranjit, S.; Zhang, P.; Liu, X. Synthesis of Aryl Sulfides by Decarboxylative C-S Cross-Couplings. *Chem. - Eur. J.* **2009**, *15*, 3666–3669.
- (127) Ranjit, S.; Duan, Z.; Zhang, P.; Liu, X. Synthesis of Vinyl Sulfides by Copper-Catalyzed Decarboxylative C-S Cross-Coupling. *Org. Lett.* **2010**, *12*, 4134–4136.
- (128) Nagashima, O.; Sato, S.; Takahashi, R.; Sodesawa, T. Ketonization of carboxylic acids over CeO<sub>2</sub>-based composite oxides. *J. Mol. Catal. A: Chem.* **2005**, *227*, 231–239.
- (129) Gaertner, C. A.; Serrano-Ruiz, J. C.; Braden, D. J.; Dumesic, J. A. Ketonization Reactions of Carboxylic Acids and Esters over Ceria-Zirconia as Biomass-Upgrading Processes. *Ind. Eng. Chem. Res.* **2010**, *49*, 6027–6033.
- (130) Pham, T. N.; Sooknoi, T.; Crossley, S. P.; Resasco, D. E. Ketonization of Carboxylic Acids: Mechanisms, Catalysts, and Implications for Biomass Conversion. *ACS Catal.* **2013**, *3*, 2456–2473.

- (131) Pestman, R.; Koster, R. M.; Pieterse, J. A. Z.; Ponec, V. Reactions of Carboxylic Acids on Oxides: 1. Selective Hydrogenation of Acetic Acid to Acetaldehyde. *J. Catal.* **1997**, *168*, 255–264.
- (132) Pestman, R.; Koster, R. M.; van Duijne, A.; Pieterse, J. A. Z.; Ponec, V. Reactions of Carboxylic Acids on Oxides: 2. Bimolecular Reaction of Aliphatic Acids to Ketones. *J. Catal.* **1997**, *168*, 265–272.
- (133) Pestman, R.; van Duijne, A.; Pieterse, J. A. Z.; Ponec, V. The formation of ketones and aldehydes from carboxylic acids, structure-activity relationship for two competitive reactions. *J. Mol. Catal. A: Chem.* **1995**, *103*, 175–180.
- (134) Pham, T. N.; Shi, D.; Sooknoi, T.; Resasco, D. E. Aqueous-phase ketonization of acetic acid over Ru/TiO<sub>2</sub>/carbon catalysts. *J. Catal.* **2012**, *295*, 169–178.
- (135) Gliński, M.; Kijeński, J.; Jakubowski, A. Ketones from monocarboxylic acids: Catalytic ketonization over oxide systems. *Appl. Catal., A* **1995**, *128*, 209–217.
- (136) Snell, R. W.; Shanks, B. H. Insights into the Ceria-Catalyzed Ketonization Reaction for Biofuels Applications. *ACS Catal.* **2013**, *3*, 783–789.
- (137) Randery, S. D.; Warren, J. S.; Dooley, K. M. Cerium oxide-based catalysts for production of ketones by acid condensation. *Appl. Catal., A* **2002**, *226*, 265–280.
- (138) Crisci, A. J.; Dou, H.; Prasomsri, T.; Román-Leshkov, Y. Cascade Reactions for the Continuous and Selective Production of Isobutene from Bioderived Acetic Acid Over Zinc-Zirconia Catalysts. *ACS Catal.* **2014**, *4*, 4196–4200.
- (139) Prasomsri, T.; Nimmanwudipong, T.; Román-Leshkov, Y. Effective hydrodeoxygenation of biomass-derived oxygenates into unsaturated hydrocarbons by MoO<sub>3</sub> using low H<sub>2</sub> pressures. *Energy Environ. Sci.* **2013**, *6*, 1732–1738.

- (140) Klein, F. G.; Banchero, J. T. Condensation of Acetone to Mesityl Oxide. *Ind. Eng. Chem.* **1956**, *48*, 1278–1286.
- (141) Salvapati, G. S.; Ramanamurty, K. V.; Janardanarao, M. Selective catalytic self-condensation of acetone. *J. Mol. Catal.* **1989**, *54*, 9–30.
- (142) Sacia, E. R.; Balakrishnan, M.; Deaner, M. H.; Goulas, K. A.; Toste, F. D.; Bell, A. T. Highly Selective Condensation of Biomass-Derived Methyl Ketones as a Source of Aviation Fuel. *ChemSusChem* **2015**, *8*, 1726–1736.
- (143) Yeap, J. H.; Héroguel, F.; Shahab, R. L.; Rozmysłowicz, B.; Studer, M. H.; Luterbacher, J. S. Selectivity Control during the Single-Step Conversion of Aliphatic Carboxylic Acids to Linear Olefins. *ACS Catal.* **2018**, *8*, 10769–10773.
- (144) Shi, W.; Zhao, J.; Yuan, X.; Wang, S.; Wang, X.; Huo, M. Effects of Brønsted and Lewis Acidities on Catalytic Activity of Heteropolyacids in Transesterification and Esterification Reactions. *Chem. Eng. Technol.* **2012**, *35*, 347–352.
- (145) Tao, Y. T. Structural comparison of self-assembled monolayers of n-alkanoic acids on the surfaces of silver, copper, and aluminum. *J. Am. Chem. Soc.* **1993**, *115*, 4350–4358.
- (146) Wühn, M.; Weckesser, J.; Wöll, C. Bonding and Orientational Ordering of Long-Chain Carboxylic Acids on Cu(111): Investigations Using X-ray Absorption Spectroscopy. *Langmuir* **2001**, *17*, 7605–7612.
- (147) Woodruff, D. P.; McConville, C. F.; Kilcoyne, A. L. D.; Lindner, T.; Somers, J.; Surman, M.; Paolucci, G.; Bradshaw, A. M. The structure of the formate species on copper surfaces: new photoelectron diffraction results and sexafs data reassessed. *Surf. Sci.* **1988**, *201*, 228–244.

- (148) Datka, J.; Kukulska-Zajac, E. IR Studies of the Activation of C=C Bond in Alkenes by Cu<sup>+</sup> Ions in Zeolites. *J. Phys. Chem. B* **2004**, *108*, 17760–17766.
- (149) Ro, I.; Liu, Y.; Ball, M. R.; Jackson, D. H. K.; Chada, J. P.; Sener, C.; Kuech, T. F.; Madon, R. J.; Huber, G. W.; Dumesic, J. A. Role of the Cu-ZrO<sub>2</sub> Interfacial Sites for Conversion of Ethanol to Ethyl Acetate and Synthesis of Methanol from CO<sub>2</sub> and H<sub>2</sub>. *ACS Catal.* **2016**, *6*, 7040–7050.
- (150) Channiwala, S. A.; Parikh, P. P. A unified correlation for estimating HHV of solid, liquid and gaseous fuels. *Fuel* **2002**, *81*, 1051–1063.
- (151) *ASTM D1655-18a: Standard Specification for Aviation Turbine Fuels*; ASTM International: West Conshohocken, PA, 2018.
- (152) Hemighaus, G.; Boval, T.; Bacha, J.; Barnes, F.; Franklin, M.; Gibbs, L.; Hogue, N.; Jones, J.; Lesnini, D.; Lind, J.; Morris, J., *Aviation Fuels Technical Review (FTR-3)*; Chevron Products Company: 2007.
- (153) Al-Nuaimi, I. A.; Bohra, M.; Selam, M.; Choudhury, H. A.; El-Halwagi, M. M.; Elbashir, N. O. Optimization of the Aromatic/Paraffinic Composition of Synthetic Jet Fuels. *Chem. Eng. Technol.* **2016**, *39*, 2217–2228.
- (154) *Aviation Fuel Quality Requirements for Jointly Operated Systems (AFQRJOS): Issue 29 - Oct 2016*; Joint Inspection Group (JIG): 2016.
- (155) Lan, W.; Amiri, M. T.; Hunston, C. M.; Luterbacher, J. S. Protection Group Effects During  $\alpha,\gamma$ -Diol Lignin Stabilization Promote High-Selectivity Monomer Production. *Angew. Chem.* **2018**, *130*, 1370–1374.

- (156) Scanlon, J. T.; Willis, D. E. Calculation of Flame Ionization Detector Relative Response Factors Using the Effective Carbon Number Concept. *J. Chromatogr. Sci.* **1985**, *23*, 333–340.
- (157) Tsoncheva, T.; Ivanova, R.; Henych, J.; Dimitrov, M.; Kormunda, M.; Kovacheva, D.; Scotti, N.; Santo, V. D.; Štengl, V. Effect of preparation procedure on the formation of nanostructured ceria–zirconia mixed oxide catalysts for ethyl acetate oxidation: Homogeneous precipitation with urea vs template-assisted hydrothermal synthesis. *Applied Catalysis A: General* **2015**, *502*, 418–432.



# Curriculum Vitae

## Jher Hau Yeap

Email: jherhau.yeap@epfl.ch  
jhyeap@hotmail.com

Avenue du Tir-Federal 92/417  
1024 Ecublens VD  
Switzerland  
Tel: +41 77 470 43 73

---

## Research Interests

- Integrated biomass conversion into fuels and value-added chemicals
- Heterogeneous & homogeneous catalyst design
- Fundamental catalyst-substrate interactions
- Catalytic process design for sustainable and eco-friendly chemical production

## Education

### École Polytechnique Fédérale de Lausanne

Ph.D. Chemical Engineering, expected December 2018

Dissertation title: Catalytic upgrading of biomass-derived carboxylic acids to fuels and chemicals

### University of Wisconsin-Madison

B.S. Chemical Engineering, December 2013

Certificate in Engineering for Energy Sustainability

GPA: 3.603/4.000

Dean's Honor List

## Research Experience

### École Polytechnique Fédérale de Lausanne

Institute of Chemical Sciences and Engineering

Laboratory of Sustainable and Catalytic Processing (LPDC), Lausanne, Switzerland

Professor Jeremy Luterbacher

*Doctoral assistant (08/14 – present)*

- Catalytic upgrading of biomass-derived carboxylic acids for fuels and chemicals
- Study of substrate interactions on catalyst surfaces
- Investigation of new biomass conversion routes

### University of Wisconsin - Madison

Department of Chemical and Biological Engineering, Madison WI, USA

Professor James Dumesic

*Undergraduate researcher (01/12 – 05/14)*

- Investigated the production of levulinic acid/furfural from corn stover
- Separation of soluble sugars from a mixture of  $\gamma$ -valerolactone and water

### University of Wisconsin - Madison

Nelson Institute for Environmental Studies

Center for Sustainability and the Global Environment (SAGE), Madison WI, USA

Dr. Erica Bickford, PhD

*Undergraduate researcher (11/10 – 01/11)*

- Optimized rail/truck routes to minimize emissions in the Midwest



## Publications

- **J. H. Yeap**, B. Rozmysłowicz, A. M. I. Elkhaiary, M. Talebi Amiri, R. L. Shahab, Y. M. Questell-Santiago, C. Xiros, M. H. Studer, J. S. Luterbacher, Catalytic valorization of the acetate fraction of biomass to aromatics and its integration into the carboxylate platform. in preparation (2018).
- **J. H. Yeap**, F. Héroguel, R. L. Shahab, B. Rozmysłowicz, M. H. Studer, J. S. Luterbacher, Selectivity control during the single-step conversion of aliphatic carboxylic acids to linear olefins. *ACS Catal.* **8**, 10769–10773 (2018).
- J. S. Luterbacher, D. M. Alonso, J. M. Rand, Y. M. Questell-Santiago, **J. H. Yeap**, B. F. Pfleger, J. A. Dumesic, Solvent-enabled nonenzymatic sugar production from biomass for chemical and biological upgrading. *ChemSusChem.* **8**, 1317–1322 (2015).
- J. M. R. Gallo, D. M. Alonso, M. A. Mellmer, **J. H. Yeap**, H. C. Wong, J. A. Dumesic, Production of furfural from lignocellulosic biomass using beta zeolite and biomass-derived solvent. *Top. Catal.* **56**, 1775–1781 (2013).

## Conferences & Workshops

- Frontiers in Biorefining 2018, St. Simons Island GA, USA  
*5 - 8 November 2018*  
Talk title: Selectivity control during the single-step conversion of aliphatic carboxylic acids to linear olefins  
Poster title: Selectivity control during the single-step conversion of aliphatic carboxylic acids to linear olefins
- American Institute of Chemical Engineers (AIChE) Annual Meeting 2018, Pittsburgh PA, USA  
*28 October - 2 November 2018*  
Talk title: Selectivity control during the single-step conversion of aliphatic carboxylic acids to linear olefins
- Clariant Chemistry Day 2018, Basel, Switzerland  
*4 October 2018*  
Poster title: Selectivity control during the single-step conversion of aliphatic carboxylic acids to linear olefins
- Swiss Chemical Society (SCS) Fall Meeting 2018, Lausanne, Switzerland  
*7 September 2018*  
Poster title: Selectivity control during the single-step conversion of aliphatic carboxylic acids to linear olefins
- American Institute of Chemical Engineers (AIChE) Annual Meeting 2017, Minneapolis MN, USA  
*29 October - 3 November 2017*  
Talk title: Selectivity control during the one-pot conversion of aliphatic carboxylic acids to linear olefins through tandem hydrogenation/dehydration

Poster title: Conversion of carboxylic acids to linear olefins by combined hydrogenation/dehydration reactions

- Swiss Competence Center for Energy Research (SCCER) School 2017, Engelberg, Switzerland  
*17 - 20 October 2017*  
Multidisciplinary talks and discussions on energy research in Switzerland
- Swiss Chemical Society (SCS) Fall Meeting 2017, Bern, Switzerland  
*21 - 22 August 2017*  
Poster title: Selectivity control during the one-pot conversion of aliphatic carboxylic acids to linear olefins through tandem hydrogenation/dehydration
- Swiss Chemical Society (SCS) Fall Meeting 2016, Zurich, Switzerland  
*15 September 2016*  
Poster title: One-pot conversion of aliphatic carboxylic acids to linear olefins through tandem hydrogenation/dehydration

## Teaching Experience

### **École Polytechnique Fédérale de Lausanne**

Section of Chemistry and Chemical Engineering (SCGC), Lausanne, Switzerland

*Teaching assistant (08/14 – present) (490 hours)*

- Chemical engineering lab & project, *4 fall semesters 2015 - 2018*
- EuroTech PhD summer school 2016, *June 6th to 17th 2016 at EPFL*
- Eco-friendly production and process intensification, *2 spring semesters 2015 - 2016*

### **University of Wisconsin - Madison**

Division of University Housing, Madison WI, USA

*Chemistry tutor (08/12 – 05/13)*

- Drop-in tutor for general, analytical, organic and physical chemistry

## Supervised Students

Name	Relationship
Ahmed Elkhaiary	M.Sc. student (co-advised with Dr. Bartosz Rozmysłowicz)
César Mercado	Undergraduate researcher
Manuel Moradell	Undergraduate researcher

## Leadership Experience

**UW-Madison Badminton Club**, Madison WI, USA

*President, Academic year 2012/2013*

*Membership coordinator, Academic year 2011/2012*

- Responsible for 50 club members
- Organized the annual Madison Open and Badger Open

## Awards and Grants

- EDCH Doctoral School Travel Fund, École Polytechnique Fédérale de Lausanne, *2018* (CHF 1000)
- John & Anne Meyer Fund, University of Wisconsin - Madison, *July 2013* (USD 500)

## Technical Skills

- Fluent in English, Mandarin, Malay, Cantonese & Hokkien
- Advanced handling of laboratory tools, including GC, HPLC, MS & NMR
- Catalyst preparation & characterization techniques, including FTIR spectroscopy, NH<sub>3</sub> TPD, H<sub>2</sub> TPR, CO/pyridine chemisorption, N<sub>2</sub> BET & air/moisture sensitive material handling
- Flow and batch reactor operation at high pressure and temperature
- Software skills: SolidWorks 3D Modeling, MATLAB, Aspen, Adobe Illustrator, Adobe Photoshop, ChemDraw & HTML/CSS
- IT manager: Responsible for the LPDC group website & server

